Bringing service to life

serco

Further Calculations Using the QSS and RTM Computer Models

Report to NDA

R.M. Mason, R. Cummings, J. G. Hosking, D. Powney,
P.J. Smith and P.N. Smith

Your Reference: NPO2140

Our Reference: SERCO/TAS - 1004 Issue 4

Date: March 2010

This page intentionally left blank

This report has been prepared by Serco under contract to NDA. The report has been reviewed by NDA, but the views expressed and conclusions drawn are those of the authors and do not necessarily represent those of NDA.

Conditions of publication

Bibliography

If you would like to see other reports available from NDA, a complete listing can be viewed at our website www.nda.gov.uk, or please write to the Library at the address below.

Feedback

Readers are invited to provide feedback to the NDA on the contents, clarity and presentation of this report and on the means of improving the range of NDA reports published. Feedback should be addressed to:

John Dalton,
Head of Communications,
Radioactive Waste Management Directorate,
Nuclear Decommissioning Authority,
Curie Avenue,
Harwell Science and Innovation Campus,
Didcot,
Oxon,
OX11 0RH, UK.

This page intentionally left blank

Title	Further Calculations Using the QSS and RTM Computer Models
Customer	NDA
Customer reference	NPO2140
Our reference	SERCO/TAS - 1004 Issue 4

Serco Technical Services
A32 Winfrith Technology Centre
Dorchester
Dorset
DT2 8DH

Telephone: +44 (0)1305 851187
Facsimile: +44 (0)1305 831105
E-mail: robert.mason@serco.com

www.serco.com/technicalservices

Serco Technical Services is a division of Serco Ltd

Serco Technical Services is certified to BS EN ISO9001 (2000) and BS EN ISO14001

	Name	Signature	Date
Author(s)	Dr R. M. Mason		04/03/2010
Reviewed by	Dr. B. D. Turland		04/03/2010
Approved by	D. W. Sweet		04/03/2010

This page intentionally left blank

Document History

Version	Author	Date	Description
Issue 1	R. M. Mason	29/09/2007	Contractor-approved version
Issue 2	R. M. Mason	18/10/2007	Error in implementation of the Tillotson equation of state for granite calculations corrected
Issue 3	R. M. Mason	11/01/2010	Revised to take account of comments from NDA
Issue 4	R. M. Mason	04/03/2010	Minor error in concentration values for Table 49 corrected.

This page intentionally left blank

Executive Summary

The Nuclear Decommissioning Authority (NDA) has been charged with implementing the UK Government's policy for the long-term management of higher-activity radioactive waste by planning, building and operating a geological disposal facility (GDF). The UK has accumulated a legacy of radioactive waste from electricity generation, defence activities and other industrial, medical, agricultural and research activities. Radioactive wastes continue to be produced from these activities. Some of these wastes will remain hazardous for hundreds of thousands of years.

Evidence to demonstrate that a geological disposal system meets all applicable regulatory requirements will be provided by the NDA Disposal System Safety Case (DSSC). This will consider the safety of radioactive waste transport, the safety of the construction and operation of the geological disposal facility, and the safety of the disposal facility in the very long term, after it has been sealed and closed. The safety case for a geological disposal facility is currently at an early stage of development, because the site and design have not yet been chosen. It is therefore termed a 'generic' safety case, and the strategies to demonstrate safety are also 'generic' because they must cover a range of possible disposal environments and facility designs. However, the DSSC will build on more than 25 years of site-specific and generic experience studying geological disposal and undertaking safety assessments in the UK, as well as learning from 20 to 30 years of such experience in other countries.

An important component of NDA's research in support of the development of a GDF is the safety of that facility once operations have ceased and the facility has been closed (post-closure performance). The wastes include a wide range of materials and radionuclides. Some radionuclides are fissile, i.e. they can cause a critical chain reaction with slow neutrons, which have thermal energies, assuming that sufficient mass of the radionuclides is present in the right conditions. The most significant fissile radionuclides in the waste inventory are the plutonium isotope ^{239}Pu and the uranium isotope ^{235}U. Engineering measures are available to prevent criticality for such time as the waste packaging affords a high level of containment. In the long term, however, after deterioration of the physical containment provided by the waste packages, there would be the possibility of movement of fissile material out of the waste packages and subsequent accumulation into new configurations, which could in principle lead to a criticality. It is conceivable that a criticality could adversely affect the performance of a GDF after closure because, for example, of the heat that would be produced affecting the engineered barriers.

It is therefore necessary to consider the post-closure criticality safety of the GDF concept in support of the DSSC. The Radioactive Waste Management Directorate (RWMD) of NDA is currently undertaking a programme of work with the objective of obtaining a better understanding of the nature of criticality under conditions within a GDF. This programme of work is known as Understanding Criticality under Repository[1] Conditions (UCuRC) and has, to date, been aimed mainly at intermediate-level wastes (ILW). Criticality is generally a well-understood phenomenon. The aim of the programme is to obtain a better understanding of the processes that would control the nature and magnitude of a criticality under the particular conditions of the NDA GDF concept. This programme is not itself an assessment of post-closure criticality safety of a GDF. The results of the work on understanding criticality feed into a programme developing an improved methodology for assessing post-closure criticality safety in the post-closure performance assessment of the NDA disposal concept. These assessments, in turn, will feed into the DSSC.

Two new transient criticality models have been developed for the UCuRC programme: the QSS (Quasi-Steady State) model and RTM (Rapid Transient Model). These models have been developed to understand two very different types of criticality: quasi-steady-state and rapid

[1] Here, and elsewhere in the report, 'Repository' is an alternative name for the GDF, and comes from earlier nomenclature.

transient (RT). Their initial development and application to test cases has been reported previously and an initial set of calculations has been undertaken. Both models continue to be developed to improve their accuracy and stability. In the study reported here, further calculations have been undertaken with both models to complement the first set of calculations using the latest developments to both the models and input supplied to them.

With the QSS Model, calculations have been undertaken in NRVB (Nirex[2] Repository Vault Backfill) where a system can encounter positive temperature feedback when the pore water boils. A QSS calculation of two or more stages is required when this occurs. The QSS Model has also been used to undertake calculations in mudstone, a potential GDF host rock that has not been studied previously.

The RTM has recently undergone improvements to the structural response model, and an analysis of stability issues has led to much greater understanding of the role the equation of state plays. An ongoing study has identified a number of potential improvements to the RTM submodels, both in terms of solution methods, and the supplied equation of state. Many of these improvements have been implemented, and previous RTM calculations undertaken in earlier studies have therefore been repeated to make use of the latest input and model features. In addition, two completely new RTM calculations have been undertaken; one to complement the set of calculations with plutonium dioxide in NRVB, and another as the first RTM calculation with uranium dioxide in NRVB. In total, this report describes ten RTM calculations.

A further part of this study has been a detailed analysis of fission product inventories for example QSS and RTM calculations. Using methodologies developed in 2004-05 as a basis, a number of calculations have been undertaken for example QSS and rapid transients from the first set of calculations. The analysis shows that for the RTM calculations the conclusions of the 2004-05 study are correct. For a QSS calculation, a more detailed analysis is required than the original outline methodology to accurately predict the fission product inventory.

This study has not only extended the range of calculations that have been undertaken previously, but has provided much more insight into the range of phenomena that can occur, why the phenomenon occur, and what further investigations and developments may be beneficial for improving confidence in both models. In addition, it provides analysis and recommendations for predicted fission product inventories for both QSS and rapid transients. Results will provide a basis for future assessments.

The technical work described in this paper was undertaken in the period July to October 2007. The work was performed by staff from Serco Technical and Assurance Services on behalf of the RWMD within NDA[2].

[2] The RWMD of NDA were formerly part of UK Nirex Ltd, which transferred to NDA in April 2007.

Contents

This page intentionally left blank

1 Introduction

1.1 Background

In 2001 the UK Government and devolved administrations initiated the Managing Radioactive Waste Safely (MWRS) programme with the aim of finding a practicable solution for the UK's higher activity wastes.

After a period of consultation, the Government published a White Paper in June 2008 that lays out the framework for inviting communities to express an interest in opening up discussions, without commitment, on the possibility of hosting a geological disposal facility (GDF) at some point in the future [1]. The Nuclear Decommissioning Authority (NDA) is supporting this process, but the Government will be responsible for initial dialogue with potential host communities. The NDA have responsibility for planning, building and operating a GDF in the future.

The NDA programme to implement geological disposal is framed by the voluntarism and partnership approach to site a GDF. To support this approach a long-term project has been developed for implementing geological disposal, the phases of which are in line with the stages in the site selection process as set out in the Government's White paper [2].

1.2 The Disposal System Safety Case

The UK has accumulated a legacy of radioactive waste from electricity generation, defence activities and other industrial, medical, agricultural and research activities. Radioactive wastes continue to be produced from these activities. Some of these wastes will remain hazardous for hundreds of thousands of years.

Evidence to demonstrate that a geological disposal system meets all applicable regulatory requirements will be provided by the NDA Disposal System Safety Case (DSSC). This will consider the safety of radioactive waste transport, the safety of the construction and operation of the geological disposal facility, and the safety of the disposal facility in the very long term, after it has been sealed and closed. The safety case for a geological disposal facility is currently at an early stage of development, because the site and design have not yet been chosen. It is therefore termed a 'generic' safety case, and the strategies to demonstrate safety are also 'generic' because they must cover a range of possible disposal environments and facility designs. However, the DSSC will build on more than 25 years of site-specific and generic experience studying geological disposal and undertaking safety assessments in the UK, as well as learning from 20 to 30 years of such experience in other countries.

The generic DSSC will consist of an overview report describing the safety of a geological disposal system and three main documents, one for each of the three components of the overall safety argument – the transport safety case, the constructional and operational safety case, and the environmental safety case.

1.3 Post-Closure Criticality

The NDA Radioactive Waste Management Directorate (RWMD) DSSC is being developed for the long-term management of higher activity wastes as introduced above. An important component of NDA's research in support of the development of the GDF concept is the consideration of the safety of a GDF once operations have ceased and the GDF has been closed (post-closure performance).

The wastes within a GDF will include a wide range of materials and radionuclides. Some radionuclides are fissile, i.e. they can cause a critical chain reaction with slow neutrons, which have thermal energies, assuming that sufficient mass of the radionuclides is present in the right conditions. The most significant fissile radionuclides in the waste inventory are the plutonium isotope ^{239}Pu and the uranium isotope ^{235}U. Engineering measures are available to prevent criticality for such time as the waste packaging affords a high level of containment [3]. In particular, limits are being established on the amount of fissile material that can be incorporated into individual waste packages. These limits will ensure that a criticality cannot occur during any credible configuration of waste packages and conditions that could occur during waste storage, transport and emplacement in a GDF. In the long term, however, after deterioration of the physical containment provided by the waste packages, there would be the possibility of movement of fissile material out of the waste packages and subsequent accumulation into new configurations that could in principle lead to a criticality. It is conceivable that a criticality could adversely affect the performance of a GDF after closure because, for example, of the heat that would be produced affecting the engineered barriers.

It is therefore necessary to consider the post-closure criticality safety of the GDF concept in support of the DSSC. The RWMD of NDA has been undertaking work on post-closure criticality safety since the early 1990s [4][3]. Both the potential for a criticality and the consequences if one occurred have been examined. The RWMD is currently undertaking a programme of work with the objective of obtaining a better understanding of the nature of criticality under GDF conditions. This programme of work is known as Understanding Criticality under Repository[4] Conditions (UCuRC) and has, to date, been aimed mainly at intermediate-level wastes (ILW). Criticality is generally a well-understood phenomenon. The aim of the programme is to obtain a better understanding of the processes that would control the nature and magnitude of a criticality under the particular conditions of a NDA GDF concept. The results of the work on understanding criticality feed into a programme developing an improved methodology for assessing post-closure criticality safety in the performance assessment of the NDA disposal concept. These assessments, in turn, will feed into the DSSC. The programme of work on UCuRC began in December 2001 after a planning stage during February to July 2001.

The main elements of the UCuRC programme are a suite of static criticality calculations and the development and application of existing or new transient models of criticality under GDF conditions. Subsequently to the reporting of the static calculations [5] and initial development of transient models and their application to test cases [6,7,8,9,10], work has continued to build confidence in, the transient criticality models [11,12,13,14,15].

A peer review of the static calculations and development of the transient criticality models, reported in References [5,6,7,8,9,10], was performed during Summer 2006. The peer review was undertaken by independent experts in criticality and rock mechanics, from the United States and United Kingdom, who had not participated previously in the NDA (and formerly Nirex[3]) programme.

An initial set of calculations with two of the models, the QSS (Quasi-Steady State) model and the RTM (Rapid Transient Model), has already been reported [16], and the calculations reported here complement and extend these earlier calculations. The intention of both this study and the initial set of calculations was to develop further understanding of criticality under GDF conditions and to provide results that could form the basis for future assessments. In conjunction with this study, an investigation has been undertaken to develop RTM, and in particular to gain improved understanding of the equations of state for NRVB (Nirex[3] Reference Vault Backfill [17]), granite

[3] The RWMD of NDA were formerly part of UK Nirex Ltd, which transferred to NDA in April 2007
[4] Here, and elsewhere in the report, 'Repository' is an alternative name for the GDF, and comes from earlier nomenclature.

and other potential host rocks [18]. The developments and findings of this investigation have been used in the calculations presented here wherever possible.

It is emphasised that the work reported here is not an assessment of post-closure criticality safety and the discussion of particular systems should not be taken to imply that the systems could or would occur.

The format of this paper is as follows:

- Section 2 – background and motivation for the calculations using the QSS and RTM Computer Models;
- Section 3 – QSS calculations;
- Section 4 – RTM calculations;
- Section 5 – Inventory calculations;
- Section 6 – Summary.

The technical work described in this paper was undertaken in the period July to October 2007. The work was performed by staff from Serco Technical and Assurance Services on behalf of the RWMD of NDA.

2 Overview of the Calculations

A specification for a suite of calculations using the QSS and RTM models developed by Serco Technical and Assurance Services, and the FETCH code developed by ICON (Imperial College Consultants), is given in Reference [19]. This is a far reaching suite of calculations to explore criticalities under many different configurations including but not limited to positive and negative temperature feedback regimes, different potential GDF host rocks, including granite, and different levels of degradation of NRVB and different critical geometries.

Following discussions with NDA, it was agreed that both Serco and ICON would undertake subsets of the calculations proposed in [19]. The first set of calculations undertaken by Serco was reported in Reference [16], and some calculations have also been undertaken by ICON. Further calculations from the specification [19] using the QSS and RTM models have now been completed by Serco, and these are presented here. These include inventory calculations for QSS and RTM transients.

Some of the RTM calculations presented here are re-runs of cases that have been reported before. These calculations have been re-run using the latest developments in the RTM and its inputs, including the latest structural response model (for all NRVB calculations), improvements in the solution methods (particularly for granite calculations), and modifications to the equation of state in formulation (NRVB calculations) and implementation (granite calculations). Explanations of the model developments are summarised in this report, with full details in References [14,15,18]. Where calculations are re-runs of earlier work, a full description of the cases is provided here to reduce the need for cross-referencing to earlier work.

3 QSS Calculations

3.1 Model Description

The QSS Model used in this study consists of a sphere containing a mixture of fissile material (FM), backfill (NRVB or rock) and water, known as the FM region, surrounded by an infinite region of the same saturated backfill or rock, known as the surrounding material (SM) region. FM is assumed to be deposited in the FM region at a user defined rate. When the FM is deposited in the FM region it is assumed to displace water from the pores in the backfill or rock. FM material continues to be deposited in the FM region until either the pores have been completely filled or a total of one tonne of FM has been deposited, or the user defined arrival rate becomes zero, which ever occurs first. The FM region is assumed to be isothermal and homogeneous. The arrival rate of FM is assumed to be sufficiently slow that the system can be approximated as being in a steady state condition at each instant in time. As more FM is added, the system moves to a different steady state.

QSS solutions are heavily dependent on the reactivity of a system, and how this changes with temperature and material composition. For a QSS solution to exist, the reactivity temperature feedback coefficient must be negative at all temperatures including the ambient temperature. A negative temperature feedback coefficient means that, as the temperature of a system at fixed composition is increased, the reactivity of that system decreases. It is assumed that the negative reactivity feedback maintains the reactivity close to zero as additional fissile material arrives. In the absence of temperature dependence, additional fissile material would typically act to increase the reactivity of the system. The reactivity is a function of various system parameters, including: nuclide and other material concentrations, temperature, saturation, and radius of the FM region. Hence, the constancy of the reactivity can be expressed in terms of the rates of change of the concentrations, temperature, saturation and radius. For the present case, the FM region is assumed to be spherical, so that the radius is the only parameter required to define the geometry. For the present calculations, the radius is assumed to remain constant.

The QSS Model has to date been developed primarily for studies of transient calculations in NRVB, the composition of which is given in Table 1. A full description of the model is given in Reference [6], and in particular a detailed description of the construction of a reactivity function for NRVB covering dependencies on temperature, mass of fissile material and composition of fissile and fissionable materials. This reactivity function removes the need to generate localised functions for reactivity variation from reactor physics codes such as WIMS9 [20] for every calculation. Instead, the generic NRVB function can be viewed as its own approximate reactor physics ‘code’ for NRVB systems, where a suitable interpolation scheme is used to estimate reactivity values at intermediate points. In the first set of calculations [16], the NRVB reactivity function was used to undertake a large number of QSS calculations in NRVB, for spheres of different initial composition, different radii and many arrival rates of fissile or fissionable materials. In this study it is used for the QSS calculations with positive temperature feedback at boiling in Section 3.3. A new reactivity function is produced for the mudstone calculations in Section 3.4.

3.2 Previous Understanding of QSS Results

The QSS Model has been used to undertake calculations for a large number of different cases in NRVB in previous studies [6,16] and a detailed sensitivity analysis for some of these cases has also been undertaken [11]. An important observation from these calculations was some general trends in the results obtained when the arrival rate of fissile/fissionable material was varied. Consider a system with a given arrival rate, which is not large enough for the system to reach temperatures where the pore water in the NRVB will boil. Suppose that at time t, while material is still arriving, this system has a temperature rise of ΔT above the ambient temperature (40℃ for all calculations in this study). Also su ppose that the power of the system is P, the neutron flux φ, and the composition of the fissile/fissionable materials is the vector $\mathbf{C}$. Now

suppose that in a new calculation, the arrival rate of material is increased by a factor X. Provided X is not large enough for the system to reach boiling temperatures (or temperatures where positive temperature feedback is reached) the following will be approximately satisfied: at time t/X the temperature rise will be $X\Delta T$, the power XP and the neutron flux $X\varphi$, but the composition will still be **C**. This general 'rule of thumb' can apply over several orders of magnitude for X, and even applies to an extent if the system does undergo boiling. It is more complicated in this case, however, since there is often a large negative temperature feedback coefficient over the boiling range, requiring a large amount of material to arrive to raise the temperature. It can therefore take a long time for the pore water to boil. More discussion of this is given in References [6] and [11].

3.3 QSS Calculations in NRVB with Positive Feedback at Boiling

In the first set of calculations the QSS model was used for fifty-eight calculations in NRVB for a variety of fissile/fissionable materials and arrival rates. These calculations gave a detailed analysis of parameter space, provided that positive temperature feedback was never encountered. In most cases, the QSS model is no longer applicable when this is encountered, but it has been shown that for some calculations where positive temperature feedback only applies over a limited range of temperatures, such as during pore water boiling, it may be applied in two stages [6]. The first progresses the calculation up to the onset of boiling (typically assumed to be 271℃ for NRVB calculations at a pressure of 6.5 MPa), and the second stage continues once the temperature has increased enough so that the temperature feedback coefficient is again negative.

From the calculations from Reference [16], the QSS calculation in NRVB with a radius of 0.5 m, and arrival of 10% enriched uranium dioxide, is a likely candidate for a two-stage QSS calculation with positive feedback at boiling. Calculations have been undertaken in Reference [16] for arrival rates of 10^{-11} and 10^{-10} kg m^{-3} s^{-1}, but larger rates gave positive temperature feedback. Figure 1 shows the reactivity function for this system at the initial composition of 202 kg m^{-3} of 10% enriched uranium dioxide. It is clear that while the reactivity initially decreases with temperature (negative temperature feedback), there is a region where the reactivity increases (positive temperature feedback), beginning at the onset of pore water boiling, here taken to be 271℃. Once the temperature increases to part way through the boiling range, the reactivity again decreases with temperature. Since the reactivity function will change slightly as material arrives, this does not guarantee that any system will encounter positive feedback at pore water boiling, but it is a likely candidate.

Using an arrival rate of 10^{-9} kg m^{-3} s^{-1} the QSS model does indeed encounter this positive feedback. Figure 2 shows that once the temperature reaches 271℃ (or the temperature increase 231℃), at about 0.6 millennia, a standard QSS calculation cannot continue. To enable it to continue, the temperature must be increased until the reactivity value is again zero, and the feedback negative. Figure 3 shows the reactivity as a function of temperature for the material composition at the onset of positive feedback. It is seen that if the temperature is increased to approximately 285.6 ℃ then these conditions on reactivity can be satisfied. Increasing the temperature, and keeping the composition fixed (through an assumed short rapid transient phase[5] [6,10]), allows a second stage to be calculated with the QSS model. The results of this two-stage calculation are summarised in Tables 2 and 3, and Figures 4 to 12.

Table 2 compares the initial concentrations of the fissionable material and fission products to that when positive feedback is encountered (approximately 0.6 millennia) and when fresh material stops arriving (approximately 152 millennia). It is seen that the composition is hardly changed from the initial values when positive feedback is encountered, but changes considerably over the duration of a complete transient. Table 3 summarises the QSS results

[5] Here the assumption is that the QSS reactivity function (which does allow for the changing density of water/steam with temperature) also applies to the assumed intermediate phase. If the intermediate phase was sufficiently short then, in principle, a larger rapid transient event could result. Alternatively, for a fixed mass of water, the temperature coefficient could remain negative.

over the entire transient, where the two lines in red show results just before and just after the deviation into positive feedback. The emboldened line shows the results at the time where fissionable material stops arriving. Figure 4 shows that after the deviation into positive temperature feedback, the temperature rises to a plateau of approximately 510℃ by about four millennia. In this, and similar figures, it is noted that the approximations of the interpolated reactivity function (which lead to step changes in gradient and hence step changes in feedback coefficients) cause non-smooth behaviour in the QSS results. For QSS results such changes are not generally significant (unless associated with a physical process such as pore water boiling) and it is the general trends that are of most interest. Figures 5 to 10 show that the concentrations of $^{235}UO_2$, $^{236}UO_2$, $^{238}UO_2$, $^{239}PuO_2$, $^{240}PuO_2$, and PbO_2 behave sensibly during the transient, with the final concentration dominated by $^{238}UO_2$, as would be expected for a 10% enriched uranium calculation. This is confirmed by Table 4. Figures 11 and 12 show the system power and neutron flux during the transient. It is seen that the power is approximately constant at 3 kW for most of the calculation, while the neutron flux rises over a period of about five millennia, then decays fairly steadily over the remainder of the calculation.

In Reference [6] it was hypothesised that oscillatory solutions may exist for calculations with positive feedback at boiling. These could occur when a system tries to settle to a steady state which is close to the switchover from positive to negative temperature feedback in the pore water boiling range. Although a study of this possible phenomenon has not been undertaken here, an additional calculation to the above has shown approximately what arrival rate may lead to such solutions. If the arrival rate is reduced to 5×10^{-10} kg m^{-3} s^{-1}, then the system has an initial temperature rise as shown in Figure 13. The QSS model again fails once the temperature reaches 271℃ (or the temperature increase is 231℃) at about 1.6 millennia. Figure 14 confirms that this is due to positive feedback at boiling. If the calculation is restarted at a temperature of 285.6℃, it will continue until mate rial stops arriving. The QSS results are summarised in Tables 4 and 5, and Figures 15 to 17, which show that the system is well behaved and qualitatively similar to the larger arrival rate of 10^{-9} kg m^{-3} s^{-1} above. Figure 15 shows that while the temperature initially increases after the positive feedback deviation at about 1.6 millennia, the ultimate plateau is for a temperature rise of about 250℃ (total temperature 290℃), which is just at the upper limi t of the pore water boiling range. This suggests that if the arrival rate is lower than 5×10^{-10} kg m^{-3} s^{-1}, but not as low as 10^{-10} kg m^{-3} s^{-1} where a calculation without positive feedback was undertaken in Reference [16], then oscillatory solutions may occur.

A summary of these two calculations, together with the lower arrival rates for the same scenario from the first set of calculations [16], is given in Table 6. It is interesting to note from this and other results (in particular Tables 2 to 5) that while the rule of thumb from Section 3.2 does not necessarily apply to similar cases with and without pore water boiling, some of the trends do hold. For example, in Table 6 the temperature rise (to plateau) is approximately 5, 50 and 500℃ for arrival rates of 10^{-11}, 10^{-10} and 10^{-9} kg m^{-3} s^{-1} respectively.

3.4 QSS Calculations in Mudstone

As discussed in Section 3.1, the QSS Model has been used primarily for NRVB systems in previous studies [6,11,16]. The implementation in Mathematica is such that any suitable host material can be modelled, provided a suitable reactivity function can be supplied to the model. This capability was used in the first set of calculations [16] to undertaken QSS calculations in granite. Using similar methods, QSS calculations for mudstone as a host material are described in this section.

3.4.1 Calculating a Reactivity Function

QSS solutions are heavily dependent on the reactivity of a system, and how this changes with temperature and material composition. For a QSS solution to exist, the reactivity temperature feedback coefficient must be negative at all temperatures including the ambient temperature. A negative temperature feedback coefficient means that as the temperature of a system is

increased, the reactivity of that system decreases. It is assumed that the negative reactivity feedback maintains the reactivity close to zero as additional fissile material arrives. In the absence of temperature dependence, additional fissile material would typically act to increase the reactivity of the system. The reactivity is a function of various system parameters, including: nuclide and other material concentrations, temperature, saturation, and radius of the FM region. Hence, the constancy of the reactivity can be expressed in terms of the rates of change of the concentrations, temperature, saturation and radius.

Before undertaking any QSS calculations, it is important to establish an initial system where a QSS transient is likely. That is, the system needs to have negative temperature feedback, positive arrival feedback, and some indication that these will continue to apply while fresh material arrives and possibly fissions, decays or captures. The change in concentration of a nuclide is due to: a source of the nuclide, loss due to decay, gain to decay of another nuclide, loss due to capture, gain due to capture in another nuclide, loss due to fission, and gain due to fission of another nuclide.

Using an ambient temperature of 40 ℃, a mudstone c alculation comparable in radius to the QSS granite in Reference [16] was sought. This radius was 1.1025 m. In the spherical cases considered in the current study, the reactivity was calculated using the spherical option of the FLURIG collision probability module in WIMS9. Resonance shielding was applied to ^{235}U by means of a subgroup treatment that is devised around the resonance integral tabulations of the standard WIMS library. A full description of the method, and an example for granite, are given in Appendix 1 of Reference [16].

A review of likely properties for mudstones has been undertaken [21]. These properties have been used to construct a reactivity function suitable for a QSS calculation in mudstone. Table 7 shows the composition of dry Opalinus Clay mudstone taken from Reference [21]. This composition (normalised to 100%) has been assumed for all reactivity values calculated for this QSS mudstone study. Reference [21] also states a mean porosity of 12% by volume, and a mean density of 2720 kg m^{-3} for Opalinus Clay, and these values have also been assumed throughout the study. Assuming a fissile material density of 10000 kg m^{-3}, this means that the maximum concentration of fissionable materials or fission products is 1200 kg m^{-3} before the pore space is completely full. Taking the variation of H_2O density with temperature as in Figure 18 (consistent with a pressure of 6.5 MPa), the density of saturated mudstone at 40℃ is 2513 kg m^{-3}.

By undertaking a number of WIMS9 calculations, a spherical system of radius 1.1025 m has been found in mudstone, which is just critical at a concentration of 11.27 kg m^{-3} of $^{235}UO_2$. This corresponds to an initial fissile mass of 63.26 kg. Table 8 summarises the initial composition of the FM (fissile material) and SM (surrounding material) regions. Figure 19 shows the reactivity as a function of temperature at the initial composition. It is noted that this is a case where positive temperature feedback at boiling is likely.

Based on this initial composition, a reactivity function has been generated with the source fissile material in the form of a mixture of $^{235}UO_2$, $^{236}UO_2$, and PbO_2. All the dioxides are assumed to have a density of 10,000 kg m^{-3}. The FM region and its surroundings contain mudstone that has 12% porosity and is fully saturated. The FM, and the already accumulated FM in the FM region, displace water in the available pore space. The ambient temperature in the host rock is 40 °C and the ambient pressure is 6.5 MPa. The maximum allowable concentration of fissile material ($^{235}UO_2$, $^{236}UO_2$, and PbO_2) is 1200 kg m^{-3}. The permissible concentration of $^{236}UO_2$ and PbO_2 is further limited by the capture and fission fraction in ^{235}U. Using the cross-sections of 98.3 barns and 582.6 barns for capture and fission in ^{235}U [6], gives a ratio of 0.144:0.856 for the concentrations of $^{236}UO_2$ and PbO_2.

For this system, the reactivity function was constructed using a detailed coverage of the (T, ^{235}U, ^{236}U, Pb) system, where T is temperature in ℃. This was obtained by calcula ting the full factorial matrix of reactivities for temperatures of (40, 90, 200, 281-δT, 281-½δT, 281, 281+½δT,

281+δ*T*, 400, 1000) °C, $^{235}UO_2$ concentrations of (5, 11.27, 20, 50, 200, 500, 800, 1100) kg m^{-3} and total $^{236}UO_2$ plus PbO_2 concentrations of (0, 50, 200, 400, 700, 1000, 1195) kg m^{-3}. The split of these concentrations between $^{236}UO_2$ and PbO_2 in the ratio 0.144368:0.855632 is shown in Table 9. The temperatures between 281-δ*T* and 281+δ*T*, where δ*T* is typically 10 °C are used to allow for the change in water density at 281 °C due to boiling. It is assumed that at 281-δ*T* the H_2O is 100% liquid and at 281+δ*T* it is 100% steam. Between these temperatures the fraction of steam increases linearly from zero to one. Figure 18 shows the density of water as a function of temperature used for these calculations. The full factorial matrix requires 10x8x7 = 560 calculations, the results of which are displayed in Tables 10 to 19. The calculated variation of reactivity with temperature and $^{235}UO_2$, $^{236}UO_2$, and PbO_2 concentration is also displayed in Figures 20 to 23. In Tables 10 to 19, additional values, indicated in red, have been added to the reactivity matrix to allow a full and correct solution to the QSS solver, which uses linear interpolation. Most of these additional values are not realistic as they correspond to FM concentrations beyond the limit imposed by the available pore space. This region of the reactivity matrix also provides positive reactivity so a QSS solution, which by definition tracks a zero reactivity path through the matrix, is no longer achievable. From Figures 19 to 23 and Tables 10 to 19, some general observations about the likely results of QSS calculations can be made. Firstly, the system is unlikely to ever reach $^{235}UO_2$ concentrations greater than 20 kg m^{-3}, in a QSS transient and certainly not 50 kg m^{-3}, as most reactivities are positive for these and larger concentrations. Since the QSS model tracks solutions of zero reactivity, it cannot get to these concentrations of $^{235}UO_2$, and it is likely that most material arriving will fission to PbO_2 or capture to $^{236}UO_2$. Larger arrival rates are likely to lead to positive feedback at boiling, so the techniques in Section 3.3 would be required. Such calculations will not be undertaken here.

3.4.2 Results

Having established a suitable reactivity function, the other inputs to the QSS Model then need to be considered. Most input parameters, such as ambient temperature and pressure, are independent of the host material. Others, such as groundwater flow rate were left at the default values for NRVB although, in reality, groundwater flow may be considerably lower. For QSS calculations this assumption is not significant because no relationship between the arrival rate and groundwater flow is assumed. The groundwater flow is only used directly in the heat transfer term which is dominated by thermal conduction. The thermal conductivity was increased from that for NRVB. Reference [21] gives values for the thermal conductivity between 1.26 and 3.22 W m^{-1} K^{-1} for damp Opalinus Clay, although the definition of 'damp' is unclear. Taking a mean value of the values given for damp clay gives a value of 2.055 W m^{-1} K^{-1}.

Tables 20 to 22 show the results for a range of arrival rates of $^{235}UO_2$ in mudstone from 10^{-13} kg m^{-3} s^{-1} to 10^{-11} kg m^{-3} s^{-1}. Larger arrival rates lead to positive temperature feedback at the onset of boiling, as expected. All calculations end when a mass of 1000 kg has arrived. The results appear to be sensible, follow the general 'rule of thumb' from Section 3.2, and do not encounter any unphysical temperatures. Table 23 gives a summary of some key times in the mudstone QSS calculations. The results are also shown in Figures 24 to 29. Figure 24 clearly demonstrates that the behaviour on the mudstone system is qualitatively similar to the NRVB and granite systems reported in Reference [16]. The same is true of Figures 25 to 27, where a clear trend for material composition can be seen. It is noted from Figures 26 and 27 that the PbO_2 concentration is indeed approximately six times that of $^{236}UO_2$, helping to justify the methodology used in construction of the reactivity function. Figures 28 and 29 show that the power and neutron flux of the system are also well behaved.

3.5 Conclusions

Two further sets of calculations using the QSS model have been undertaken. The first set has applied a two-stage QSS method, first reported in Reference [6]. The second set has extended the QSS set of calculations for a further host rock type, mudstone, building on the calculations in NRVB and granite undertaken previously.

The two-stage QSS calculations for 10% enriched uranium systems with positive temperature feedback at pore water boiling have further tested the method developed during earlier studies. The method has been successfully employed for an example from earlier calculations, but with larger arrival rates. Two arrival rates have been used, the lower of which appears to be close to an arrival rate which could lead to oscillatory solutions, should they exist for this 10% enriched uranium system.

The QSS calculations for $^{235}UO_2$ systems in mudstone add to those already reported for NRVB and granite systems [16]. It has again been established that the QSS model can easily handle reactivity functions for different host materials, provided they are suitably defined. Results can be achieved without pore water boiling, and the methods of Section 3.3 should be applicable to mudstone calculations with positive feedback at pore water boiling for larger arrival rates. Qualitatively the results are very similar to those in NRVB and granite, with the general 'rule of thumb' described in Section 3.2 being applicable for most times during a calculation, the exception being the time to reach the plateau temperature, which does not follow the rule. Calculating the sensitivity of the mudstone QSS results to input parameters might give further insight into the behaviour of these systems. Furthermore it is noted that for a given volume the arrival rates in mudstone could be significantly lower than those for granite or NRVB due to the lower permeability of mudstone as a potential host rock for a GDF.

4 RTM Calculations

4.1 Model Description

The RTM Model consists of a sphere containing a mixture of fissile material, other initially solid material, and water, known as the Fissile Material (FM) region, surrounded by an infinite region (the surrounding material, or SM region) of saturated material. This material is either NRVB or granite, the same material being used for the FM and SM regions. The FM region is assumed to be isothermal and homogeneous. The FM region is assumed to become critical, with a positive reactivity temperature feedback coefficient. For RTM it is assumed that, once a criticality starts, positive temperature feedback results in a runaway power excursion, with fission energy typically being released over a short time interval. During this short time interval it is assumed that no water can be expelled from the pores of the FM region, and hence the effect of water density on the temperature feedback is neglected. This enables a reactivity function that is independent of water density variation to be constructed and essentially means that a system must initially have a positive feedback coefficient for changes in nuclear data with temperature (including resonance broadening and changes to the neutron spectrum) for an RT criticality to be modelled. If the effect of water density were significant, then RTM would tend to overestimate the energy release of a criticality where the density temperature feedback were negative (i.e. a little water escaping would tend to shut the system down more quickly). RTM would tend to underestimate the energy release of a criticality where the density temperature feedback were positive (i.e. a little water escaping would tend to increase the reactivity of the system). For systems where the criticality lasts for order 10 ms, it is not believed that the water density effect would be significant.

The positive nuclear data feedback ensures that the system quickly becomes prompt-critical. Hence, in RTM it is adequate to assume that the FM region is prompt-critical at the start of the transient. Due to the exponential growth of the neutron flux, delayed neutrons can be neglected in RTM. For most systems which initially have positive temperature reactivity feedback coefficients, the nuclear data effect and spectral hardening will result in the temperature feedback coefficient becoming negative at sufficiently high temperatures. The heat up and consequent pressurisation will cause the FM region to expand, which will also reduce the reactivity of the system. Thus the expansion of the FM region also contributes to the termination of the criticality event. The possibility of the region forming a critical configuration again after cooling has not been addressed in the present study.

For the present purpose, it is sufficient to consider a transient that becomes prompt critical. Once prompt criticality is reached, the point kinetics equation can be approximated by:

$$\dot{P} = \frac{10^{-5}}{\Lambda}(\rho_{mN} - 210)P \qquad (1)$$

Where ρ_{mN} is the reactivity in mNiles
P is the power in Watts
Λ is the neutron generation time in seconds (set to 10^{-4} for thermal neutrons), and the dot denotes the time derivative.

The factor of 10^{-5} originates from the expressing the reactivity in mNiles, since the reactivity in mNiles is calculated from the neutron multiplication factor k_{eff} with a factor of 10^5. The value of 210 mN is the reactivity at which the system becomes prompt critical for systems with ^{239}Pu. For different fissile materials the value of this constant should be changed to the appropriate value for the material modelled. It is also noted that the neutron generation time can depend on the system temperature and geometry. For the calculations reported here it is assumed constant, but noted that more recent calculations have shown the results of the RTM model to be quite sensitive to changes in this parameter [22].
.
The reactivity function varies with temperature, radius and composition. The amount, or mass, of fissile material in the FM region remains constant throughout the transient. SM may be added to the FM region due to vaporisation. However, there is negligible vaporisation of SM during the criticality transient due to the very short timescale. Therefore, the composition of the system can be assumed to be constant during the criticality transient. Hence, the reactivity can be taken to be a function of the FM region temperature and radius.

From above, one of the inputs required by RTM is the reactivity of the system as a function of the radius, *R* (m), and temperature (K) of the FM region. Suitable reactor physics software, the WIMS9 code, is used to evaluate the reactivity at a number of points in parameter space, and a linear or physics-based interpolation scheme is implemented for other points in parameter space. In this scheme, a matrix of radii and temperature values is chosen for a given system, where the radii are spread between the initial value and an estimated upper value. The WIMS9 code was used to estimate the appropriate cross-sections and reactivity values for systems of the chosen composition and mass. In the current application, a sphere of fully saturated NRVB or granite containing the chosen concentration and mass of fissile material was surrounded by a larger sphere consisting of fully saturated NRVB or granite respectively.

Previous RTM calculations [7,10,16] and the calculations described in this report indicate that temperatures in excess of 10,000 K may be attained in the FM region. In view of the large resonance in the ^{239}Pu fission cross-section at about 3,300 K, it is necessary to allow for variation in cross-sections with temperature when estimating system reactivities. Therefore, a series of WIMS9 libraries were generated containing data at temperatures of 293 K, 900 K, 1,900 K, 2,900 K, 3,300 K, 4,050 K, 7,025 K, 10,000 K, 100,000 K and 1,000,000 K. The chosen temperatures provide additional detail in the region of the ^{239}Pu resonance and provide data up to 1,000,000 K in case unexpectedly high temperatures are attained in any future transient calculations. A separate library was created for each temperature. Initially, each of the libraries contained data for the nuclides H, O, Na, Al, Si, K, Ca, Ti, Fe, Mg, S and ^{239}Pu. These have now been extended to include uranium isotopes ^{235}U, ^{236}U and ^{238}U for uranium calculations. A free gas thermal scattering model was used for all nuclides. The standard WIMS 172 energy group scheme was used, although the partitions between the fast, resonance, and thermal regions were modified.

The evaluated nuclear data source for all nuclides was JEF2.2; with the exception of Fe, elemental or mono-isotopic data were used. For Fe, isotopic data were mixed to form elemental

data according to the natural abundances of the individual isotopes. In addition to the nuclides specified above, the 293.16K and 900K libraries also contain data for H in water, taken from the standard 1997 WIMS8 library. The WIMS library generation route also requires that data are present for room temperature and so it was necessary to include data at 293.16K in each of the libraries, in addition to the required temperatures. This is useful as lower temperature data is required for the surrounding material region in reactivity calculations.

The data were generated using the standard route for WIMS library generation with the following changes:

- A temperature dependent weighting spectrum was used.
- The partitions between the fast, resonance and thermal energy regions were varied with temperature.
- Dummy burn-up and PHODAT data were used (i.e. all nuclides are non-burnable).

The within-group weighting spectrum used in the group condensation for WIMS libraries comprises a thermal Maxwellian joined to 1/E and to a fission spectrum. This is specified using a standard NJOY weighting option. With this option, the user supplies the energies of the breakpoints between the three components of the weighting spectrum and the energies of the thermal and fission Maxwellian spectra. Thus for each temperature, the appropriate thermal temperature and breakpoint were specified (the fission spectrum energy and breakpoint were unchanged). A thermal breakpoint of 2.5kT was used, where kT is the energy of the thermal Maxwellian peak (here k is Boltzman's constant and T is the temperature in K). The thermal temperatures and breakpoints used are given in Reference [7].

The standard WIMS 172 group structure defines three energy regions; thermal (0 to 4 eV), resonance (4 eV to 911 keV) and fast (911 keV to 20 MeV). WIMS curtails thermal scattering (upscatter) at the top of the thermal range (4 eV). For the higher temperatures used in this study, there is significant thermal scattering above this energy. Experience with previous high temperature work has indicated that a thermal limit of 40kT is appropriate for the range of temperatures in this study. Reference [7] gives the peak energies and 40kT energies for thermal Maxwellian spectra at the required temperatures. For the temperatures above 3000 K, alternative group structures were used in which the thermal range was extended up to the 40kT energy. For 293.16 and 900 K, the standard group scheme (i.e. thermal limit of 4 eV) was used to avoid extending the resonance range down in energy. The group schemes used for each of the temperatures are displayed in Reference [7].

In the spherical cases considered in the current study, the reactivity was calculated using the spherical option of the FLURIG collision probability module in WIMS9. The WIMS calculation sequence is shown in Appendix 2 of Reference [16]. The validity of WIMS calculations at the high temperatures required for the construction of reactivity functions for use in RTM is very important. Some confidence is gained from 'sensible' behaviour of the system reactivity as the temperature increases. Physical arguments show that the reactivity should not increase as a function of temperature for ever but should, at suitably high temperatures start to decrease and eventually become sub-critical. This behaviour is observed in the WIMS calculations undertaken. Following the calculations reported here further work has been undertaken to compare high temperature reactivity calculations using not only different reactor physics codes, but different high temperature libraries. This work has confirmed good agreement in the reactivity values calculated, giving much greater confidence in the use of reactivity values calculated at high temperature [22].

4.2 Overview of Rapid Transient Calculations

In this study, three classes of RTM calculations are considered. The first group of calculations is for NRVB where the system is initially just critical (i.e. the reactivity is just above 210 mNiles). This includes the first report of an RTM calculation for a uranium system. The second group is

for NRVB where the system is initially supercritical (i.e. the reactivity is significantly above 210 mNiles). Such systems might arise if an initially heterogeneous system were homogenised, as described in detail in Reference [16]. The final set of calculations is for initially just critical granite systems.

It is noted that some of the RTM calculations presented here are re-runs of scenarios that have been reported before [7,16]. These calculations have been re-run using the latest developments in the RTM and its inputs, including the latest structural response model (for all NRVB calculations), improvements in the solution methods (particularly for granite calculations), and modifications to the equation of state in formulation (NRVB calculations) and implementation (granite calculations). Explanations of the model developments are summarised below, with full details in References [14,15,18]. Where calculations are re-runs of earlier work, a full description of the case is provided here to reduce the need for cross-referencing earlier work.

Alongside this set of calculations, parallel work has been undertaken to investigate and improve the implementation of the equations of state for NRVB. This study will be reported in Reference [18]. For NRVB the main conclusion is that the 'fix' identified in a previous study [15] is not required if there is better consistency between the equation of state and other model inputs. These changes are not huge, but because the results can be very sensitive to potential singularities in the equation of state, it is important to align all model inputs where possible. The recommended changes for NRVB are summarised in Figures 30 to 32, where it is seen that the enthalpy, and the model inputs f_s an θ need to have slightly different temperature dependence. The new functions have been used for all NRVB calculations in this study. For granite, it is the solution method that needs to be modified. Previously it has been necessary to use a look-up table to approximate the Tillotson equation of state. This is not ideal as it introduces potentially large errors in holding the true equation of state at zero. By modifying the way in which the governing equations are presented to the numerical solver, and invoking a newer algebraic-differential solver (not available when RTM was first developed), a look-up table approximation is no longer required. In addition, two errors have been corrected for the granite calculations: the first an error in the implementation of one component of the Tillotson equation of state, and the second an inconsistency in the treatment of vaporisation terms in the governing equations. The correction to the Tillotson equation prevents the occurrence of negative pressure regions for the granite calculations presented in this report.

4.3 NRVB Systems which are Initially Just Critical

Six initially just critical cases are studied in NRVB, including 3.684 kg, 10 kg, 100 kg, 200 kg and 1000 kg of $^{239}PuO_2$ and 15.7 kg of $^{235}UO_2$. The compositions of the FM and SM regions for the $^{239}PuO_2$ cases are given in Table 24. A RTM $^{235}UO_2$ scenario has not been undertaken before, so more details are given in Section 4.3.7.

4.3.1 Case 1 - 3.684 kg of $^{239}PuO_2$ in NRVB

In the spherical case presented here, 3.684 kg of $^{239}PuO_2$ at a concentration of 10 kg m^{-3} was placed in the FM region, with a radius of 0.4447 m.

The reactivity was evaluated for a range of temperatures and radii as shown in Table 25. The prompt-critical values are indicated in red: once the transient strays outside of the red region the reactivity will fall and power will be driven to zero. The value of k_∞ is independent of radius and is displayed as a function of temperature in Table 26. It is seen to peak at a temperature around 2,000 K and falls back below the initial value just before the temperature reaches 10,000 K. This suggests that temperatures are unlikely to significantly exceed about 10,000 K. The calculated variation of reactivity with temperature and radius of the FM region is also displayed in Figure 33. It is seen that for temperatures above about 7,000 K the reactivity is negative and so the transient will shut down if it gets hotter than this. The reactivity also becomes negative before the radius has expanded to 0.6 m. Therefore, the criticality transient

will shut down as a radius of 0.6 m is approached. This case was first presented in Reference [7].

As discussed in detail in Section 4.6 it is important to note that inertia in the system can lead to significant energy release after the reactivity has fallen below prompt critical. There are also inertial terms in the structural response model. As a result the 'shut-down' temperature and radius from examining the reactivity function alone are likely to be an underestimate of the actual maxima achieved. This observation applies to all discussions of the reactivity functions below.

4.3.2 Case 2 - 10 kg of $^{239}PuO_2$ in NRVB

In the spherical geometry used here, 10 kg of $^{239}PuO_2$ at a concentration of 10.1 kg m^{-3} was placed in the FM region, with a radius of 0.619 m.

The reactivity was evaluated for a range of temperatures and radii as shown in Table 27. The prompt-critical values are indicated in red: once the transient strays outside the red region the reactivity will fall and power will be driven to zero. The value of k_∞ is independent of radius and is displayed as a function of temperature in Table 28. It is seen to peak at a temperature around 2,000 K and falls back below the initial values as the temperature exceeds 100,000 K. From Table 28 it is seen that the system will become sub-critical if the temperature rises above roughly 8,000 K, irrespective of the radius of the FM region. This suggests that temperatures are unlikely to rise significantly above about 8,000 K. The calculated variation of reactivity with temperature and radius of the FM region is also displayed in Figure 34. It is seen that for temperatures above about 7,025 K, the reactivity is negative and so the transient will shut down if it gets hotter than this. The reactivity also becomes negative before the radius has expanded to 0.93 m. Therefore, the criticality transient will shut down as a radius of 0.93 m is approached. This case was first presented in Reference [16].

4.3.3 Case 3 - 100 kg of $^{239}PuO_2$ in NRVB

In the spherical geometry used here, 100 kg of $^{239}PuO_2$ at a concentration of 8.99 kg m^{-3} was placed in the FM region, with a radius of 1.3852 m.

The reactivity was evaluated for a range of temperatures and radii as shown in Table 29. The prompt-critical values are indicated in red: once the transient strays outside the red region the reactivity will fall and power will be driven to zero. The value of k_∞ is independent of radius and is displayed as a function of temperature in Table 30. It is seen to peak at a temperature around 2,000 K and falls back close to the initial values as the temperature exceeds 100,000 K. The calculated variation of reactivity with temperature and radius of the FM region is also displayed in Figure 35. It is seen that for temperatures above about 7,025 K, the reactivity is negative and so the transient will shut down if it gets hotter than this. The reactivity also becomes negative before the radius has expanded to 3.46 m. Therefore, the criticality transient will shut down as a radius of 3.46 m is approached. This case was first presented in Reference [16].

4.3.4 Case 4 - 200 kg of $^{239}PuO_2$ in NRVB

In the spherical geometry used here, 200 kg of $^{239}PuO_2$ at a concentration of 8.936 kg m^{-3} was placed in the FM region, with a radius of 1.7483 m.

The reactivity was evaluated for a range of temperatures and radii as shown in Table 31. The prompt-critical values are indicated in red: once the transient strays outside the red region the reactivity will fall and power will be driven to zero. The value of k_∞ is independent of radius and is displayed as a function of temperature in Table 32. It is seen to peak at a temperature around 2,000 K and falls back close to the initial values as the temperature exceeds 100,000 K. The calculated variation of reactivity with temperature and radius of the FM region is also displayed in Figure 36. It is seen that for temperatures above about 10,000 K the reactivity is negative and

so the transient will shut down if it gets hotter than this. The reactivity also becomes negative before the radius has expanded to approximately 4.4 m. Therefore, the criticality transient will shut down as a radius of 4.4 m is approached. This case is new to this suite of calculations.

4.3.5 Case 5 - 1000 kg of $^{239}PuO_2$ in NRVB

In the spherical geometry used here, 1000 kg of $^{239}PuO_2$ at a concentration of 8.77 kg m^{-3} was placed in the FM region, with a radius of 3.008 m.

The reactivity was evaluated for a range of temperatures and radii as shown in Table 33. The prompt-critical values are indicated in red: once the transient strays outside the red region the reactivity will fall and power will be driven to zero. The value of k_∞ is independent of radius and is displayed as a function of temperature in Table 34. It is seen to peak at a temperature around 2,000 K and falls back close to the initial values as the temperature exceeds 100,000 K. The calculated variation of reactivity with temperature and radius of the FM region is also displayed in Figure 37. It is seen that for temperatures above about 100,000 K, the reactivity becomes negative and so the transient will shut down rapidly if it gets hotter than this. The reactivity also becomes negative before the radius has expanded to 10.53 m. Therefore, the criticality transient will shut down as a radius of 10.53 m is approached. This case was first presented in Reference [16].

4.3.6 Summary of Cases 1 to 5

With five cases of similar design gathered it is useful to consider any trends. It is clear that as the fissile mass is increased the likely maxima for temperature and radius increase, and alongside this so does the potential for more energetic transients. However, before any RTM calculations are undertaken there are some other observations that can be made. For example, if the initial radii of the just critical systems are plotted against fissile mass, then there appears to be a clear correlation, and even the suggestion of an empirical relationship, as seen in Figure 38. This relationship should provide a reasonable estimate of the initial radius for a system of any initial mass within the range above, 3.684 to 1000 kg.

4.3.7 Case 6 - 15.7 kg of $^{235}UO_2$ in NRVB

In static analysis of systems in NRVB it has been observed that at elevated ambient temperatures of 90 °C it is possible to find uranium systems with total positive temperature feedback [5] (the combination of the nuclear data and density temperature effects). For RTM calculations it is assumed that only the nuclear data effect is significant and for a very limited range of parameter space uranium systems were found to have this property. It is worth noting, however, that these calculations were for cylinders, and used a different solution method and nuclear data to current methods.

An initial study was therefore undertaken to see if similar results could be found for uranium ($^{235}UO_2$) in spheres using WIMS9 as the method for calculating reactivities. The results are shown in Table 35. These are similar to the results in Reference [5], but a positive nuclear data coefficient only exists at a concentration of 1000 kg m^{-3}, whereas before this was predicted at 200 and 2000 kg m^{-3} as well. To enable a RTM calculation to be undertaken, the 1000 kg m^{-3} case has therefore been taken as a starting point, which has a critical radius of 0.1554 m, and a mass of 15.7 kg. The initial composition of the SM and FM regions is shown in Table 36

Using WIMS9 a RTM reactivity function has been constructed for this $^{235}UO_2$ case. Unlike the plutonium cases, the positive nuclear data coefficient only persists for a few tens of °C, and the reactivity soon starts to decrease. The reactivity was evaluated for a range of temperatures and

radii as shown in Table 37[6]. The prompt-critical values are indicated in red: once the transient strays outside the red region the reactivity will fall and power will be driven rapidly to zero. The value of k_∞ is independent of radius and is displayed as a function of temperature in Table 37. It is seen to be a slightly decreasing function of temperature. The calculated variation of reactivity with temperature and radius of the FM region is also displayed in Figure 39 and 40, the second being a zoom to the initial radius of the first. It is seen that for temperatures above about 400 K, the reactivity is negative and so the transient will shut down if it gets hotter than this. The reactivity also becomes negative before the radius has expanded to 0.157 m, an expansion of just 1%. Therefore, the criticality transient will shut down almost as soon as the radius increases. This case is new to this suite of calculations.

4.4 NRVB Systems which are Initially Supercritical

The cases in this section are different to the other NRVB cases above. Instead of determining systems where the initial reactivity is just above prompt critical (210 mNiles for ^{239}Pu), a system with a much larger initial reactivity is sought. The idea is that a heterogeneous system can have much lower reactivity than a homogeneous system with the same fissile mass. If the system is suddenly homogenised then the reactivity could increase to a supercritical value, of many Niles. A detailed study of this phenomena was presented in Reference [16]. Such cases were also hypothesized and studied by Kastenberg et. al. [23].

Two such cases have been undertaken with RTM before, but neither using all of the latest features. Both have therefore been re-run for this study. The initial compositions of the FM and SM regions is shown in Table 39.

4.4.1 Case 7 - 13.4 kg of $^{239}PuO_2$ in NRVB

A spherical system within NRVB has been undertaken using a larger mass of $^{239}PuO_2$ at a concentration of 10 kg m^{-3}. In this case a sphere of radius 0.684 m, containing 13.4 kg of $^{239}PuO_2$, was used. A WIMS9 calculation estimated the initial reactivity of such a system to be 6899.4 mNiles.

Figure 41 and Table 40 show how the reactivity is calculated to vary, as a function of radius and temperature. It is seen that as a temperature of 10,000 K or a radius of 1 m is approached, the reactivity becomes negative. The variation of k_∞ with temperature is displayed in Table 41. It is seen to rise to a peak value at around 1,900 K and then falls back to roughly the initial value by the time the temperature has reached 10,000 K. This case was first presented in Reference [7].

4.4.2 Case 8 - 200 kg of $^{239}PuO_2$ in NRVB

In the spherical geometry used here, 200 kg of $^{239}PuO_2$ at a concentration of 201.3 kg m^{-3} was placed in the FM region, with a radius of 0.619 m.

The reactivity was evaluated for a range of temperatures and radii as shown in Table 42. The prompt-critical values are indicated in red: once the transient strays outside the red region the reactivity will fall and power will be driven to zero. The value of k_∞ is independent of radius and is displayed as a function of temperature in Table 43. It is seen to peak at a temperature around 2,000 K, but to fall back close to the initial value the temperature must rise significantly above 100,000 K. The calculated variation of reactivity with temperature and radius of the FM region is also displayed in Figure 42. It is seen that at small radii the temperature must rise considerably

[6] Due to an oversight, the assumption for these calculations was that prompt-criticality occurs at 210 mNIles. This is the value for ^{239}Pu and the value for ^{235}U is nearer to 700 mNiles. However, given the calculations of reactivity undertaken it is clear that regions of positive temperature feedback are difficult to find and do not persist over large temperature ranges as for the $^{239}PuO_2$ systems considered. Further checks to compare the prompt-critical reactivity predicted by WIMS has also shown that the positive temperature feedback region found may be an artefact of numerical convergence only. The RTM calculation for $^{235}UO_2$ reported here should therefore be considered as presenting preliminary results.

above 100,000 K for the reactivity to become negative and cause the criticality to shut down. The reactivity also becomes negative before the radius has expanded to 1.5 m. Therefore, the criticality transient will shut down if the radius exceeds 1.5 m. This case was first presented in Reference [16].

4.5 Granite Systems which are Initially Just Critical

For the granite case, the granite surrounding the cavity has a density of 2683 kg m^{-3}, with a porosity of 0.01 saturated with water. The composition at 40°C for the SM region is as shown in Table 44. In the FM region $^{239}PuO_2$ is added by displacing some of the water from the pores in the granite. Two granite calculations have been undertaken in previous studies, both of which are initially just critical [7,16]. Neither of these used the latest solution methods for granite systems, which removes the need for an equation of state look-up table, so they have been re-run. The initial composition of the FM region for both cases is given in Table 44.

4.5.1 Case 9 - 500 kg of $^{239}PuO_2$ in Granite

In the spherical geometry used here, 500 kg of $^{239}PuO_2$ at a concentration of 3.82 kg m^{-3} was placed in the FM region, with a radius of 3.15 m.

The reactivity was evaluated for a range of temperatures and radii as shown in Table 45. The prompt-critical values are indicated in red: once the transient strays outside the red region the reactivity will fall and power will be driven to zero. The value of k_∞ is independent of radius and is displayed as a function of temperature in Table 46. It is seen to peak at a temperature around 2,000 K and falls back close to the initial value as the temperature exceeds about 5,500 K. The calculated variation of reactivity with temperature and radius of the FM region is also displayed in Figure 43. It is seen that for temperatures above about 6,000 K, the reactivity becomes negative and so the transient will shut down if it gets hotter than this. The reactivity also becomes negative before the radius has expanded to 4.41 m. Therefore, the criticality transient will shut down as a radius of 4.41 m is approached. This case was first presented in Reference [16].

4.5.2 Case 10 - 988 kg of $^{239}PuO_2$ in Granite

In the spherical geometry used here, 988 kg of $^{239}PuO_2$ at a concentration of 3.62 kg m^{-3} was placed in the FM region, with a radius of 4.0249 m.

The reactivity was evaluated for a range of temperatures and radii as shown in Table 47. The prompt-critical values are indicated in red: once the transient strays outside the red region the reactivity will fall and power will be driven to zero. The value of k_∞ is independent of radius and is displayed as a function of temperature in Table 48. It is seen to initially increase with temperature, reaching a maximum at around 1,900 K. Above that it starts to fall, returning to its initial value just above 4,050 K and becoming less than one before 7,000 K is reached. The calculated variation of reactivity with temperature and radius of the FM region is also displayed in Figure 44. It is seen that for temperatures above about 6,000 K the reactivity becomes negative and so the transient will shut down if it gets hotter than this. The reactivity also becomes negative before the radius has expanded to 7 m. Therefore, the criticality transient will shut down as a radius of 7 m is approached. This case was first presented in Reference [7].

4.6 RTM Results

The results of the RTM calculations for systems which are initially just critical and the host material is NRVB (Cases 1 to 6) are presented in Table 49. Results for systems which are initially supercritical and the host material is NRVB (Cases 7 and 8) are presented in Table 50. Results for systems which are initially just critical and the host material is granite (Cases 9 and 10) are presented in Table 51. In these tables the energy release (or yield) is given in units of kt (kilotonnes of TNT equivalent), where 1 kt is equal to 4.18×10^{12} J.

Consider Case 4 first, as this clearly exhibits all of the major phenomena, and is also a case new to this suite of calculations while being extreme in terms of possibly criticality events due to the requirement for 200 kg of $^{239}PuO_2$ to accumulate. Figures 45 to 49 show the behaviour of the system during the transient. Figure 45 shows the variation of reactivity with time. During the rise of the reactivity, two plateaus can clearly be seen. The first corresponds to the boiling of the pore water in the NRVB and the second to the dehydration of the NRVB. In the model both of these phase changes hold the temperature nearly constant for a while due to the large latent heats of the phase changes. In reality the effect would be spread over a temperature range and the variation in the results would be smoother. There is little change in radius at these early times and, therefore, when the temperature is approximately constant the reactivity is approximately constant. The next major change is the vaporisation of the NRVB, which corresponds to the initial “slow” rate of decrease of the reactivity. However, once the NRVB has all vaporised the temperature starts to climb rapidly (see Figure 47). By the time the temperature has risen to about 9,300 K and the radius increased to just approximately 2.19 m the reactivity has become negative (see Table 49).

Even when the reactivity has become negative, the energy continues to rise briefly (see Figure 46). This is due to the appearance of the power on the right-hand-side of equation 1 (see Section 4.1). When the reactivity is smaller than 210 mNiles, the right-hand-side of equation 1 will be negative, so that power must decrease with time. However, as the power decreases the right-hand-side becomes smaller, and the power will decrease less rapidly. As a result the power always remains positive, even if it asymptotes to zero rapidly once the system has a reactivity below prompt-critical. Since energy is the integral of power with respect to time this explains the brief energy rise after the system has become sub-(prompt)-critical. This behaviour is termed neutronic inertia. This inertia is also evident from the smoothness of the power curve, with the inertia having smoothed out the major features of the reactivity curve in Figure 45. When the system goes sub-critical, only 50% of the total energy has been released. The remaining 50% is generated in the 1.9 milliseconds after the reactivity becomes negative.

The temperature history is displayed in Figure 47, which shows brief temperature plateaus around 554 K, 853 K and 2,983 K, corresponding to the boiling of pore water, dehydration of NRVB and vaporisation of NRVB, respectively. Due to the scale of the vertical axis in this plot these are not as obvious as in Figure 45, for example.

The pressure history is shown in Figure 48.The pressure is seen to fall during the boiling of the pore water. Under the model approximations this is because the temperature is approximately constant at this time, but the density of the FM region is falling due to the expansion of the region. The fall in density at constant temperature leads to a fall in pressure. On the other hand, the dehydration of the NRVB releases more moles of water vapour into the pores. Hence, during this phase change the temperature remains approximately constant, but the fluid density actually increases due to the water vapour production from the NRVB. Consequently, the pressure rises very steeply during the dehydration of the NRVB. The final phase change is the vaporisation of the NRVB. Although this produces more moles of pressurising fluid, it also increases the free volume that the fluid occupies and, additionally, the volume of the FM region is increasing more rapidly at this time. Hence, under the approximate equation of state for the RTM calculation the pressure falls a little during the boiling of the NRVB. Once the NRVB has all vaporised the pressure once again rises, until the energy generation rate becomes too small and the expansion of the FM region starts to relieve the pressure.

The evolution of the cavity radius with time is depicted in Figure 49. The radius has increased from its initial value of 1.748 m to 2.19 m by the time the reactivity has fallen back to zero. It has further increased to approximately 4 m by the time the power generation has fallen to zero, and approximately 14 m by the time the pressure has returned to the ambient value. Over longer timescales the radius is seen to keep increasing to a peak value of over 30 m. This long-term increase is entirely due to the inertia of the surrounding material, since there is no pressure gradient between the cavity and surrounding region. It is noted that (except along the vault) the

largest dimension of NRVB in the concept model for a GDF is 20 m (vault height and width). As such, a sphere of NRVB of radius greater than 10 m will not be possible. In RTM calculations the NRVB is assumed to be infinite so, in practice, cavity radii greater than 10 m (and possibly less) will be affected by the presence of the host rock.

Cases 1 to 3 and 5 are similar to Case 4, but with different amounts of fissile material, and different radii. Qualitatively, the behaviour of the transients is similar, and the trends with increasing fissile mass are best seen from Table 49. This table shows that as the fissile mass is increased so do the maximum values for reactivity, power, temperature, pressure and radius. The only minor discrepancy is that the maximum pressure for the Case 2 is marginally lower than for Case 1. These relationships are clearly non-linear. For example, the peak reactivity for Cases 3 to 5 varies by less than 2 Niles, whereas there is 10 Niles difference between Case 2 and 3. One trend that is clear is that the yield increases with the fissile mass of the system. Figure 50 shows the variation for Cases 1 to 5, and suggests that it may be possible to estimate intermediate yields from an empirical rule. It is also noted that Cases 1 and 2 do not reach large enough temperatures to vaporise the FM region, while Cases 3 to 5 are calculated also to vaporise surrounding material.

Case 6 is very different to Cases 1 to 5. Despite being in the same host material, the presence of $^{235}UO_2$ as the fissile material in this preliminary investigation of such a system causes a transient of much lower energy release than for the $^{239}PuO_2$ calculations, consistent with the observations of the reactivity function in Section 4.3.7 above . This is confirmed by the preliminary RTM results in Table 49. The peak temperature and radius are less than 1% larger than the initial values, and the peak pressure only 5% larger. The energy release is also very small at 2.793×10^{-8} kt, some six orders of magnitude smaller than for a comparable $^{239}PuO_2$ mass (Case 2). Figures 51 and 52 also show that the transient is longer lived than for the $^{239}PuO_2$ cases. Figure 51 shows that the reactivity decreases over a period of about three seconds, and this is confirmed by Figure 52, where the main release of energy is over the same period. This is 300 times longer than the 10 ms typical for $^{239}PuO_2$ cases. This brings into question whether such a rapid transient criticality could occur at all, since if any water were able to escape from the system, the large negative density effect (Table 35) would terminate the criticality much earlier. At present the RTM does not have the capability to model the effects of water escaping the FM region during a criticality. Such cases could be studied further with FETCH.

Table 50 summarises the results for systems that are initially supercritical and the host material is NRVB (Cases 7 and 8). The expected trends are observed with the higher mass (200 kg) system having higher peak pressure, temperature and radius than the lower mass system (13.4 kg). An interesting comparison is between Cases 4 and 8, which both have the same fissile mass, but where Case 4 is initially just critical, and Case 8 supercritical. While the supercritical case reaches higher temperatures than the just critical case by a factor of 2.5, it is the just critical Case 4 that has the larger energy release (by an order of magnitude), and largest radius (by a factor of 2.2). In such a comparison it is important to consider the size of the critical regions. Case 4 has a volume approximately 22 times that of case 8, and hence despite the larger energy release in Case 4, it is entirely consistent that the peak temperature should be lower as there is more mass that needs to be heated.

Table 51 summarises the results for systems that are initially just critical and the host material is granite (Cases 9 and 10). The expected trends are observed with the higher mass (988 kg) system having higher peak power, reactivity, pressure, temperature and radius than the lower mass system (500 kg). It is also interesting to compare Case 5 in NRVB and Case 10 in granite as they are both initially just critical, and have very similar fissile mass (although the granite system has a larger volume by a factor of approximately 2.4). It is noted that the yields of the two calculations are within a factor of two, 4.5 kt for 1000 kg of $^{239}PuO_2$ in NRVB, and 2.4 kt for 988 kg of $^{239}PuO_2$ in granite.

4.7 Conclusions

A set of eight calculations has been run with the RTM including the New Structural Response Model for NRVB systems. This set brings together six cases defined during earlier studies [7,16] and two new cases defined specifically for this study. All of the calculations have been undertaken using the latest model developments for structural response in NRVB, and using the latest improvements to the equation of state for NRVB, which has caused stability issues in previous studies. A further two calculations in granite have been undertaken. These are both re-runs of cases defined in earlier studies [7,16], with the significant modelling improvement to the RTM to remove the need to approximate the Equation of State with an approximate look-up table. The results in both NRVB and granite identify some interesting trends and help to give a better understanding of parameter space for RT criticalities.

5 Estimating the Actinide and Fission Product Inventory

The radiological impact of a GDF depends partly on the radionuclide inventory in the wastes. A criticality transient would change the GDF inventory. It is therefore necessary to be able to estimate the change in the inventory caused by a criticality and to determine the fission products present in the GDF after the transient has occurred. Detailed estimates of the change in the actinide and fission product inventory can be accomplished by performing a series of calculations with the FISPIN fuel inventory code [24]. The FISPIN inventory code calculates the changes in the number of atoms of the nuclides of various types (heavy isotopes, actinides, fission products, structural or activation materials) as the fissile material is subjected to periods of irradiation and cooling. To calculate the changes in the number of atoms of the various nuclides FISPIN requires the following data:

- The radioactive decay constants and the modes of decay and branching ratio between the various nuclides.
- The independent yields of the fission products created by fission in the main fissioning actinides.
- The cross-sections for the various neutron induced reactions. Typically, the main actinides undergo fission, (n,2n) reactions and neutron capture (n,γ), sometimes to several distinct states of the daughter product nuclide.

The radioactive decay data and the fission yield data depend on whether a thermal fission or fast spectrum system is being considered. For the fuel inventory calculations being discussed in this report these data have been taken from the thermal JEF2.2 evaluation.

The cross-section data is strongly dependent on the type of fissile material and the neutron energy spectrum. The irradiation of the fissile material may also change cross-section data through changes in the spectrum and resonance shielding. The WIMS9 reactor physics code [20] has been used in the current study, together with the TRAIL programme [25], to produce neutron spectra and cross-sections for those actinides which are subject to resonance shielding. Data for the remaining non-shielded nuclides is taken directly from the relevant TRAIL database, which contains information for 129 actinides, 1,038 fission products or significant capture products of fission products, and 708 structural material nuclides. The cross-section data for the non-shielded nuclides has been taken from the JEF2.2 evaluation. The TRAIL programme then uses the spectra generated by WIMS9, in 172 energy groups, to condense the cross-section data taken from the TRAIL database, plus that generated by WIMS9 for the resonance shielded nuclides, into a format in three energy groups that is suitable for use in FISPIN.

Inventory Calculations for both the QSS and RTM models are presented below using calculations from Reference [16] as a basis.

5.1 QSS Inventory Calculations

The reactivity function used by the QSS model contains seven nuclides that are potentially important to the energy generation during criticality. In addition, an inert nuclide is included to represent the fission products, which have been found to have little impact on power generation. For a chosen scenario, a calculation can be undertaken using FISPIN to estimate the evolution of the radionuclide inventory (including the fission products and actinides neglected in the QSS model), based on the power history calculated by the QSS code. The FISPIN calculation can be continued beyond the end time of the QSS calculation, to estimate the evolution of the nuclide inventory due to radioactive decay after the criticality transient has terminated.

A sample calculation was performed in a previous study to demonstrate the methodology [6]. This sample calculation involved a number of approximations:

- A neutron energy spectrum from a 17x17 array of PWR fuel pins was used to condense the cross-section data to the three group cross-sections required by FISPIN, rather than a neutron spectrum calculated from the reactor physics calculations used to construct reactivity functions for use in the QSS GDF model.
- The duration of the QSS simulation was divided into six time steps, rather than following the more detailed power history calculated by the QSS code.
- A mean flux, chosen to approximately match burn-up, was used throughout the transient, rather than following the variation of flux with time calculated by the QSS code.

A more detailed calculation has been performed in this study to illustrate the robustness of the methodology, and the magnitude of the uncertainties associated with the approximations described above. The QSS model in this study consists of a sphere containing a mixture of fissile material (FM), backfill (NRVB) and water, known as the FM region surrounded by an infinite region of saturated backfill, known as the surrounding material (SM) region. The NRVB is composed mainly of hydrated metal oxides and mineral oxides. The main constituent is hydrated lime ($CaO.H_2O$ or $Ca(OH)_2$). The composition of the NRVB is shown in Table 1. The FM region has a radius of 0.105 m. The FM considered in this study is $^{235}UO_2$. FM is assumed to be deposited in the FM region at a user defined rate. When the FM is deposited in the FM region it is assumed to displace water from the pores in the backfill. FM material continues to be deposited in the FM region until the pores have been completely filled. The initial concentration of fissile material (in the pores of the NRVB) is 3,923 kg m^{-3}, which for a sphere of the given radius equates to 19.0 kg of fissile material. The arrival rate of fissile material is 10^{-10} kg m^{-3} s^{-1}, which ends after 1.077×10^{13} s when the pores are full of fissile material. A summary of the main characteristics of this QSS system is given in Table 52. The variation of flux, power and temperature throughout the transient, as predicted by the QSS code, is shown in Figures 53, 54 and 55 respectively.

In order to allow for the arrival of fresh fissile material, the FISPIN inventory calculation is broken into a series of time steps. For the first step the initial inventory is taken and subjected to the an appropriate initial neutron flux, for the chosen duration of the FISPIN inventory calculation. At the start of the second time step the fresh fissile material that arrived during the first time step is taken as the initial inventory, and subjected to the calculated neutron flux from the start of the second time step onwards, in a second FISPIN calculation. This process is repeated for the chosen number of time steps, with an additional FISPIN calculation being performed for each time step. Once this process is complete, the inventory at a given time is obtained by summing the inventories from all of the FISPIN calculations at the chosen time.

Four different FISPIN calculation routes have been used to investigate the approximations and uncertainties in the methodology.

For the first calculation route, the 341,000-year duration of the QSS simulation was divided into seven time steps, each of approximately 50,000 years, and therefore seven FISPIN calculations were performed. A constant neutron flux of 1.63×10^{11} neutrons m^{-2} s^{-1} was used. This is the mean flux for the transient, as seen from Figure 53. The neutron spectrum and cross-sections for those actinides which are subject to resonance shielding were generated by WIMS9 for a 17x17 array of $^{235}UO_2$ fuel pins subject to burn ups up to 46 GW days te^{-1}. This approach corresponds to that used in the earlier sample study.

For the second calculation route, the 341,000-year duration of the QSS simulation was again divided into seven time steps, each of approximately 50,000 years, and therefore seven FISPIN calculations were performed. A constant mean neutron flux of 1.63×10^{11} neutrons m^{-2} s^{-1} was used. The neutron spectrum and cross-sections for those actinides, which are subject to resonance shielding, have been generated by WIMS9 from a spherical model of the fissile material using the spherical option of the FLURIG collision probability module in WIMS9. Resonance shielding was applied to ^{235}U by means of a subgroup treatment that is devised around the resonance integral tabulations of the standard WIMS library. The WIMS HEAD module generates microscopic cross-sections for all nuclides in the problem by performing an equivalence treatment of resonance shielding. However, the equivalence treatment is not adequate to represent the ^{235}U resonances and so the PRES-FLURIG-RES sequence is invoked. PRES generates subgroup cross-sections that have been obtained by fitting to the library resonance integrals. Collision probabilities are then generated for these cross-sections by FLURIG in spherical geometry. The RES module uses the collision probabilities to calculate the subgroup fluxes, a set of weights for each WIMS library resonance group, and an appropriately weighted broad group resonance cross-section. The FLURIG-PIP sequence is then used to calculate the fluxes and reactivity for the system. The WIMS9 HEAD module uses a ^{235}U thermal fission spectrum to form a macroscopic fission spectrum for all fissionable nuclides. This approach is adequate for a system containing a significant proportion of ^{235}U.

The 172 energy group neutron spectrum generated by WIMS9 for the PWR array and the QSS calculation are shown in Figure 56, where energy values are plotted for the 172 group WIMS scheme at the mean group energy. Values of flux are not plotted as a function of lethargy, and not all energy groups are of equal lethargy. The PWR spectrum is similar to that found within the QSS calculations, but the neutron energy spectrum within the QSS calculation is slightly softer at thermal energy, which may have an impact on the predicted actinide and fission product inventory.

For the third calculation route, the 341,000-year duration of the QSS simulation was divided into 79 time steps to follow more closely the actual flux and power history during the transient. Particular attention was given to accurately representing the rapid change in flux at the beginning and end of the transient. The flux used for each time step was that predicted by the QSS model. The neutron spectrum and cross-sections for those actinides which are subject to resonance shielding were generated by WIMS9 for a 17x17 array of $^{235}UO_2$ fuel pins subject to burn ups up to 46 GW days te^{-1}.

For the fourth calculation route, the 341,000-year duration of the QSS simulation was again divided into 79 time steps to follow the actual flux and power history during the transient. The flux used for each time step was that predicted by the QSS model. The neutron spectrum and cross-sections for those actinides, which are subject to resonance shielding, have been generated by WIMS9 from a spherical model of the fissile material using the spherical option of the FLURIG collision probability module in WIMS9.

Thus, it has been possible to determine the impact of approximations to the neutron spectrum and the flux and power history on the predicted actinide and fission product inventories. The power history followed in FISPIN for each of the four calculation routes is shown in Figure 57,

together with the power history predicted by the QSS model. The variation in ^{235}U mass (g) throughout the transient is similarly shown in Figure 58. Results are displayed in Figures 59 to 62 and Figures 63 to 66, in terms of the variation in fission product mass (g) and activity (Bq) throughout the transient, and for a further 280,000 years after the system is considered to be shutdown. For convenience, all isotopes of a given element have been summed. The results are displayed for nine selected elements. Others are available, although not displayed in the figures.

Figure 57 shows that the choice of neutron spectrum used to condense the cross-section data, and the number of time steps and the value of the flux have an important impact on the power history calculated by FISPIN. This results in significant differences in the predicted values of mass and activity. The most accurate calculation route, employing a neutron spectrum calculated from the spherical fissile material model and the detailed flux history from the QSS model, provides inventory results that are in good agreement with those predicted by the QSS model, indicating the viability of the methodology. The least accurate calculation route, employing a neutron spectrum from a PWR array model and fewer time steps with an average value for the flux, underestimates the ^{235}U mass at the end of the transient by up to 1.5 kg. The activity differs by more than a factor of two, depending on the calculation route. All the calculation routes show that U dominates in terms of mass for this transient. The chosen fission product elements differ by less than an order of magnitude, in terms of activity.

It has been shown that the FISPIN methodology provides an accurate prediction of the GDF inventory and its evolution through a QSS transient providing that a sufficiently detailed calculation route is employed. Further evaluation is required on a variety of QSS transients to fully determine the robustness of the FISPIN calculation route.

5.2 RTM Inventory Calculations

For RTM calculations the reactivity function is constructed using high temperature libraries for a limited range of nuclides, as discussed in Section 4.1. For a chosen RTM scenario, a calculation can be undertaken using FISPIN to estimate the radionuclide inventory, including fission products and actinides neglected in the RTM model, based on the power history calculated by the RTM code. The FISPIN calculation can be continued beyond the end time of the RTM calculation, to estimate the evolution of the nuclide inventory due to radioactive decay after the criticality transient has terminated.

A sample calculation was performed in a previous study to demonstrate the methodology [7]. This sample calculation involved a number of approximations.

- A neutron energy spectrum used to produce WIMS cross-sections at a temperature of 3,300 K was used to condense the cross-section data to the three group cross-sections required by FISPIN, rather than using a different neutron spectrum at different temperatures throughout the transient.
- The duration of the RTM simulation was represented as a single time step, with a peak value for the power, rather than following the more detailed power history calculated by RTM.
- The burn-up for an RTM transient was found to be low (< 0.5 GWd/te) and so the relative abundance of the inventory was similar to that of the fission yield data. It was therefore deemed sufficient to perform a single inventory calculation for all transients for a given system, and then scale the results according to the number of fissions, or, equivalently the yield.

A more detailed calculation has been performed in this study to illustrate the robustness of the methodology, and the magnitude of the uncertainties associated with the approximations described above. The model in this study consists of a sphere containing a mixture of fissile

material (FM), backfill (NRVB) and water, known as the FM region surrounded by an infinite region of saturated backfill, known as the surrounding material (SM) region. The NRVB is composed mainly of hydrated metal oxides and mineral oxides. The main constituent is hydrated lime ($CaO.H_2O$ or $Ca(OH)_2$). The composition of the NRVB is shown in Table 1. The FM considered in this study is $^{239}PuO_2$. Three different transients were considered in this study:

- 10 kg of $^{239}PuO_2$, at a concentration of 10.1 kg/m^3, was placed in the FM region, with a radius of 0.619 m. The variation of power throughout the transient, as predicted by the RTM code, is shown in Figure 67.
- 100 kg of $^{239}PuO_2$, at a concentration of 8.99 kg/m^3, was placed in the FM region, with a radius of 1.3852 m. The variation of power throughout the transient, as predicted by the RTM code, is shown in Figure 68.
- 1000 kg of $^{239}PuO_2$, at a concentration of 8.77 kg/m^3, was placed in the FM region, with a radius of 3.008 m. The variation of power throughout the transient, as predicted by the RTM code, is shown in Figure 69.

For each transient, four different FISPIN calculation routes have been used to investigate the approximations and uncertainties in the methodology.
For the first calculation route, the duration of the RTM simulation was represented by a single 1 ms time step at a power of $1.3x10^{14}$ W, corresponding to the peak power during the transient, as predicted by RTM. A neutron energy spectrum used to produce WIMS cross-sections at a temperature of 3,300 K was used to condense the cross-section data to the three group cross-sections required by FISPIN. This approach corresponds to that used in the earlier sample study.

For the second calculation route, the duration of the RTM simulation was represented by a single 1 ms time step at a power of $1.3x10^{14}$ W, corresponding to the peak power during the transient, as predicted by RTM. The neutron spectrum and cross-sections for those actinides that are subject to resonance shielding have been generated by WIMS9 from a spherical model of the fissile material using the spherical option of the FLURIG collision probability module in WIMS9. Resonance shielding was applied to ^{239}Pu by means of a subgroup treatment that is devised around the resonance integral tabulations of the standard WIMS library. The WIMS HEAD module generates microscopic cross-sections for all nuclides in the problem by performing an equivalence treatment of resonance shielding. However, the equivalence treatment is not adequate to represent the ^{239}Pu resonances and so the PRES-FLURIG-RES sequence is invoked. PRES generates subgroup cross-sections that have been obtained by fitting to the library resonance integrals. Collision probabilities are then generated for these cross-sections by FLURIG in spherical geometry. The RES module uses the collision probabilities to calculate the subgroup fluxes, a set of weights for each WIMS library resonance group, and an appropriately weighted broad group resonance cross-section. The FLURIG-PIP sequence is then used to calculate the fluxes and reactivity for the system. The neutron spectrum and cross-sections were generated at both 2,900 K and 3,300 K, as these temperatures correspond roughly to the middle of the predicted reactivity peak during the transient.

For the third calculation route, the duration of the RTM simulation was divided into a number of time steps to more accurately represent the power history during the transient. The power at each time step was taken from the power history predicted by RTM. Particular attention was given to accurately represent the rapid change in power throughout the transient. A neutron energy spectrum used to produce WIMS cross-sections at a temperature of 3,300 K was used to condense the cross-section data to the three group cross-sections required by FISPIN. This approach corresponds to that used in the earlier sample study.

For the fourth calculation route, the duration of the RTM simulation was divided into a number of time steps to more accurately represent the power history during the transient. The power at each time step was taken from the power history predicted by the RTM code. The neutron

spectrum and cross-sections for those actinides which are subject to resonance shielding have been generated by WIMS9 from a spherical model of the fissile material using the spherical option of the FLURIG collision probability module in WIMS9. The neutron spectrum and cross-sections were generated at both 2,900 K and 3,300 K, as these temperatures correspond roughly to the middle of the predicted reactivity peak during the transient.

Thus, it has been possible to determine the impact of approximations to the neutron spectrum and the flux and power history on the predicted fission product inventory. For each transient considered in this study, and for all of the FISPIN calculation routes, the estimated relative abundance of the fission product inventory one hour after the criticality transient has ended was found to be identical, as displayed in Figure 70 and Table 53. Table 53 display the relative abundance of the various nuclides. Figure 70 gives the relative abundance as a function of mass number. There is a clear similarity with the fission yield data. The maximum burnup, found in the case of 10 kg of $^{239}PuO_2$, was 0.2 GWd per tonne. In view of the low burnup, it is considered sufficient to run a single inventory calculation to represent the progeny of ^{239}Pu for all transients. The relative abundance of the fission product inventory shown here can then be scaled on the number of fissions, or, equivalently the yield, to determine the actual inventory.

It has been shown that the FISPIN methodology provides an accurate prediction of the GDF inventory and its evolution through an RTM transient. It is sufficient to run a single inventory calculation to represent the progeny of selected actinides for all transients.

6 Summary

Two new transient criticality models have been developed in the understanding programme: the QSS and RTM computer models. These models have been developed to understand two very different types of criticality: quasi-steady-state and rapid transient. Their initial development and application to test cases has been reported previously and an initial set of calculations has been undertaken. Both models continue to be developed to improve their accuracy and stability. In the study reported here, further calculations have been undertaken with both models to complement the first set of calculations using the latest developments to both the models, and input supplied to them.

With the QSS Model, calculations have been undertaken in NRVB where a system can encounter positive temperature feedback when the pore water boils. A QSS calculation of two or more stages is required when this occurs. The QSS Model has also been used to undertake calculations in mudstone, a potential GDF host rock, which has not been studied previously.

RTM has recently undergone improvements to the structural response model, and an analysis of stability issues has led to much greater understanding of the role the equation of state plays. An ongoing study has identified a number of potential improvements to RTM, both in terms of solution methods, and the supplied equation of state. Many of these improvements have been implemented, and previous RTM calculations undertaken in earlier studies have therefore been repeated to make use of the latest input and model features. In addition, two completely new RTM calculations have been undertaken; one to complement the set of calculations with plutonium dioxide in NRVB, and another as the first RTM calculation with uranium dioxide in NRVB. In total, this report summarises ten RTM calculations. Gathering a number of calculations together allows trends to be deduced which may be useful in assessment studies. For, example, using the RTM calculations for systems which are initially just critical there appear to be fairly simple correlations between fissile mass and yield from the RT criticality.

A further part of this study has been a detailed analysis of fission product inventories for example QSS and RTM calculations. Using methodologies developed in 2004-05 (reported in References [6,7]) as a basis, a number of calculations have been undertaken for example QSS and rapid transients from the first set of calculations. The analysis shows that, for the RTM calculations, the conclusions of the 2004-05 study are correct. For a QSS calculation, a more

detailed analysis is required than the original outline methodology to accurately predict the fission product inventory.

This study has not only extended the range of calculations that have been undertaken previously, but has provided much more insight into the range of phenomena that can occur, why the phenomenon occur, and what further investigations and developments may be beneficial for improving confidence in both models. In addition, it provides analysis and recommendations for predicting fission product inventories for both QSS and rapid transients. Results will provide a basis for future assessments.

This page intentionally left blank

References

Note that the mark * indicates reports for which a further issue is expected. This includes revisions following peer review, or reviews by NDA or its contractors. All reports are Contractor-Approved.

1 Defra, BERR, Welsh Assembly Government, Department of the Environment Northern Ireland, *Managing Radioactive Waste Safely: A Framework for Implementing Geological Disposal*, Cm7386, 2008.

2 Nuclear Decommissioning Authority, *The NDA's Research and development Strategy to Underpin Geological Disposal on the United Kingdom's Higher-activity Radioactive Wastes*, NDA Report no. NDA/RWMD/011c – Issue 1, March 2009.

3 United Kingdom Nirex Limited, *Generic Repository Studies: The Nirex Phased Disposal Concept*, Nirex Report N/074, 2003.

4 United Kingdom Nirex Limited, *Topical Report on Post-closure Criticality Safety Assessment*, Nirex Science Report S/98/004, 1998.

5 R. Cummings, P.N. Smith and K. Ghabaee, *Understanding Criticality Under Repository Conditions: Results of Static Calculations*, Serco Report SA/ENV- 0770 Issue 3, 2007.

6 P.N. Smith, R.M. Mason and R. Cummings, *Understanding Criticality Under Repository Conditions: QSS – A Model for Quasi-Steady-State Criticalities*, Serco Report SA/ENV-0771 Issue 3, 2007.

7 P.N. Smith, R.M. Mason and R. Cummings, *Understanding Criticality Under Repository Conditions: RTM – A Model for Rapid Transient Criticalities*, Serco Report SA/ENV-0772 Issue 3, 2007.

8* A.K. Ziver, C.C. Pain, A.J.H. Goddard, M.D. Eaton, J.L.M.A. Gomes, A.P. Umpleby and C.R.E. de Oliveira, *Modelling of Energetic Transients due to Slow Accumulation of Plutonium in Homogeneous Matrices*, ICON(05)01, 2006.

9 A.K. Ziver, C.C. Pain, M.D. Eaton, J.L.M.A. Gomes, A.P. Umpleby, A.J.H. Goddard and C.R.E. de Oliveira, *Stack Slumping/Amorphous Media Studies Carried Out Using FETCH*, ICON(05)02, Issue 6, 2008.

10 P.N. Smith, R.M. Mason, R. Cummings, K. Ghabaee, A.J.H. Goddard, C.C. Pain and A.K. Ziver, *Understanding Criticality Under Repository Conditions: Comparison of Results from Rapid Transient Models*, Serco Report SA/ENV-0773 Issue 3, 2008.

11 R.M. Mason, P.N. Smith and R. Cummings, *Sensitivity Studies Using the QSS Solver*, Serco Report SA/ENV-0830 Issue 2, 2007.

12 R.M. Mason, P.N. Smith, K. Ghabaee and R. Cummings, *Sensitivity Studies Using the RTM Solver*, Serco Report SA/ENV-0846 Issue 2, 2007.

13 P.N. Smith, R.M. Mason, N. Butler, R. Cummings, K. Ghabaee and S. Mandica, *Further Studies to Improve Confidence in the RTM and QSS Models*, Serco Report SA/ENV-0858 Issue 2, 2007.

14 N. Butler, P.N. Smith and R.M. Mason, *Development of an Improved Structural Response Model for the Rapid Transient Solver*, Serco Report SA/ENV-0945 Issue 2, 2010.

15 R.M. Mason and P.N. Smith, *An Investigation into Improving Numerical Stability of the Rapid Transient Solver*, Serco Report SA/ENV-0946 Issue 2, 2010.

16 R.M. Mason, R. Cummings, Y. Kudelin, J. Martindill, P.J. Smith and P.N. Smith, *A Suite of Calculations Using the QSS and RT Models*, Serco Report SA/ENV-0944 Issue 2, 2009.

17 United Kingdom Nirex Limited, *Development of the Nirex Reference Vault Backfill; Report on Current Status in 1994*, Nirex Science Report S/97/014, 1997.

18 M. Dillistone, R. Cummings, R.M. Mason and P.N. Smith, *Development of the RTM Equation of State for Different Potential Host Materials*, Serco Report SERCO/TAS – 1005, Issue 2, 2010.

19 R. Cummings and P.N. Smith, *Understanding Criticality Under Repository Conditions: Specification of a Suite of Calculations*, Serco Report SA/ENV-0893 Draft A, September 2006.

20 WIMS9 User Guide*, Serco, ANSWERS report.*

21 G.H. Towler, R. Metcalfe, S.P. Watson, T.J. McEwen and A.H. Bath, *Properties of Mudstone of a Kind that could prove Suitable to Host a Geological Disposal Facility for Radioactive Wastes*, QRS-1378A-1, Version 2.0, March 2008.

22* R.M. Mason, B.M. Franklin & C.J. Dean, *An Investigation of the Sensitivity to Nuclear Data of the QSS and RT Models*, SERCO/TAS/P3871/W001 Issue 1, 2008.

23 W.E. Kastenberg, P.F. Peterson, J. Ahn, J. Burch, G. Casher, P.L. Chambré, E. Greenspan, D.R. Olander, J.L. Vujic, B. Bessinger, N.G.W. Cook, F.M. Doyle and L.B. Hilbert, *Considerations of Autocatalytic Criticality of Fissile Materials in Geologic Repositories*, Nucl. Tech. **115**, 298-310 (1996).

24 E. B. Webster, *FISPIN for Nuclide Inventory Calculations. Introductory Guide for Version 7B*, ANSWERS/FISPIN(98)3, 1999.

25 E. B. Webster, TRAIL User Guide for Version 1A, ANSWERS/TRAIL/REPORT/001, 2001.

Glossary

Term	Meaning
Autocatalytic criticality	Criticality with positive reactivity temperature coefficient.
Burn-up	The amount of energy produced per unit weight of fuel irradiated or 'burned.'
Critical Mass	Mass of fissile material that can sustain a nuclear chain reaction.
Chain Reaction	A self-sustaining nuclear reaction. I.e. a system of nuclear reactions in which, on average, for every fission that occurs one or more neutrons is produced that go on to cause further fissions.
Feedback coefficient	Change in reactivity per unit change in a parameter, such as temperature or a nuclide concentration.
Fissile material	Nuclides that are capable of undergoing nuclear fission with neutrons at thermal energies.
Fissile material region	Region containing fissile material.
Fissionable material	Nuclides that are capable of undergoing nuclear fission with neutrons at fast energies, but not normally at thermal energies
k_{eff}	Neutron multiplication factor, i.e. the number of neutrons created per fission that go on to cause further fissions.
Minimum Critical Mass	For a given system it is the minimum mass of fissile material that can sustain a nuclear chain reaction.
Neutron absorption cross-sections	The effective area that has to be attributed to a nucleus to geometrically account for its absorption of a beam of incident neutrons.
Nile	One Nile is defined as a reactivity of 0.01. Hence in relation to k_{eff}, the reactivity in Niles is defined as $100(k_{eff} - 1) / k_{eff}$
mNile	One mNile is defined as 10^{-3} Niles. Hence in relation to k_{eff}, the reactivity in mNiles is defined as $100{,}000(k_{eff} - 1) / k_{eff}$
NRVB	Nirex Reference Vault Backfill.
Prompt neutron	A neutron emitted immediately by a nuclear fission, as opposed to a delayed neutron, that is emitted some time later by the decay of a fission product.
Prompt critical	A system is prompt critical if for each nuclear fission, one or more of the prompt neutrons produced goes on to cause a fission.
QSS criticality	Quasi-Steady-State criticality, i.e. a criticality transient that evolves via a series of near steady states.

Rapid transient criticality	Criticality with positive temperature feedback coefficient.
Reactivity	$(k_{eff} - 1) / k_{eff}$
Static calculation	Calculation for a time independent (steady-state) system.
Transient calculation	Calculation for a system that changes with time.

Tables

Table 1: Composition of Saturated Pristine NRVB

Element	Concentration ($kg\ m^{-3}$)	Weight %
Ca	459	26.98
Mg	18	1.06
Si	44	2.59
Al	12	0.71
Fe	9.2	0.54
K	1.8	0.11
Na	0.8	0.05
S	5.2	0.31
H	98	5.76
O	1053	61.90
Total	1703	100

Table 2: Concentrations of Fissile, Fissionable and Fission Product Materials for an NRVB QSS System with an Arrival Rate of 10^{-9} kg m^{-3} s^{-1} of 10% Enriched UO_2 in a Sphere of Radius 0.5 m. All materials are present as dioxides.

Time	Concentration ($kg\ m^{-3}$)							
	$^{235}UO_2$	$^{236}UO_2$	$^{238}UO_2$	$^{239}PuO_2$	$^{240}PuO_2$	$^{241}PuO_2$	$^{242}PuO_2$	PbO_2
Start of Calculation – 0 millennia.	20.22	0	182.0	0	0	0	0	0
Positive Feedback Break – 0.6 millennia	21.71	0.04853	198.4	0.01180	3.61×10^{-5}	1.64×10^{-8}	3.50×10^{-11}	0.2899
End of Arrival – 152 millennia	110.6	67.84	4442	5.953	0.4648	8.63×10^{-5}	7.59×10^{-4}	377.5

Notes for Tables 3, 5 and 20-22:

1) **All concentrations and masses are for material in the dioxide form. E.g. $^{235}UO_2$.**
2) **The concentration arrived (Column 3) is the initial concentration of fissile and fissionable materials (as dioxide) plus the product of the arrival rate (also for oxide in kg m^{-3} s^{-1}) and the time (s).**
3) **The total fissile mass arrived (Column 4) is the total concentration arrived multiplied by the volume of the fissile region, but also multiplied by the amount of fissile materials ($^{235}UO_2$, $^{239}PuO_2$ or $^{241}PuO_2$) arriving compared to all materials. Hence, for $^{235}UO_2$ arrival the factor is 1, but for 3% enriched UO_2 it would be 0.03.**
4) **The fissile concentration (Column 6) is the total concentration of $^{235}UO_2$, $^{239}PuO_2$ and $^{241}PuO_2$ in the fissile material region, during the QSS transient, taking into account any production, fission, decay or capture within the QSS model.**
5) **The fissile mass (Column 7) is the mass of $^{235}UO_2$, $^{239}PuO_2$ and $^{241}PuO_2$ in the fissile material region and is the fissile concentration (Column 6) multiplied by the volume of the fissile region.**
6) **The total power is given, along with the fraction of that power in the neutrons and gamma rays (See Reference [6] for details of their derivation).**

Table 3: Summary of NRVB QSS System with an Arrival Rate of 10^{-9} kg m^{-3} $s^{-1}$of 10% Enriched UO_2 in a Sphere of Radius 0.5 m

Time (s)	Time (millenia)	Total Concentration Arrived (kg m^{-3})	Total Fissile Mass Arrived (kg)	Temperature (℃)	Fissile Concentration (kg m^{-3})	Fissile Mass (kg)	Power (W)			Neutron Flux ($m^{-2}s^{-1}$)
							Total	Neutron	Gamma	
0	0	202.24	10.59	40.00	20.22	10.59	0.00	0.00	0.00	0.00
3.156×10^{7}	0.001	202.27	10.59	40.31	20.23	10.59	1.93	0.05	0.24	4.33×10^{10}
3.156×10^{8}	0.01	202.55	10.61	43.06	20.26	10.61	19.25	0.46	2.37	4.31×10^{11}
3.156×10^{9}	0.1	205.39	10.75	69.91	20.53	10.75	188.05	4.51	23.13	4.15×10^{12}
1.824×10^{10}	0.578	220.47	11.54	271.00	21.72	11.37	1452.21	34.86	178.63	3.03×10^{13}
1.824×10^{10}	0.578	220.47	11.54	285.62	21.72	11.37	1544.99	37.09	190.04	3.23×10^{13}
3.156×10^{10}	1	233.79	12.24	288.01	22.44	11.75	1560.17	37.46	191.93	3.15×10^{13}
3.156×10^{11}	10	517.81	27.11	534.93	27.47	14.38	3112.36	75.24	383.76	5.11×10^{13}
3.156×10^{12}	100	3358.00	175.82	482.71	72.46	37.94	2784.16	68.11	344.69	1.71×10^{13}
4.798×10^{12}	**152**	**5000.00**	**261.80**	**446.72**	**116.52**	**61.01**	**2557.93**	**62.29**	**316.18**	**9.82×10^{12}**
4.888×10^{12}	155	5000.00	261.80	310.13	111.59	58.43	1699.43	41.40	210.09	6.81×10^{12}

Table 4: Concentrations of Fissile, Fissionable and Fission Product Materials for an NRVB QSS System with an Arrival Rate of 5×10^{-10} kg m^{-3} s^{-1} of 10% Enriched UO_2 in a Sphere of Radius 0.5 m. All materials are present as dioxides.

Time	Concentration (kg m^{-3})							
	$^{235}UO_2$	$^{236}UO_2$	$^{238}UO_2$	$^{239}PuO_2$	$^{240}PuO_2$	$^{241}PuO_2$	$^{242}PuO_2$	PbO_2
Start of Calculation	20.22	0	182.0	0	0	0	0	0
Positive Feedback Break	21.59	0.1645	204.5	0.03924	3.98×10^{-4}	1.54×10^{-8}	1.82×10^{-9}	0.9832
End of Arrival	98.11	71.50	4431	4.619	0.2128	2.04×10^{-5}	2.54×10^{-4}	397.8

Table 5: Summary of NRVB QSS System with an Arrival Rate of 5×10^{-10} kg m^{-3} s^{-1} of 10% Enriched UO_2 in a Sphere of Radius 0.5 m. See notes above Table 3 for further information on the data presented.

Time (s)	Time (millenia)	Total Concentration Arrived (kg m^{-3})	Total Fissile Mass Arrived (kg)	Temperature (℃)	Fissile Concentration (kg m^{-3})	Fissile Mass (kg)	Power (W)			Neutron Flux ($m^{-2}s^{-1}$)
							Total	Neutron	Gamma	
0	0	202.24	10.59	40.00	20.22	10.59	0.00	0.00	0.00	0.00
3.156×10^{7}	0.001	202.25	10.59	40.17	20.23	10.59	1.05	0.03	0.13	2.36×10^{10}
3.156×10^{8}	0.01	202.39	10.60	41.67	20.24	10.60	10.48	0.25	1.29	2.35×10^{11}
3.156×10^{9}	0.1	203.81	10.67	56.22	20.38	10.67	101.94	2.45	12.54	2.27×10^{12}
3.156×10^{10}	1	218.01	11.42	182.32	21.35	11.18	894.70	21.48	110.06	1.90×10^{13}
1.824×10^{10}	1.589	227.30	11.90	271.00	21.63	11.33	1452.21	34.87	178.65	3.04×10^{13}
1.824×10^{10}	1.589	227.30	11.90	285.55	21.63	11.33	1544.57	37.09	190.02	3.24×10^{13}
3.156×10^{11}	10	360.02	18.85	286.18	22.79	11.93	1548.54	37.35	190.79	3.07×10^{13}
3.156×10^{12}	100	1780.12	93.21	287.88	41.91	21.94	1559.34	38.06	192.90	1.66×10^{13}
9.596×10^{12}	**304**	**5000.00**	**261.80**	**224.94**	**102.75**	**53.80**	**1162.60**	**28.26**	**143.62**	**5.07×10^{12}**
1.041×10^{13}	330	5000.00	261.80	40.04	95.67	50.09	0.23	0.01	0.03	1.08×10^{9}

Table 6: Summary of NRVB QSS Systems with 10% Enriched UO_2 in a Sphere of Radius 0.5 m

Arrival rate (kg m^{-3} s^{-1})	Material Arriving	Radius of System (m)	Other Details	Time boiling starts, if applicable (millennia)	Time boiling ends, if applicable (millennia)	Time of temperature plateau, if reached (millennia)	Approximate Plateau Temperature (ºC)	Time new material stops arriving (millennia)
10^{-11}	10% $^{235}UO_2$, 90% $^{238}UO_2$	0.5	-	N/A	N/A	5	45	15203
10^{-10}	10% $^{235}UO_2$, 90% $^{238}UO_2$	0.5	-	N/A	N/A	5	90	1520
5×10^{-10}	10% $^{235}UO_2$, 90% $^{238}UO_2$	0.5	Two stage QSS calculation – positive feedback at boiling of pore water	1.589	141	50	290, although smaller period at approx 310	304
10^{-9}	10% $^{235}UO_2$, 90% $^{238}UO_2$	0.5	Two stage QSS calculation – positive feedback at boiling of pore water	0.578	2	4	510	152

Table 7: Composition of Dry Opalinus Clay from Reference [21]

Component	wt%
SiO_2	58.1
Al_2O_3	15.4
Fe_2O_3	4.0
FeO	2.5
MgO	2.4
CaO	3.1
Na_2O	1.3
K_2O	3.2
CO_2	2.6
C	0.6
H_2O	5.0

Table 8: Composition of Mudstone

Material Region	Total Density (kg m^{-3})	Weight Percent for Element										
		Al	C	Ca	Fe	H	K	Mg	Na	O	Si	^{235}U
SM	2513	7.905295	1.270226	2.148986	4.59859	1.074339	2.576655	1.40379	0.935443	51.74266	26.34401	0
FM	2523.15	7.873499	1.265117	2.140343	4.580094	1.065044	2.566291	1.398143	0.931681	51.54859	26.23805	0.393142

Table 9: Concentrations of $^{236}UO_2$ and PbO_2 Used to Generate a Reactivity Function for Mudstone.

Concentration of $^{236}UO_2$ and PbO_2 (kg m^{-3})	50	200	400	700	1000	1195
Concentration of $^{236}UO_2$ (kg m^{-3})	7.22	28.87	57.75	101.06	144.37	172.52
Concentration of PbO_2 (kg m^{-3})	42.78	171.13	342.25	598.94	855.63	1022.48

Table 10: Reactivity as a Function of $^{235}UO_2$, $^{236}UO_2$, and PbO_2 Concentration for an FM Region of 1.1025 Radius at a Temperature of 40 °C and a Water Density of 995 kg m^{-3}

Concentration of $^{235}UO_2$ (kg m^{-3})	Combined Concentration of $^{236}UO_2$ and PbO_2 (kg m^{-3})						
	0	50	200	400	700	1000	1195
5	-59233.9	-61273.2	-65624.1	-70089.1	-76521.3	-84153.9	-90414.5
11.27	0.0	-1337.9	-4248.2	-7304.5	-11783.4	-17094.4	-23355.0
20	20473.2	19396.6	17035.9	14529.5	10850.1	6476.2	215.6
50	35828.5	34964.9	33056.1	31000.1	27963.5	24367.6	18107.0
200	41250.3	40538.5	38934.2	37166.9	34573.5	31653.8	25393.2
500	40087.1	39553.2	38335.0	37018.9	35227.1	32307.4	26046.7
800	39671.6	39306.4	38497.3	37655.0	35863.2	32943.5	26682.9
1100	40098.3	39874.9	39065.8	38223.5	36431.7	33512.0	27251.4

Table 11: Reactivity as a Function of $^{235}UO_2$, $^{236}UO_2$, and PbO_2 Concentration for an FM Region of 1.1025 Radius at a Temperature of 90 °C and a Water Density of 968 kg m^{-3}

Concentration of $^{235}UO_2$ (kg m^{-3})	Combined Concentration of $^{236}UO_2$ and PbO_2 (kg m^{-3})						
	0	50	200	400	700	1000	1195
5	-60011.5	-62116.9	-66637.5	-71285.4	-77945.4	-85749.7	-92091.2
11.27	-336.5	-1709.2	-4717.5	-7875.4	-12463.8	-17868.7	-24210.2
20	20279.2	19179.0	16754.0	14180.7	10422.7	6000.7	-340.8
50	35736.0	34857.4	32897.2	30802.0	27725.5	24114.6	17773.1
200	41160.5	40442.2	38815.8	37029.5	34430.9	31519.2	25177.7
500	40001.3	39467.2	38245.1	36928.1	35149.6	32238.0	25896.4
800	39613.3	39243.5	38434.9	37605.4	35827.0	32915.4	26573.8
1100	40062.7	39841.2	39032.6	38203.2	36424.7	33513.1	27171.5

Table 12: Reactivity as a Function of $^{235}UO_2$, $^{236}UO_2$, and PbO_2 Concentration for an FM Region of 1.1025 Radius at a Temperature of 200 °C and a Water Density of 868 kg m^{-3}

Concentration of $^{235}UO_2$ (kg m^{-3})	Combined Concentration of $^{236}UO_2$ and PbO_2 (kg m^{-3})						
	0	50	200	400	700	1000	1195
5	-60980.3	-63261.0	-68266.9	-73477.4	-80744.6	-88994.5	-95445.0
11.27	-844.6	-2314.9	-5574.4	-9023.9	-13911.6	-19491.7	-25942.2
20	19927.8	18759.5	16157.0	13392.8	9458.2	4955.5	-1495.0
50	35470.0	34547.0	32483.5	30265.3	27121.0	23520.9	17070.4
200	40852.7	40112.2	38444.6	36627.0	34059.1	31251.4	24800.9
500	39745.3	39210.6	38000.3	36696.0	34997.2	32189.5	25739.1
800	39462.4	39108.9	38316.2	37508.0	35809.2	33001.5	26551.0
1100	39988.9	39773.7	38981.1	38172.8	36474.0	33666.4	27215.9

Table 13: Reactivity as a Function of $^{235}UO_2$, $^{236}UO_2$, and PbO_2 Concentration for an FM Region of 1.1025 Radius at a Temperature of 281 °C and a Water Density of 750 kg m^{-3}

Concentration of $^{235}UO_2$ (kg m^{-3})	Combined Concentration of $^{236}UO_2$ and PbO_2 (kg m^{-3})						
	0	50	200	400	700	1000	1195
5	-60949.5	-63436.1	-68919.2	-74688.4	-82527.4	-91126.7	-97595.3
11.27	-968.4	-2551.7	-6070.9	-9801.2	-14942.4	-20637.3	-27105.8
20	19738.7	18488.4	15712.7	12767.4	8699.2	4176.8	-2291.7
50	35200.9	34228.5	32063.4	29759.7	26578.6	23049.9	16581.4
200	40484.0	39727.7	38032.4	36203.1	33716.5	31069.1	24600.6
500	39466.5	38940.1	37754.1	36497.0	34895.7	32248.4	25779.9
800	39327.2	38975.7	38222.4	37443.3	35842.1	33194.8	26726.3
1100	39935.7	39727.0	38973.7	38194.6	36593.4	33946.0	27477.5

Table 14: Reactivity as a Function of $^{235}UO_2$, $^{236}UO_2$, and PbO_2 Concentration for an FM Region of 1.1025 Radius at a Temperature of 281 °C and a Water Density of 571 kg m^{-3}

Concentration of $^{235}UO_2$ (kg m^{-3})	Combined Concentration of $^{236}UO_2$ and PbO_2 (kg m^{-3})						
	0	50	200	400	700	1000	1195
5	-59053.3	-61815.4	-67861.3	-74208.7	-82581.0	-91359.7	-97595.3
11.27	-401.0	-2138.6	-5942.1	-9950.9	-15265.8	-20898.8	-27134.4
20	19831.5	18470.7	15509.7	12393.1	8288.6	3913.2	-2322.3
50	34894.1	33850.1	31590.5	29216.4	26116.4	22829.4	16593.8
200	39932.1	39156.5	37462.5	35701.3	33406.5	31069.1	24833.6
500	39103.2	38591.8	37466.3	36317.6	34895.7	32558.4	26322.9
800	39189.1	38858.6	38157.3	37443.3	36021.5	33684.2	27448.6
1100	39920.1	39720.1	39018.8	38304.9	36883.0	34545.7	28310.1

Table 15: Reactivity as a Function of $^{235}UO_2$, $^{236}UO_2$, and PbO_2 Concentration for an FM Region of 1.1025 Radius at a Temperature of 281 °C and a Water Density of 392 kg m^{-3}

Concentration of $^{235}UO_2$ (kg m^{-3})	Combined Concentration of $^{236}UO_2$ and PbO_2 (kg m^{-3})						
	0	50	200	400	700	1000	1195
5	-57411.2	-60481.4	-67081.0	-73959.9	-82786.0	-91627.4	-97595.3
11.27	3.1	-1937.3	-5999.7	-10244.6	-15683.6	-21185.7	-27153.5
20	19788.5	18291.9	15140.4	11922.5	7804.1	3639.5	-2328.3
50	34456.1	33340.5	30985.5	28607.2	25608.8	22600.9	16633.0
200	39291.3	38498.1	36832.2	35153.8	33083.8	31069.1	25101.3
500	38719.0	38223.2	37178.7	36136.8	34895.7	32881.1	26913.3
800	39052.8	38747.1	38093.3	37443.3	36202.3	34187.7	28219.8
1100	39904.6	39712.9	39059.1	38409.1	37168.0	35153.4	29185.5

Table 16: Reactivity as a Function of $^{235}UO_2$, $^{236}UO_2$, and PbO_2 Concentration for an FM Region of 1.1025 Radius at a Temperature of 281 °C and a Water Density of 213 kg m^{-3}

Concentration of $^{235}UO_2$ (kg m^{-3})	Combined Concentration of $^{236}UO_2$ and PbO_2 (kg m^{-3})						
	0	50	200	400	700	1000	1195
5	-56107.3	-59511.0	-66671.1	-73987.5	-83155.2	-91926.4	-97595.3
11.27	188.2	-1920.3	-6299.1	-10717.9	-16206.4	-21490.0	-27158.8
20	19558.0	17933.8	14604.7	11276.6	7236.4	3347.1	-2321.8
50	33884.8	32677.6	30241.4	27873.4	25039.2	22363.3	16694.4
200	38539.6	37733.4	36115.2	34552.8	32738.3	31069.1	25400.3
500	38305.3	37833.4	36880.8	35951.4	34895.7	33226.6	27557.8
800	38915.8	38634.9	38030.9	37443.3	36387.7	34718.5	29049.7
1100	39889.4	39706.0	39101.9	38514.4	37458.7	35789.6	30120.7

Table 17: Reactivity as a Function $^{235}UO_2$, $^{236}UO_2$, and PbO_2 Concentration for an FM Region of 1.1025 Radius at a Temperature of 281 °C and a Water Density of 34 kg m^{-3}

Concentration of $^{235}UO_2$ (kg m^{-3})	Combined Concentration of $^{236}UO_2$ and PbO_2 (kg m^{-3})						
	0	50	200	400	700	1000	1195
5	-55259.0	-59040.4	-66748.1	-74474.7	-83713.1	-92263.7	-97595.3
11.27	64.6	-2266.3	-6950.0	-11448.7	-16861.7	-21818.1	-27149.7
20	19076.0	17296.2	13781.6	10461.4	6570.5	3048.4	-2283.1
50	33087.5	31781.1	29282.8	26986.8	24402.4	22116.6	16785.0
200	37650.8	36839.5	35294.5	33892.2	32378.8	31069.1	25737.6
500	37867.0	37430.6	36564.4	35761.8	34895.7	33586.1	28254.5
800	38781.4	38516.2	37968.4	37443.3	36577.3	35267.6	29936.1
1100	39874.1	39698.8	39150.9	38625.9	37759.8	36450.2	31118.6

Table 18: Reactivity as a Function of $^{235}UO_2$, $^{236}UO_2$, and PbO_2 Concentration for an FM Region of 1.1025 Radius at a Temperature of 400 °C and a Water Density of 23 kg m^{-3}

Concentration of $^{235}UO_2$ (kg m^{-3})	Combined Concentration of $^{236}UO_2$ and PbO_2 (kg m^{-3})						
	0	50	200	400	700	1000	1195
5	-56776.9	-60656.5	-68636.3	-76545.6	-86107.5	-94842.1	-100284.4
11.27	-630.7	-3021.9	-7822.1	-12504.2	-18061.1	-23127.7	-28570.0
20	18680.4	16854.2	13221.6	9765.5	5797.7	2196.8	-3245.5
50	32890.9	31555.8	28983.1	26606.2	23970.7	21635.9	16193.7
200	37529.2	36710.3	35125.2	33689.3	32149.5	30820.6	25378.3
500	37770.0	37334.5	36452.2	35636.4	34758.6	33429.6	27987.4
800	38707.6	38445.7	37890.3	37356.4	36478.6	35149.6	29707.4
1100	39817.9	39644.8	39089.3	38555.4	37677.6	36348.6	30906.4

Table 19: Reactivity as a Function of $^{235}UO_2$, $^{236}UO_2$, and PbO_2 Concentration for an FM Region of 1.1025 Radius at a Temperature of 1000 °C and a Water Density of 11 kg m^{-3}

Concentration of $^{235}UO_2$ (kg m^{-3})	Combined Concentration of $^{236}UO_2$ and PbO_2 (kg m^{-3})						
	0	50	200	400	700	1000	1195
5	-61532.9	-65693.5	-74644.4	-83527.3	-94003.0	-103575.6	-109503.1
11.27	-2800.5	-5350.2	-10759.0	-16043.7	-22178.6	-27762.7	-33690.2
20	17398.3	15439.6	11388.6	7488.7	3059.8	-931.2	-6858.6
50	32296.4	30888.3	28002.8	25311.9	22367.0	19771.9	13844.4
200	37201.0	36347.2	34606.4	32994.7	31278.9	29810.4	23882.9
500	37450.2	37007.8	36069.0	35164.5	34204.2	32735.7	26808.3
800	38436.9	38174.8	37587.4	37008.8	36048.5	34580.0	28652.5
1100	39596.9	39422.5	38835.1	38256.5	37296.2	35827.7	29900.2

Table 20: Summary of Mudstone QSS System with an arrival rate of 10^{-13} kg m^{-3} s^{-1} of $^{235}UO_2$. See notes above Table 3 for further information on the data presented.

Time (s)	Time (millenia)	Total Concentration Arrived (kg m^{-3})	Total Fissile Mass Arrived (kg)	Temperature (°C)	Fissile Concentration (kg m^{-3})	Fissile Mass (kg)	Power (W)			Neutron Flux ($m^{-2}s^{-1}$)
							Total	Neutron	Gamma	
0	0.000	11.27	63.26	40.00	11.27	63.26	0.00	0.00	0.00	0.00
3.156×10^{7}	0.001	11.27	63.26	40.00	11.27	63.26	0.03	0.00	0.00	9.79×10^{7}
3.156×10^{8}	0.01	11.27	63.26	40.01	11.27	63.26	0.26	0.01	0.03	9.76×10^{8}
3.156×10^{9}	0.1	11.27	63.26	40.11	11.27	63.26	2.51	0.06	0.31	9.44×10^{9}
3.156×10^{10}	1	11.27	63.28	40.77	11.27	63.28	18.28	0.44	2.25	6.86×10^{10}
3.156×10^{11}	10	11.30	63.44	41.44	11.27	63.29	34.30	0.82	4.22	1.29×10^{11}
3.156×10^{12}	100	11.59	65.03	41.45	11.28	63.31	34.32	0.82	4.22	1.29×10^{11}
3.156×10^{13}	1000	14.43	80.98	41.45	11.31	63.49	34.32	0.82	4.22	1.28×10^{11}
3.156×10^{14}	10000	42.83	240.41	41.45	11.63	65.28	34.33	0.82	4.22	1.25×10^{11}
1.669×10^{15}	**52880**	**178.15**	**1000.00**	**41.45**	**12.76**	**71.60**	**34.44**	**0.83**	**4.24**	**1.14×10^{11}**
1.669×10^{15}	52896	178.15	1000.00	40.00	12.75	71.57	0.00	0.00	0.00	3.15×10^{6}

Table 21: Summary of Mudstone QSS System with an Arrival Rate of 10^{-12} kg m^{-3} $s^{-1}$of $^{235}UO_2$. See notes above Table 3 for further information on the data presented.

Time (s)	Time (millenia)	Total Concentration Arrived (kg m^{-3})	Total Fissile Mass Arrived (kg)	Temperature (℃)	Fissile Concentration (kg m^{-3})	Fissile Mass (kg)	Power (W)			Neutron Flux ($m^{-2}s^{-1}$)
							Total	Neutron	Gamma	
0	0.000	11.27	63.26	40.00	11.27	63.26	0.00	0.00	0.00	0.00
3.156×10^{7}	0.001	11.27	63.26	40.01	11.27	63.26	0.26	0.01	0.03	9.80×10^{8}
3.156×10^{8}	0.01	11.27	63.26	40.11	11.27	63.26	2.60	0.06	0.32	9.76×10^{9}
3.156×10^{9}	0.1	11.27	63.28	41.06	11.27	63.28	25.14	0.60	3.09	9.44×10^{10}
3.156×10^{10}	1	11.30	63.44	47.71	11.29	63.39	182.95	4.39	22.50	6.85×10^{11}
3.156×10^{11}	10	11.59	65.03	54.45	11.31	63.51	343.02	8.23	42.19	1.28×10^{12}
3.156×10^{12}	100	14.43	80.98	54.46	11.35	63.69	343.19	8.24	42.21	1.28×10^{12}
3.156×10^{13}	1000	42.83	240.41	54.46	11.67	65.49	343.24	8.24	42.22	1.24×10^{12}
1.670×10^{14}	**5288**	**178.15**	**1000.00**	**54.51**	**12.80**	**71.85**	**344.43**	**8.27**	**42.37**	**1.14×10^{12}**
1.680×10^{14}	5308	178.15	1000.00	40.00	12.75	71.57	0.00	0.00	0.00	3.15×10^{6}

Table 22: Summary of Mudstone QSS System with an Arrival Rate of 10^{-11} kg m^{-3} $s^{-1}$of $^{235}UO_2$. See notes above Table 3 for further information on the data presented.

Time (s)	Time (millenia)	Total Concentration Arrived (kg m^{-3})	Total Fissile Mass Arrived (kg)	Temperature (℃)	Fissile Concentration (kg m^{-3})	Fissile Mass (kg)	Power (W)			Neutron Flux ($m^{-2}s^{-1}$)
							Total	Neutron	Gamma	
0	0.000	11.27	63.26	40.00	11.27	63.26	0.00	0.00	0.00	0.00
3.156×10^{7}	0.001	11.27	63.26	40.11	11.27	63.26	2.61	0.06	0.32	9.80×10^{9}
3.156×10^{8}	0.01	11.27	63.28	41.10	11.27	63.28	26.01	0.62	3.20	9.76×10^{10}
3.156×10^{9}	0.1	11.30	63.44	50.60	11.30	63.43	251.73	6.04	30.96	9.42×10^{11}
3.156×10^{10}	1	11.59	65.03	127.29	11.49	64.48	2072.50	49.74	254.92	7.63×10^{12}
3.156×10^{11}	10	14.43	80.98	184.45	11.63	65.28	3429.43	82.31	421.82	1.25×10^{13}
3.156×10^{12}	100	42.83	240.41	184.48	11.97	67.18	3430.14	82.32	421.91	1.21×10^{13}
1.669×10^{13}	**529**	**178.15**	**1000.00**	**185.00**	**13.18**	**73.99**	**3442.51**	**82.62**	**423.43**	**1.10×10^{13}**
1.743×10^{13}	552	178.15	1000.00	40.00	12.75	71.57	0.00	0.00	0.00	3.15×10^{6}

Table 23: Summary of Mudstone QSS Systems

Arrival rate (kg m^{-3} s^{-1})	Time of the onset of boiling, if applicable (millennia)	End of boiling, if applicable (millennia)	Time of temperature plateau, if reached (millennia)	Approximate Plateau Temperature (ºC)	Time new material stops arriving (millennia)
10^{-13}	N/A	N/A	5	41.5	52880
10^{-12}	N/A	N/A	5	54.5	5288
10^{-11}	N/A	N/A	4	185	528

Table 24: Composition of FM and SM Regions for Just Critical $^{239}PuO_2$ Systems in NRVB at 40ºC

Region	Concentration of $^{239}PuO_2$ (kg m^{-3})	Weight % for species:										
		Ca	Mg	Si	Al	Fe	K	Na	^{32}S	H	O	^{239}Pu
SM	0.000	26.984	1.058	2.587	0.705	0.541	0.106	0.047	0.306	5.761	61.905	0.000
FM – 3.684 kg $^{239}PuO_2$ in a sphere radius of 0.4447 m	10.000	26.826	1.052	2.572	0.701	0.538	0.105	0.047	0.304	5.728	61.612	0.515
FM - 10 kg $^{239}PuO_2$ in a sphere radius of 0.619 m	10.066	26.825	1.052	2.571	0.701	0.538	0.105	0.047	0.304	5.727	61.610	0.519
FM - 100 kg $^{239}PuO_2$ in a sphere radius of 1.3852 m	8.982	26.842	1.053	2.573	0.702	0.538	0.105	0.047	0.304	5.731	61.642	0.463
FM - 200 kg $^{239}PuO_2$ in a sphere radius of 1.7483 m	8.936	26.843	1.053	2.573	0.702	0.538	0.105	0.047	0.304	5.731	61.643	0.461
FM - 1000 kg $^{239}PuO_2$ in a sphere radius of 3.008 m	8.772	26.846	1.053	2.573	0.702	0.538	0.105	0.047	0.304	5.732	61.648	0.452

Table 25: Reactivity as a Function of Temperature and Radius for the 3.684 kg $^{239}PuO_2$ at 10 kg m^{-3} NRVB System. The red text indicates where the system is prompt critical

Temp. (K) → / Radius (m) ↓	313.16	900	1900	2900	3300	4050	7025	10000	100000
0.4447	243	14147	18613	17054	15911	13312	-598	-18007	-57791
0.447	12	13940	18403	16821	15667	13042	-1019	-18630	-59248
0.45	-292	13666	18125	16514	15344	12682	-1574	-19454	-61192
0.4625	-1620	12471	16908	15170	13927	11109	-4027	-23079	-69727
0.475	-3046	11185	15594	13720	12399	9410	-6683	-27025	-79055
0.5	-6214	8325	12668	10480	8984	5601	-12684	-35966	-100306
0.6	-23689	-7560	-3646	-7803	-10400	-16218	-47981	-89284	-229299
0.8	-88240	-66971	-65229	-79594	-87666	-105437	-201798	-327440	-825189

Table 26: k_∞ as a Function of Temperature for the 3.684 kg $^{239}PuO_2$ at 10 kg m^{-3}NRVB System

Temp. (K)	k_∞
313.16	1.137921
900	1.328168
1900	1.416364
2900	1.404348
3300	1.392891
4050	1.367140
7025	1.248935
10000	1.135440
100000	1.124052

Table 27: Reactivity as a Function of Temperature and Radius for the 10 kg $^{239}PuO_2$ NRVB System in a Sphere of Radius 0.619 m.
The red text indicates where the system is prompt critical

Temp. (K) → / Radius (m) ↓	313.16	900	1900	2900	3300	4050	7025	10000	100000
0.619	255.2	16401.9	21860.3	20627.6	19636.7	17372.4	5450.5	-9074.4	-31559.4
0.619464	236.1	16387.4	21844.3	20609.8	19618.2	17351.5	5419.6	-9124.9	-31676.7
0.62007	209.6	16364.9	21822.5	20586.2	19592.9	17324.6	5376.6	-9186.2	-31821.1
0.6345	-397.8	15838.5	21290.1	20000.4	18977.6	16640.3	4309.2	-10766.3	-35544.9
0.64995	-1095.4	15236.4	20680.5	19329.2	18270.8	15854.6	3081.3	-12588.0	-39832.0
0.6809	-2628.0	13911.6	19338.1	17849.2	16711.4	14115.9	355.6	-16641.7	-49418.8
0.7428	-6285.2	10740.8	16122.6	14286.7	12950.6	9917.4	-6296.9	-26591.1	-73129.3
0.8047	-10810.8	6799.9	12119.2	9822.4	8226.1	4614.1	-14810.3	-39413.4	-103985.5
0.8666	-16294.5	1999.2	7232.0	4331.3	2397.8	-1961.5	-25523.4	-55665.8	-143486.1
0.9285	-22838.2	-3752.1	1365.2	-2315.1	-4680.7	-9993.0	-38806.6	-75956.0	-193286.1
0.9904	-30521.0	-10535.3	-5574.8	-10244.1	-13156.0	-19665.7	-55050.1	-100943.2	-255150.2
1.238	-73996.0	-49302.5	-45543.9	-57125.7	-63743.8	-78342.4	-157450.6	-260491.6	-658552.7

Table 28: k_∞ as a Function of Temperature for the 10 kg $^{239}PuO_2$ NRVB System in a Sphere of Radius 0.619 m

Temp. (K)	k_∞
313.16	1.076807
900	1.286224
1900	1.384506
2900	1.371507
3300	1.359001
4050	1.330974
7025	1.204038
10000	1.084633
100000	1.080572

Table 29: Reactivity as a Function of Temperature and Radius for the 100 kg $^{239}PuO_2$ NRVB System in a Sphere of Radius 1.3852 m.
The red text indicates where the system is prompt critical

Temp. (K) → / Radius (m) ↓	313.16	900	1900	2900	3300	4050	7025	10000	100000
1.3852	271.1	18345.2	24737.2	23835.8	22997.6	21070.5	11150.4	-458.6	-5432.5
1.41983	119.9	18221.3	24612.3	23697.9	22852.8	20909.4	10899.2	-834.3	-6310.5
1.45446	-40.3	18086.9	24477.2	23546.6	22696.9	20735.9	10627.2	-1236.3	-7247.1
1.52372	-395.1	17789.5	24176.8	23219.0	22351.6	20351.7	10028.2	-2123.5	-9318.2
1.66224	-1244.2	17073.1	23457.8	22428.1	21519.4	19426.6	8581.5	-4274.1	-14336.8
1.80076	-2307.0	16176.2	22556.4	21433.5	20474.1	18261.3	6758.0	-6987.7	-20719.4
1.93928	-3608.3	15075.8	21448.2	20209.4	19180.4	16818.3	4482.1	-10380.8	-28731.8
2.0778	-5172.0	13746.9	20109.3	18726.4	17612.1	15065.4	1696.1	-14552.9	-38634.7
2.21632	-7028.3	12168.9	18516.8	16955.8	15739.9	12963.0	-1668.9	-19613.5	-50720.0
2.7704	-17820.9	2912.8	9137.6	6391.8	4509.7	269.5	-22461.7	-51236.7	-127429.9
3.463	-40505.7	-16780.8	-11028.2	-16895.6	-20477.0	-28447.2	-71531.3	-127217.5	-316836.9
4.1556	-75049.5	-47162.9	-42540.1	-54383.2	-61148.4	-76039.3	-156181.7	-259788.6	-656223.7
5.5408	-179807.9	-141255.1	-141310.4	-176104.3	-194807.0	-235234.1	-445982.7	-708505.5	-1863556.4

Table 30: k_∞ as a Function of Temperature for the 100 kg $^{239}PuO_2$ NRVB System in a Sphere of Radius 1.3852 m.

Temp. (K)	k_∞
313.16	1.019415
900	1.245288
1900	1.352932
2900	1.339032
3300	1.32554
4050	1.295394
7025	1.160672
10000	1.036429
100000	1.038739

Table 31: Reactivity as a Function of Temperature and Radius for the 200 kg $^{239}PuO_2$ NRVB System in a Sphere of Radius 1.7483 m.
The red text indicates where the system is prompt critical

Temp. (K) → / Radius (m) ↓	313.16	900	1900	2900	3300	4050	7025	10000	100000
1.74825	288.0	18642.0	24837.5	23985.4	23239.6	21167.1	11618.4	473.2	-2599.6
1.79196	25.7	18322.4	24846.2	24032.4	23107.3	21134.7	11313.1	378.5	-3316.8
1.83566	-144.7	18474.0	24734.8	23764.1	22893.3	21079.3	11543.9	116.9	-3839.1
1.92308	-558.0	18116.1	24561.5	23601.0	22765.9	20539.0	10815.2	-414.4	-5280.6
2.09790	-603.1	17859.1	24165.7	23359.2	22481.6	20504.1	10068.5	-1770.4	-8296.5
2.27273	-1122.3	17283.3	23724.0	22731.1	21820.8	19621.9	9104.2	-3475.0	-12303.5
2.44755	-1988.4	16574.1	23006.6	21938.7	20879.5	18849.4	7683.8	-5609.2	-17285.7
2.62238	-2991.6	15718.7	22145.2	20983.2	19995.9	17732.9	5917.1	-8233.4	-23865.5
2.79720	-4194.2	14696.7	21110.4	19845.9	18791.9	16382.2	3798.1	-11444.0	-31093.0
3.49650	-11335.8	8618.3	14972.4	12978.3	11519.9	8209.6	-9406.8	-31321.3	-78840.3
4.37063	-26600.2	-4539.3	1565.6	-2292.8	-4773.3	-10357.9	-40435.2	-79051.7	-195981.5
5.24475	-50467.1	-25348.0	-19866.0	-27340.2	-31777.7	-41624.4	-94844.4	-163855.0	-409408.8

Table 32: k_∞ as a Function of Temperature for the 200 kg $^{239}PuO_2$ NRVB System in a Sphere of Radius 1.7483 m

Temp. (K)	k_∞
313.16	1.016751
900	1.243355
1900	1.351418
2900	1.337470
3300	1.323958
4050	1.293707
7025	1.158630
10000	1.034203
100000	1.036711

Table 33: Reactivity as a Function of Temperature and Radius for the 1000 kg $^{239}PuO_2$ NRVB System in a Sphere of Radius 3.008 m.
The red text indicates where the system is prompt critical

Temp. (K) → / Radius (m) ↓	313.16	900	1900	2900	3300	4050	7025	10000	100000
3.008	223.6	18705.9	25314.2	24485.0	23663.5	21883.3	12427.6	1484.3	472.1
3.0832	160.4	18740.5	25293.6	24451.1	23696.0	21842.5	12368.0	1390.6	274.1
3.1584	197.5	18677.4	25296.5	24430.5	23661.1	21802.4	12305.0	1308.0	58.6
3.3088	90.7	18640.0	25228.3	24390.1	23580.7	21674.6	12168.6	1104.7	-438.5
3.6096	-75.1	18474.4	25061.7	24208.5	23389.2	21504.1	11835.6	611.0	-1555.2
3.9104	-320.0	18265.3	24852.2	23978.6	23147.8	21231.9	11418.5	-5.2	-2996.2
4.2112	-636.1	18005.6	24590.5	23693.7	22845.3	20901.2	10898.0	-772.6	-4779.6
4.512	-1008.9	17690.7	24274.0	23345.0	22479.9	20492.7	10266.3	-1711.2	-6971.3
4.8128	-1465.8	17302.5	23896.3	22927.9	22041.1	20005.2	9498.7	-2844.9	-9623.9
6.016	-4172.6	15031.9	21600.9	20392.7	19367.9	17022.0	4795.6	-9860.9	-26117.1
7.52	-10193.2	9921.8	16439.0	14632.1	13270.0	10171.7	-6220.1	-26467.2	-65800.4
9.024	-20002.4	1520.8	7896.5	4955.6	2962.7	-1526.1	-25572.8	-56030.8	-137854.6
10.528	-34321.2	-10866.5	-4805.8	-9702.5	-12762.1	-19589.3	-56392.5	-103723.7	-256465.6
12.032	-53822.0	-27898.7	-22437.8	-30458.2	-35195.6	-45679.4	-102206.1	-175294.0	-437851.3

Table 34: k_∞ as a Function of Temperature for the 1000 kg $^{239}PuO_2$ NRVB System in a Sphere of Radius 3.008 m

Temp. (K)	k_∞
313.16	1.007423
900	1.236521
1900	1.346094
2900	1.332002
3300	1.318313
4050	1.287731
7025	1.151424
10000	1.026256
100000	1.029887

Table 35: $^{235}UO_2$ in Fully Saturated Backfill at 90°C Ambient Temperature and 6.5 MPa Ambient Pressure

UO_2 Concent-ration (kg m^{-3})	Critical radius (m)	Critical mass (kg)	Nuclear data. Coefficient (mN per °C)	Expansion Coefficient (mN per °C)	Total Temp. Coefficient (mN per °C)
5000.00	0.1539	76.40	-0.448	0.000	-0.448
2000.00	0.1569	32.36	-1.891	-25.246	-27.137
1000.00	0.1554	15.72	1.244	-34.626	-33.382
200.00	0.1625	3.595	-6.226	-42.645	-48.871

Table 36: Composition of FM and SM Regions for a Just Critical $^{235}UO_2$ Systems in NRVB at 90ºC

Region	Concentration of $^{235}UO_2$ (kg m^{-3})	Weight % for species:										
		Al	^{32}S	Ca	Fe	H	K	Mg	Na	O	Si	^{235}U
SM	0.000	0.7119	0.3132	27.323	0.5482	5.7238	0.1068	1.0679	0.0498	61.536	2.6198	0.0000
FM – 15.7 kg $^{235}UO_2$ in a sphere radius of 0.1554 m	1000.0	0.4630	0.2037	17.770	0.3565	3.3030	0.0694	0.6945	0.0324	41.288	1.7038	34.116

Table 37: Reactivity as a Function of Temperature and Radius for the 15.7 kg $^{235}UO_2$ NRVB System in a Sphere of Radius 0.1554 m.
The red text indicates where the system is prompt critical

Temp. (K) → / Radius (m) ↓	363.16	373.16	383.16	393.16	403.16	573.16
0.1554	236.4	249.4	261.3	207.6	195.6	32.0
0.1570	-1465.2	-1424.0	-1485.8	-1496.1	-1487.8	-1693.2
0.1632	-8745.3	-8755.9	-8769.0	-8779.6	-8731.1	-8919.4

Table 38: k_∞ as a Function of Temperature for the 15.7 kg $^{235}UO_2$ NRVB System in a Sphere of Radius 0.1554 m

Temp. (K)	k_∞
363.16	1.8385
373.16	1.8383
383.16	1.8381
393.16	1.8379
403.16	1.8377
573.16	1.8346

Table 39: Composition of FM and SM Regions for Supercritical $^{239}PuO_2$ Systems in NRVB at 40ºC

Region	Concentration of $^{239}PuO_2$ (kg m^{-3})	Weight % for species:										
		Ca	Mg	Si	Al	Fe	K	Na	^{32}S	H	O	^{239}Pu
SM	0.000	26.984	1.058	2.587	0.705	0.541	0.106	0.047	0.306	5.761	61.905	0.000
FM – 13.40 kg $^{239}PuO_2$ in a sphere radius of 0.684 m	10.000	26.826	1.052	2.572	0.701	0.538	0.105	0.047	0.304	5.728	61.612	0.515
FM - 200 kg $^{239}PuO_2$ in a sphere radius of 0.619 m	201.312	24.129	0.946	2.313	0.631	0.484	0.095	0.042	0.273	5.152	56.603	9.333

Table 40: Reactivity as a Function of Temperature and Radius for the 13.4 kg $^{239}PuO_2$ NRVB System in a Sphere of Radius 0.684 m.
The red text indicates where the system is prompt critical

Temp. (K) → / Radius (m) ↓	313.16	900	1900	2900	3300	4050	7025	10000	100000
0.6842	6899.4	20113.9	24715.2	23707.6	22886.1	21011.4	11171.4	-753.2	-17721.4
0.71	6145.8	19435.5	24026.6	22955.3	22098.3	20142.3	9847.0	-2687.6	-22187.1
0.74	5169.4	18563.6	23135.3	21979.4	21074.5	19011.3	8120.3	-5214.9	-28052.5
0.8	2876.4	16516.2	21039.7	19682.4	18660.9	16339.4	4006.5	-11265.4	-42132.9
0.875	-679.2	13328.6	17781.1	16084.5	14873.2	12128.7	-2554.2	-20981.0	-65009.1
0.95	-5088.7	9371.4	13723.2	11572.0	10106.5	6802.1	-10978.2	-33549.5	-94917.3
1.2	-27035.3	-10471.5	-6704.7	-11603.4	-14567.6	-21160.1	-56931.7	-103388.9	-265347.5
1.7	-110104.8	-86123.7	-85603.1	-105864.2	-116895.3	-140893.6	-268489.7	-431733.9	-1106709.

Table 41: k_∞ as a Function of Temperature for the 13.4 kg $^{239}PuO_2$ NRVB System in a Sphere of Radius 0.684 m

Temp. (K)	k_∞
313.16	1.137921
900	1.328168
1900	1.416364
2900	1.404348
3300	1.392891
4050	1.367140
7025	1.248935
10000	1.135440
100000	1.124052

Table 42: Reactivity as a Function of Temperature and Radius for the 200 kg $^{239}PuO_2$ NRVB System in a Sphere of Radius 0.619 m.
The red text indicates where the system is prompt critical

Temp. (K) → / Radius (m) ↓	313.16	900	1900	2900	3300	4050	7025	10000	100000
0.619	41051.6	39499.5	38569.4	38465.5	38476.6	38475.0	38425.1	38270.2	32091.4
0.7428	38090.7	36294.4	35462.5	35303.2	35290.6	35239.9	34956.3	34522.7	27290.5
0.8666	33875.9	31950.3	31032.1	30757.5	30698.5	30555.6	29843.2	28914.7	19900.0
0.9904	28462.1	26358.9	25328.2	24847.2	24704.4	24395.1	22955.7	21212.4	9364.9
1.1142	22086.4	19757.3	18591.8	17779.4	17501.0	16927.0	14349.5	11364.7	-4793.1
1.238	15114.5	12520.1	11201.4	9919.0	9445.1	8490.9	4287.7	-446.0	-22665.4
1.3618	7939.2	5056.8	3572.8	1697.1	969.8	-476.3	-6788.4	-13784.4	-44226.9
1.4856	901.7	-2298.8	-3934.0	-6494.0	-7515.8	-9542.3	-18358.2	-28039.7	-68901.8
1.6094	-5806.1	-9307.3	-11101.5	-14388.7	-15731.6	-18388.7	-29964.8	-42647.5	-95943.2
1.7332	-12080.9	-15872.6	-17809.9	-21830.0	-23501.6	-26810.1	-41256.5	-56978.7	-124410.0
1.857	-17903.1	-21965.9	-24038.2	-28771.4	-30768.9	-34725.3	-52043.8	-70838.3	-153593.4

Table 43: k_∞ as a Function of Temperature for the 200 kg $^{239}PuO_2$ NRVB System in a Sphere of Radius 0.619 m

Temp. (K)	k_∞
313.16	1.795875
900	1.74516
1900	1.723746
2900	1.72196
3300	1.722797
4050	1.723864
7025	1.728167
10000	1.730889
100000	1.588114

Table 44: Composition of FM and SM Regions in Granite Calculations with 1% porosity

Region	Concentration of $^{239}PuO_2$ (kg m^{-3})	Weight % for species:									
		^{239}Pu	O	H	Si	Al	K	Na	Ca	Fe	Ti
SM	0.0	0.000	48.679	0.045	34.264	6.854	3.308	2.956	0.712	2.943	0.239
FM - 500 kg $^{239}PuO_2$ in a sphere radius of 3.15 m	3.819	0.125	48.627	0.044	34.215	6.845	3.304	2.952	0.711	2.938	0.239
FM - 988 kg $^{239}PuO_2$ in a sphere radius of 4.025 m	3.620	0.1189	48.629	0.044	34.218	6.845	3.304	2.952	0.711	2.939	0.239

Table 45: Reactivity as a Function of Temperature and Radius for the 500 kg $^{239}PuO_2$ Granite System in a Sphere of Radius 3.15 m.
The red text indicates where the system is prompt critical

Temp. (K) → / Radius (m) ↓	313.16	900	1900	2900	3300	4050	7025	10000	100000
3.15	233.5	7067.9	9851.2	7993.3	6844.6	4432.3	-7426.8	-20108.0	-15805.7
3.158	251.8	7086.3	9869.7	8011.3	6863.0	4452.3	-7401.3	-20078.7	-15759.0
3.1608	234.8	7069.8	9852.5	7993.9	6845.8	4433.4	-7425.6	-20107.6	-15806.3
3.23	-187.2	6672.5	9457.9	7576.7	6416.1	3978.4	-8003.6	-20824.5	-16877.9
3.31	-683.3	6203.8	8992.5	7085.4	5912.1	3445.0	-8679.5	-21662.3	-18125.8
3.46	-1773.2	5179.9	7973.2	6006.8	4802.4	2272.9	-10170.5	-23503.0	-20896.0
3.78	-4368.3	2730.5	5545.4	3435.9	2154.8	-530.9	-13730.7	-27916.5	-27537.2
4.1	-7579.6	-294.1	2544.9	258.9	-1116.2	-3993.2	-18139.8	-33386.7	-35820.5
4.41	-11469.4	-3957.2	-1086.4	-3587.3	-5078.4	-8191.9	-23494.9	-40029.2	-45980.1
4.73	-16099.1	-8316.1	-5400.1	-8160.7	-9790.1	-13188.8	-29880.6	-47948.9	-58211.1
5.04	-21509.3	-13407.2	-10435.0	-13500.3	-15293.0	-19026.6	-37351.5	-57214.2	-72700.8
6.3	-51585.2	-41674.6	-38260.2	-43012.0	-45729.3	-51356.2	-78778.6	-108426.3	-156606.3

Table 46: k_∞ as a Function of Temperature for the 500 kg $^{239}PuO_2$ Granite System in a Sphere of Radius 3.15 m

Temp. (K)	k_∞
313.16	1.056335
900	1.134831
1900	1.171461
2900	1.1501
3300	1.136958
4050	1.110231
7025	0.99527
10000	0.896762
100000	0.970468

Table 47: Reactivity as a Function of Temperature and Radius for the 988 kg $^{239}PuO_2$ Granite System in a Sphere of Radius 4.02 m.
The red text indicates where the system is prompt critical

Temp. (K) → / Radius (m) ↓	313.16	900	1900	2900	3300	4050	7025	10000	100000
4.024923	226.9	7387.0	10443.1	8606.8	7448.8	5012.5	-6961.0	-19747.3	-13602.0
4.046875	162.8	7326.9	10385.0	8542.4	7384.8	4943.1	-7050.6	-19860.0	-13758.9
4.09375	22.8	7192.7	10253.5	8403.7	7241.6	4789.6	-7242.5	-20099.6	-14121.4
4.1875	-270.3	6915.7	9977.7	8109.3	6940.7	4473.0	-7650.0	-20600.5	-14888.4
4.375	-909.2	6310.1	9376.5	7474.6	6285.4	3779.1	-8530.9	-21701.1	-16533.5
4.75	-2422.8	4875.6	7955.3	5971.4	4736.9	2137.4	-10626.2	-24305.8	-20464.9
5.5	-6530.2	987.2	4105.0	1888.3	531.0	-2320.0	-16325.9	-31402.9	-31235.8
7	-20128.8	-11872.6	-8608.8	-11601.9	-13376.9	-17086.0	-35288.2	-55023.9	-67850.0
9	-51954.2	-41919.5	-38130.9	-42958.2	-45737.3	-51510.8	-79637.7	-110088.0	-158273.1

Table 48: k_∞ as a Function of Temperature for the 988 kg $^{239}PuO_2$ Granite System in a Sphere of Radius 4.02 m

Temp. (K)	k_∞
313.16	1.036877
900	1.117849
1900	1.157099
2900	1.135353
3300	1.121851
4050	1.094355
7025	0.976835
10000	0.876843
100000	0.951614

Table 49: RTM Results for Initially Just Critical Systems in NRVB

	Case 1	Case 2	Case 3	Case 4	Case 5	Case 6
Host material	NRVB	NRVB	NRVB	NRVB	NRVB	NRVB
Structural Response Model	New	New	New	New	New	New
Fissile Material	$^{239}PuO_2$	$^{239}PuO_2$	$^{239}PuO_2$	$^{239}PuO_2$	$^{239}PuO_2$	$^{235}UO_2$
Fissile mass (kg)	3.684	10	100	200	1000	15.7
Fissile concentration (kg m^{-3})	10.0	10.1	8.99	8.94	8.77	1000
Initial Radius (m)	0.4447	0.619	1.385	1.748	3.008	0.1554
Initial reactivity (mNiles)	243.0	255.2	271.1	288.0	223.6	236.4
Maximum reactivity (mNiles)	9471	13017	23856	24503	25273	236.4
Temperature at reactivity = 210 mN (K)	2352	2901	8499	9337	15880	364.4
Radius at reactivity = 210 mN (m)	0.557	0.903	1.803	2.190	3.713	0.1554
Total Energy Released (kt)	0.001049	0.04360	0.1973	0.5157	4.505	2.793×10^{-8}
Maximum Power (W)	1.537×10^{12}	9.773×10^{12}	6.803×10^{14}	1.465×10^{15}	7.551×10^{15}	77080
Maximum Temperature (K)	2918	3029	16850	22030	37760	365.6
Maximum Pressure (MPa)	385.5	306.4	2973	4090	7529	6.887
Maximum Radius (m)	2.015	4.717	21.73	30.59	62.85	0.15545

Table 50: RTM Results for Initially Supercritical Systems in NRVB

	Case 7	Case 8
Host material	NRVB	NRVB
Structural Response Model	New	New
Fissile Material	$^{239}PuO_2$	$^{239}PuO_2$
Fissile mass (kg)	13.4	200
Fissile concentration (kg m^{-3})	10.0	201.3
Initial Radius (m)	0.684	0.619
Initial reactivity (mNiles)	6899	41052
Maximum reactivity (mNiles)	20845	41052
Temperature at reactivity = 210 mN (K)	3740	37230
Radius at reactivity = 210 mN (m)	1.001	1.167
Total Energy Released (kt)	0.01150	0.05668
Maximum Power (W)	4.320×10^{13}	2.904×10^{14}
Maximum Temperature (K)	6920	55336
Maximum Pressure (MPa)	732.5	3016
Maximum Radius (m)	7.421	13.73

Table 51: RTM Results for Initially Just Critical Systems in Granite

	Case 9	Case 10
Host material	Granite	Granite
Structural Response Model	Inertial	Inertial
Fissile Material	$^{239}PuO_2$	$^{239}PuO_2$
Fissile mass (kg)	500	988
Fissile concentration (kg m^{-3})	3.819	3.620
Initial Radius (m)	3.15	4.025
Initial reactivity (mNiles)	233.5	226.9
Maximum reactivity (mNiles)	7957	9406
Temperature at reactivity = 210 mN (K)	3409	3791
Radius at reactivity = 210 mN (m)	3.917	5.177
Total Energy Released (kt)	0.9461	2.424
Maximum Power (W)	7.075×10^{14}	2.529×10^{15}
Maximum Temperature (K)	3742	5574
Maximum Pressure (MPa)	2720	4064
Maximum Radius (m)	5.825	12.75

Table 52: Summary of NRVB QSS System with an arrival rate of 10^{-10} kg m^{-3} $s^{-1}$of $^{235}UO_2$ in a Sphere of Radius 0.105 m.

Time (s)	Time (millennia)	Total Concentration Arrived (kg m^{-3})	Total Fissile Mass Arrived (kg)	Temperature (℃)	Fissile Concentration (kg m^{-3})	Fissile Mass (kg)	Power (W)			Neutron Flux ($m^{-2}s^{-1}$)
							Total	Neutron	Gamma	
0	0	3923.01	19.02	40.00	3923.01	19.02	0.00	0.00	0.00	0
3.156×10^{7}	0.001	3923.01	19.02	40.00	3923.01	19.02	0.00	0.00	0.00	1.57×10^{7}
3.156×10^{8}	0.01	3923.04	19.02	40.01	3923.04	19.02	0.01	0.00	0.00	1.57×10^{8}
3.156×10^{9}	0.1	3923.32	19.02	40.10	3923.32	19.02	0.13	0.00	0.02	1.57×10^{9}
3.156×10^{10}	1	3926.16	19.04	40.92	3926.10	19.04	1.21	0.03	0.15	1.51×10^{10}
3.156×10^{11}	10	3954.56	19.18	46.51	3949.43	19.15	8.59	0.21	1.06	1.07×10^{11}
3.156×10^{12}	100	4238.58	20.55	51.56	4098.28	19.87	15.26	0.37	1.88	1.82×10^{11}
1.077×10^{13}	**341**	**5000.00**	**24.25**	**52.58**	**4454.34**	**21.60**	**16.60**	**0.40**	**2.04**	**1.83×10^{11}**
1.175×10^{13}	372	5000.00	24.25	40.04	4445.02	21.55	0.05	0.00	0.01	5.82×10^{8}

Table 53: Fission Product Inventory at One Hour After the RTM NRVB Transient

Isotope	% of Total Activity	Isotope	% of total Activity
Cs138	7.52	Nd149	0.88
Tc101	7.42	Pr145	0.82
I134	6.35	Pr147	0.81
Ba139	4.88	Kr87	0.76
Te134	4.42	Cs139	0.74
La142	4.07	Y93	0.63
Te131	4.00	Sn128	0.63
Tc104	3.86	Rb88	0.61
Pr146	3.35	Kr88	0.59
Te133m	3.32	Xe135m	0.57
Ba141	3.13	Rh105m	0.57
Y94	2.88	Zr97	0.52
Rh107	2.81	I134m	0.50
Mo101	2.64	Nb97m	0.49
Sb131	2.17	Sb129	0.43
Ru105	2.03	Br84	0.43
Xe138	2.02	Sr91	0.42
La141	1.88	I133	0.42
La143	1.79	Tc105	0.36
Sr92	1.51	Y92	0.31
Sb130	1.50	Xe135	0.29
I135	1.50	Nb97	0.26
Te133	1.43	Ag111m	0.25
Tc102	1.43		
Mo102	1.42	Total	95.38
Ce146	1.00		
Ba142	0.95		
Rb89	0.91		
Y95	0.90		

Figures

Figure 1: Reactivity as a Function of Temperature for a 10% Enriched UO_2 Critical System with Radius 0.5 m

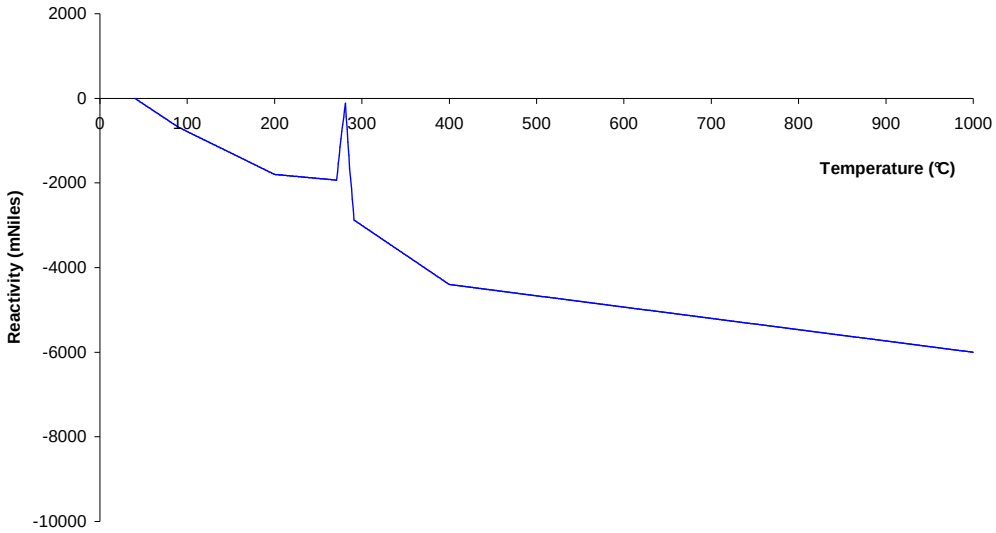

Figure 2: Initial Increase in Temperature for a 10% Enriched UO_2 System with Radius 0.5 m and Arrival rate 10^{-9} $kgm^{-3}s^{-1}$. Positive temperature feedback is encountered at a temperature increase of 231 ℃ (absolute temperatur e 271 ℃)

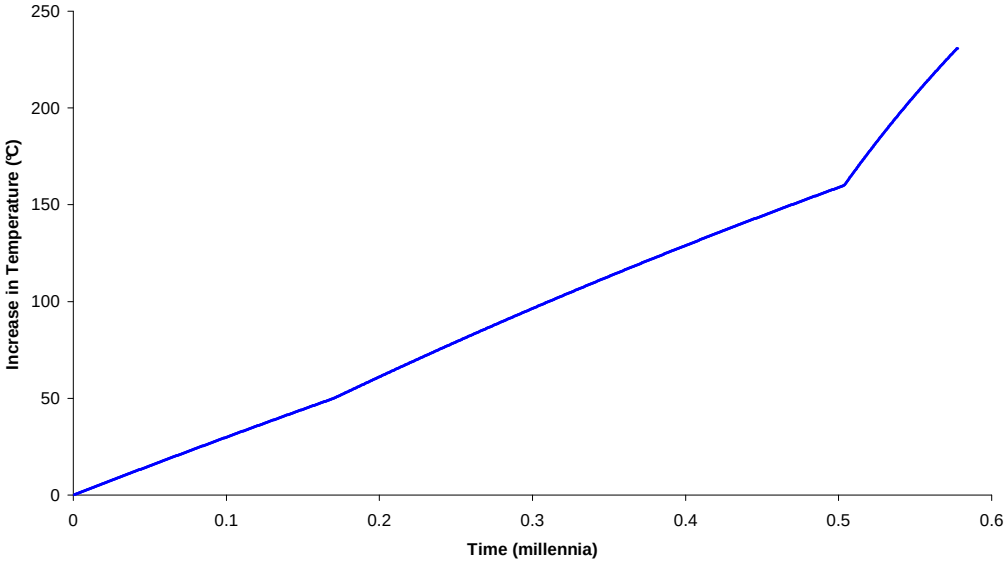

Figure 3: Reactivity as a Function of Temperature for an Initially 10% Enriched UO_2 Critical System upon the Onset of Pore Water Boiling. Arrival Rate 10^{-9} kg m^{-3} s^{-1}

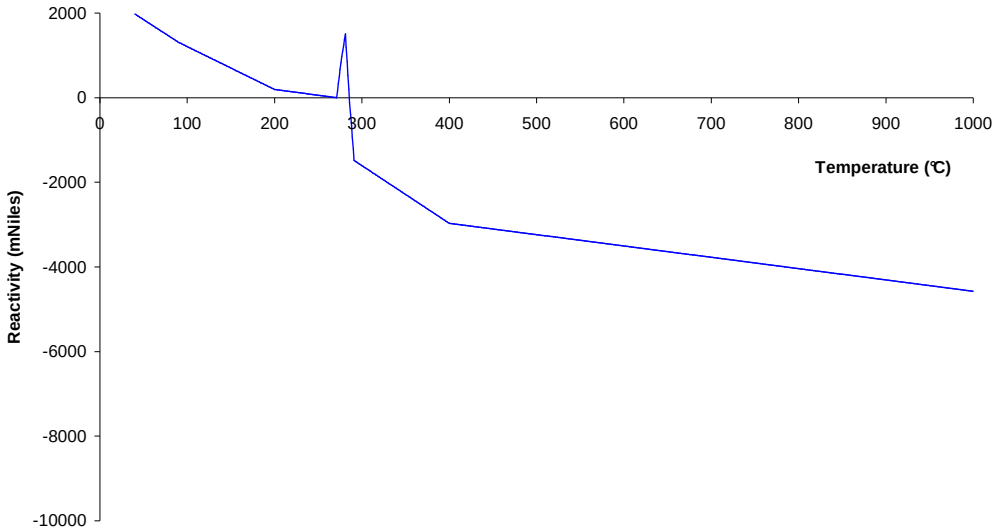

Figure 4: Temperature Increase as a Function of Time for a 10% Enriched UO_2 System with Radius 0.5 m and Arrival Rate 10^{-9} kg m^{-3} s^{-1}

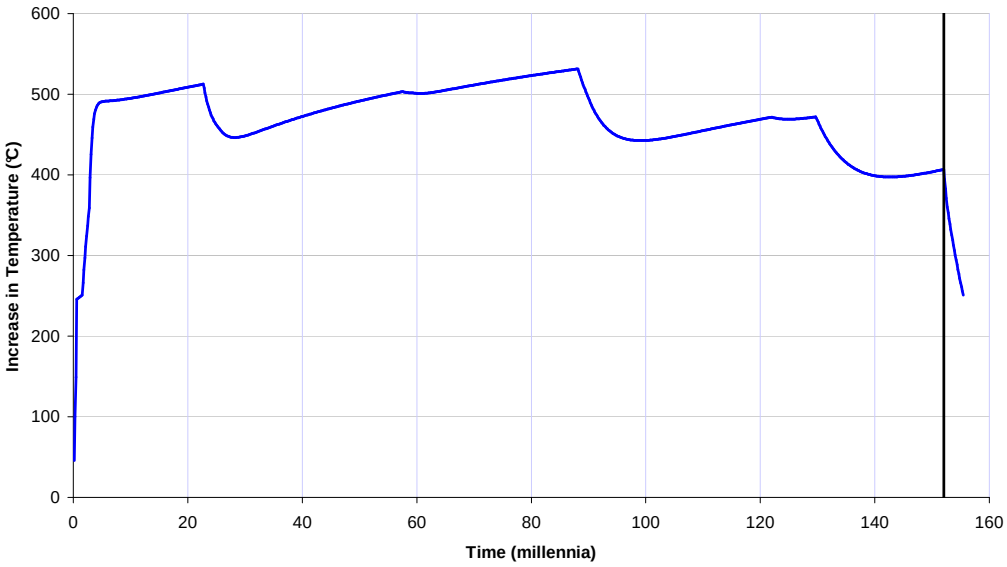

Figure 5: $^{235}UO_2$ Concentration as a Function of Time for a 10% Enriched UO_2 System with Radius 0.5 m and Arrival Rate 10^{-9} kg m^{-3} s^{-1}

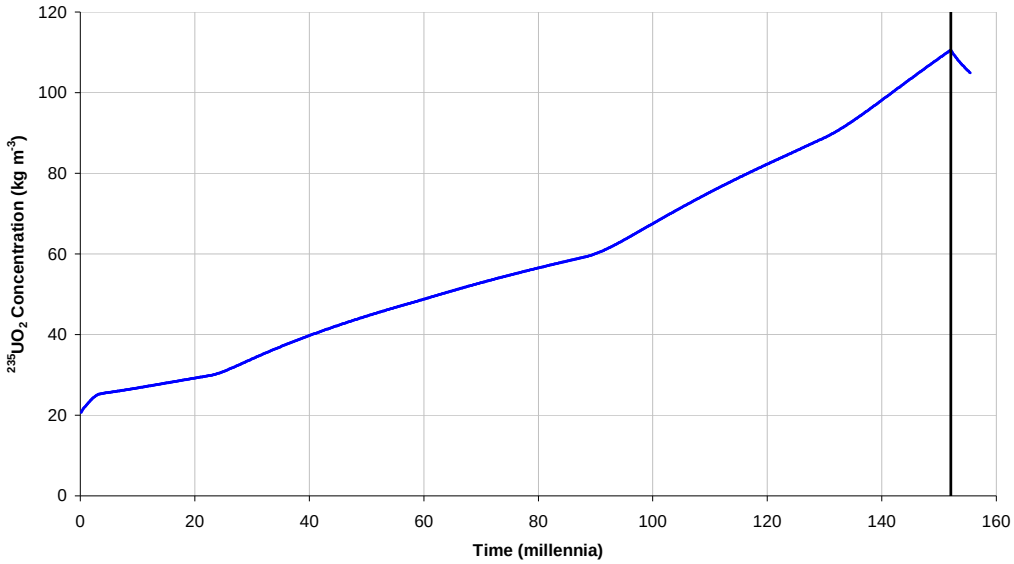

Figure 6: $^{236}UO_2$ Concentration as a Function of Time for a 10% Enriched UO_2 System with Radius 0.5 m and Arrival Rate 10^{-9} kg m^{-3} s^{-1}

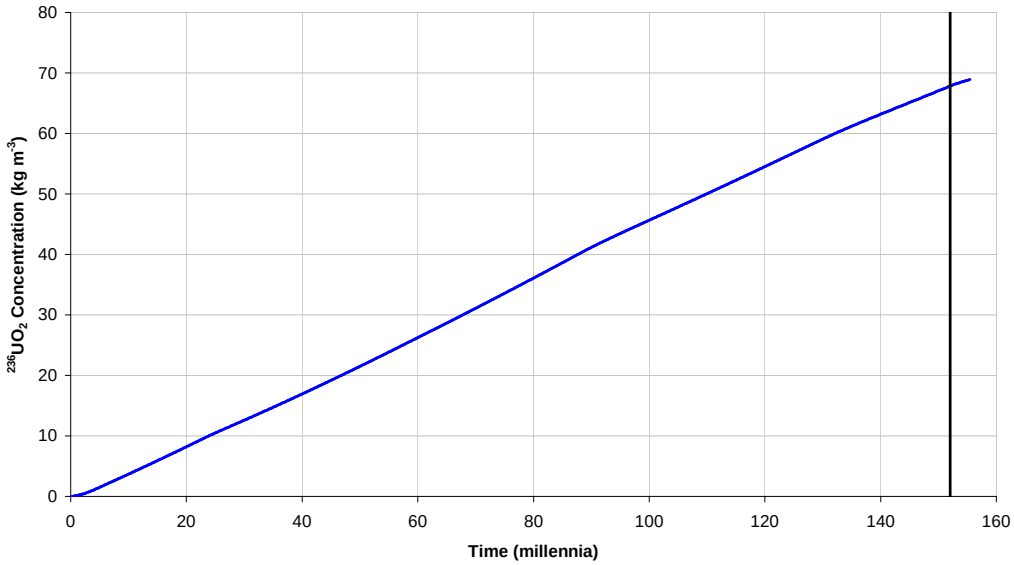

Figure 7: $^{238}UO_2$ Concentration as a Function of Time for a 10% Enriched UO_2 System with Radius 0.5 m and Arrival Rate 10^{-9} kg m^{-3} s^{-1}

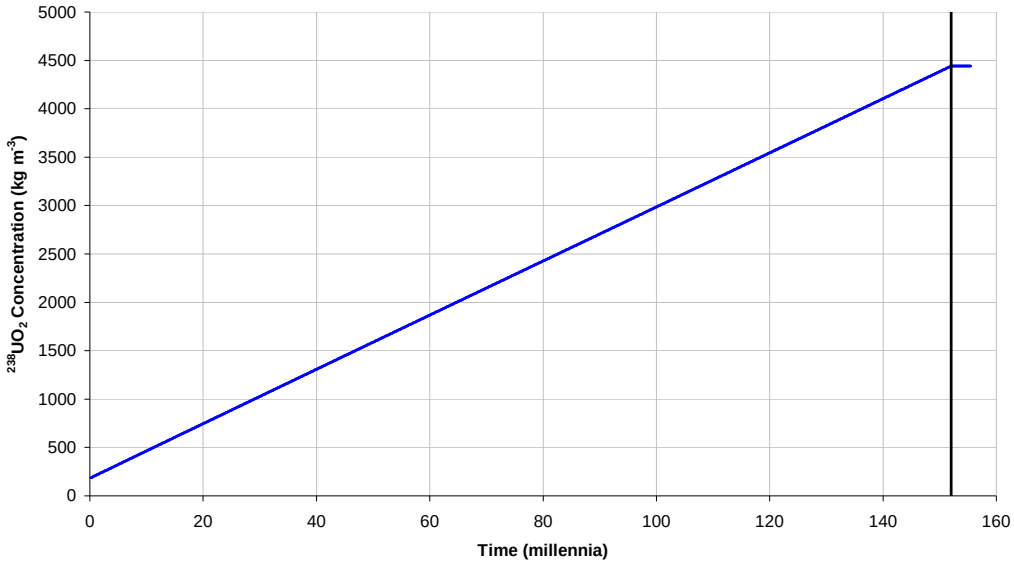

Figure 8: $^{239}PuO_2$ Concentration as a Function of Time for a 10% Enriched UO_2 System with Radius 0.5 m and Arrival Rate 10^{-9} kg m^{-3} s^{-1}

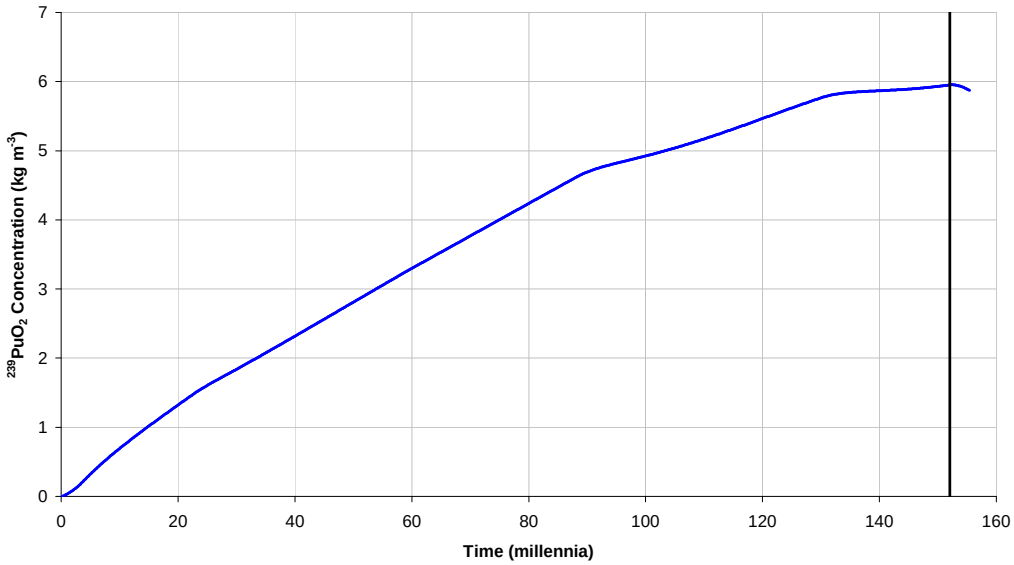

Figure 9: $^{240}PuO_2$ Concentration as a Function of Time for a 10% Enriched UO_2 System with Radius 0.5 m and Arrival Rate 10^{-9} kg m^{-3} s^{-1}

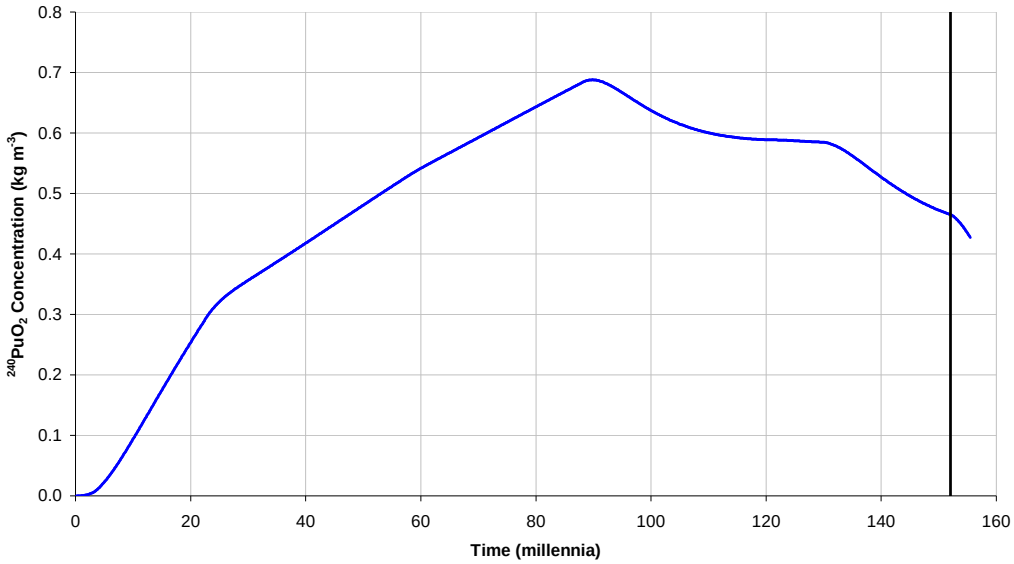

Figure 10: PbO_2 Concentration as a Function of Time for a 10% Enriched UO_2 System with Radius 0.5 m and Arrival Rate 10^{-9} kg m^{-3} s^{-1}

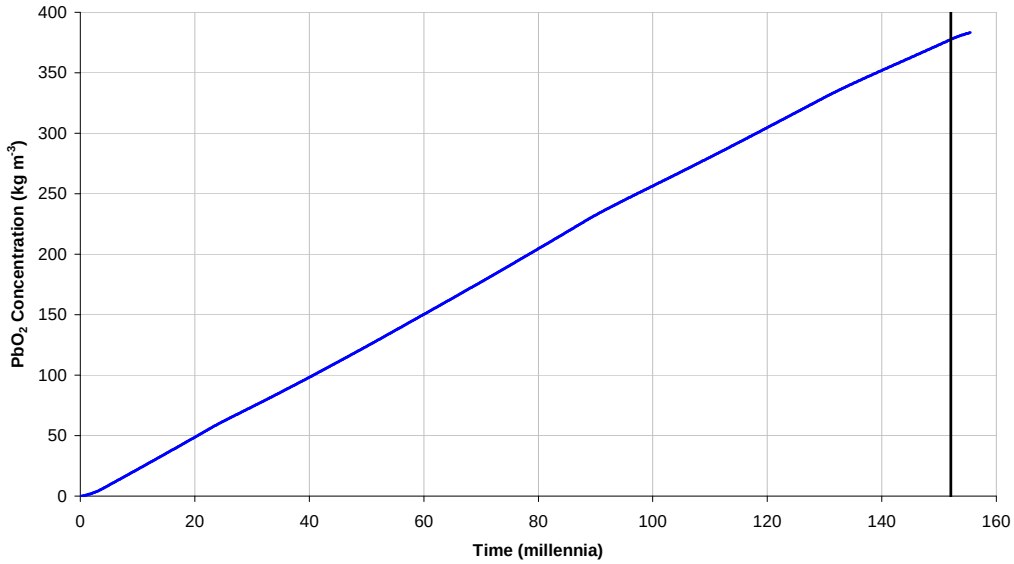

Figure 11: Power as a Function of Time for a 10% Enriched UO_2 System with Radius 0.5 m and Arrival Rate 10^{-9} kg m^{-3} s^{-1}

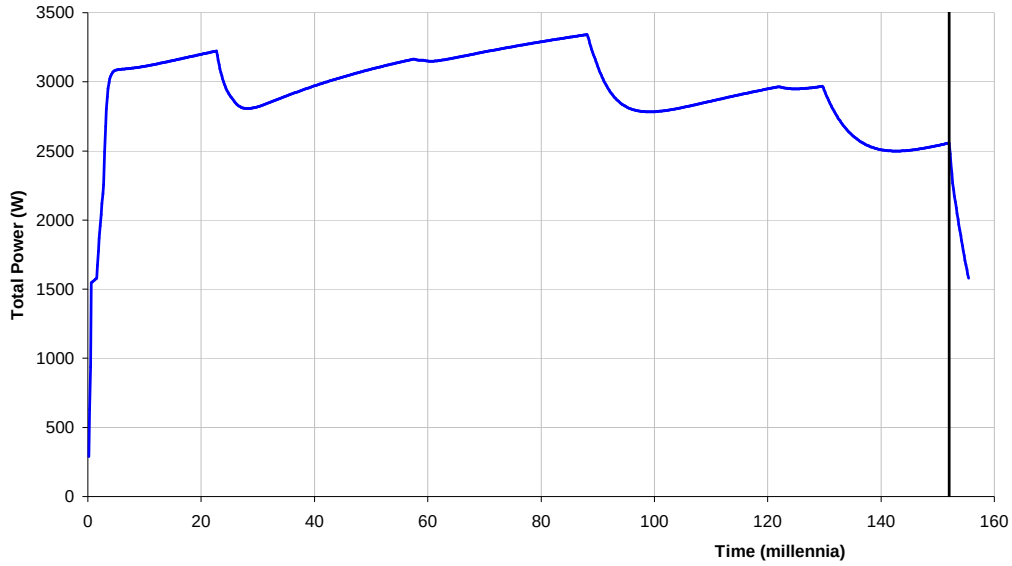

Figure 12: Neutron Flux as a Function of Time for a 10% Enriched UO_2 System with Radius 0.5 m and Arrival Rate 10^{-9} kg m^{-3} s^{-1}

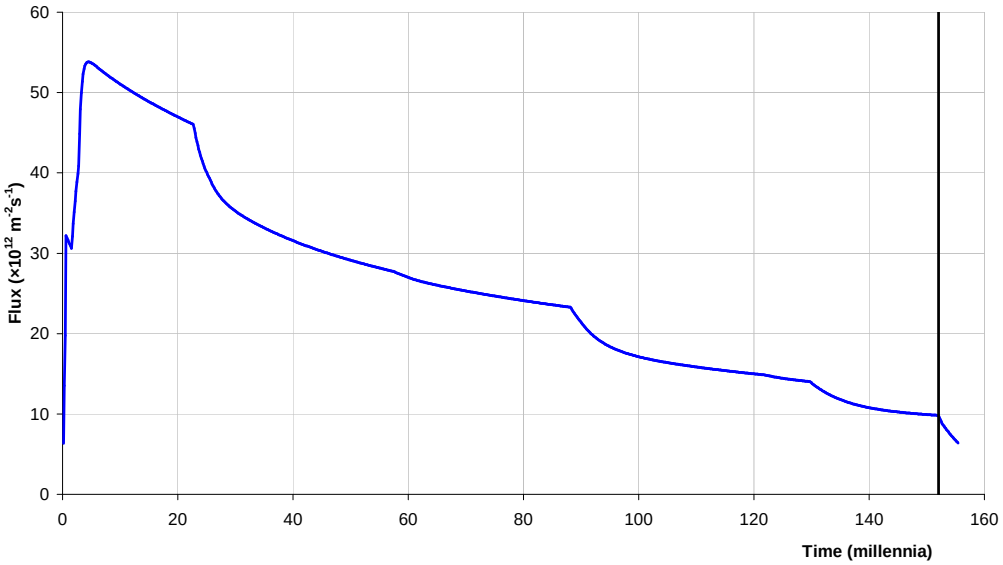

Figure 13: Initial Increase in Temperature for a 10% Enriched UO_2 System with Radius 0.5 m and Arrival Rate 5×10^{-10} $kgm^{-3}s^{-1}$. Positive temperature feedback is encountered at a temperature increase of 231 ℃ (absolute temperatur e 271 ℃)

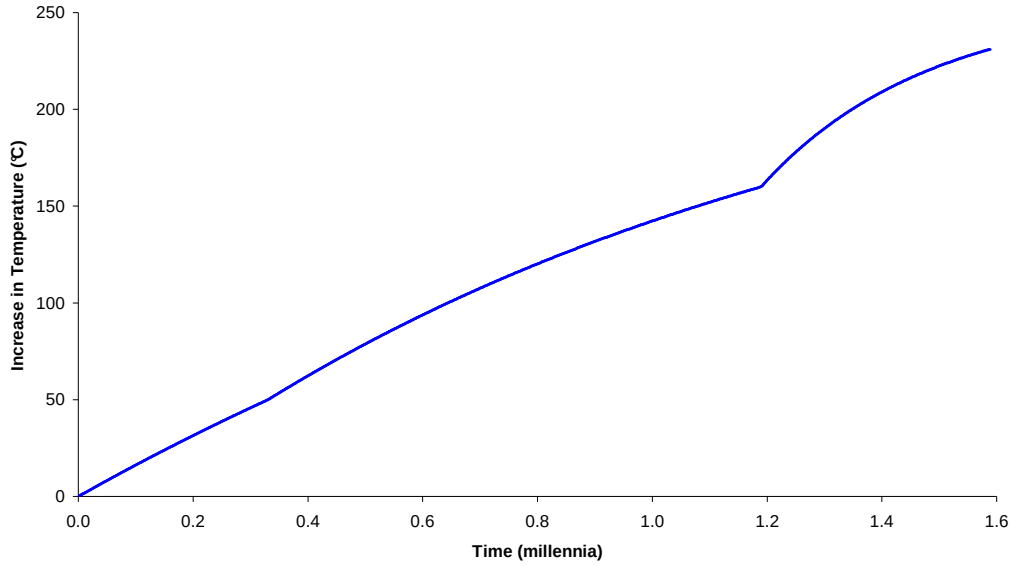

Figure 14: Reactivity as a Function of Temperature for an Initially 10% Enriched UO_2 Critical System upon the Onset of Pore Water Boiling. Arrival Rate 5×10^{-10} kg m^{-3} s^{-1}

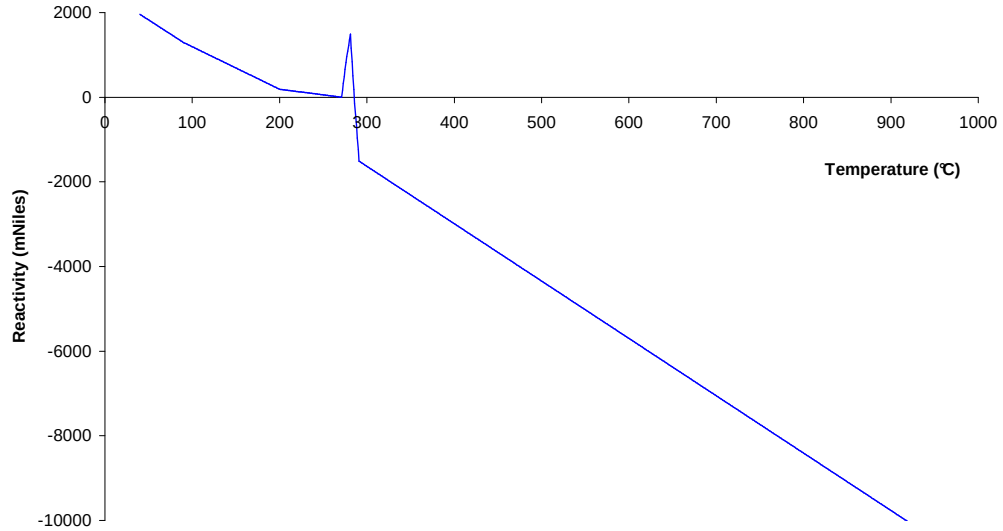

Figure 15: Temperature Increase as a Function of Time for a 10% Enriched UO_2 System with Radius 0.5 m and Arrival Rate 5×10^{-10} kg m^{-3} s^{-1}

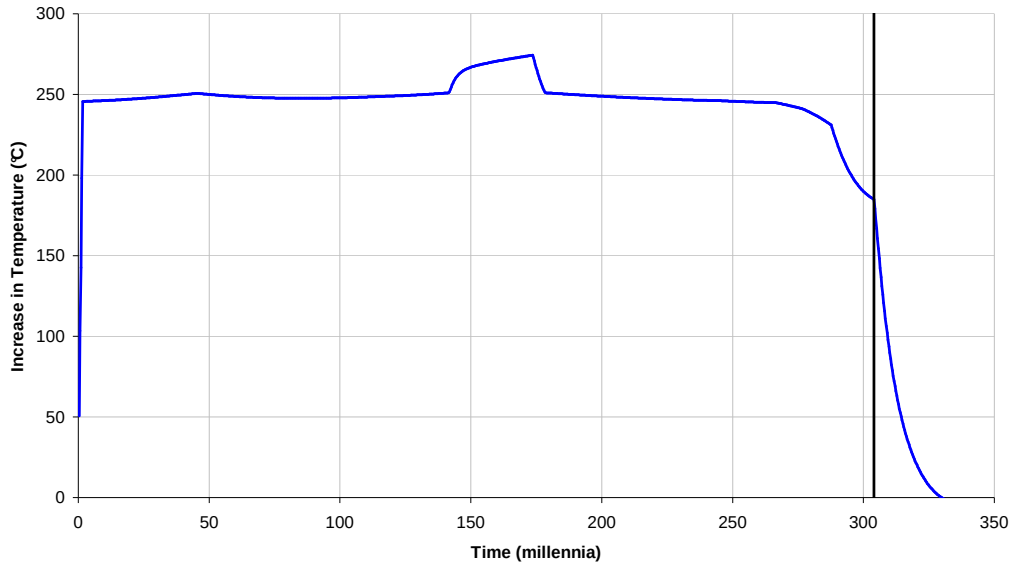

Figure 16: Power as a Function of Time for a 10% Enriched UO_2 System with Radius 0.5 m and Arrival Rate 5×10^{-10} kg m^{-3} s^{-1}

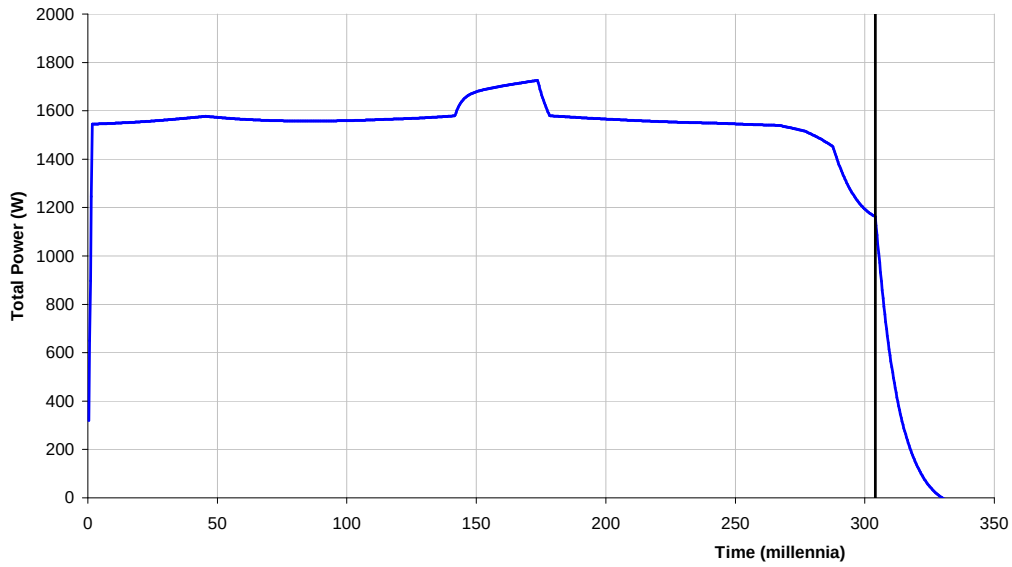

Figure 17: Neutron Flux as a Function of Time for a 10% Enriched UO_2 System with Radius 0.5 m and Arrival Rate 5×10^{-10} kg m^{-3} s^{-1}

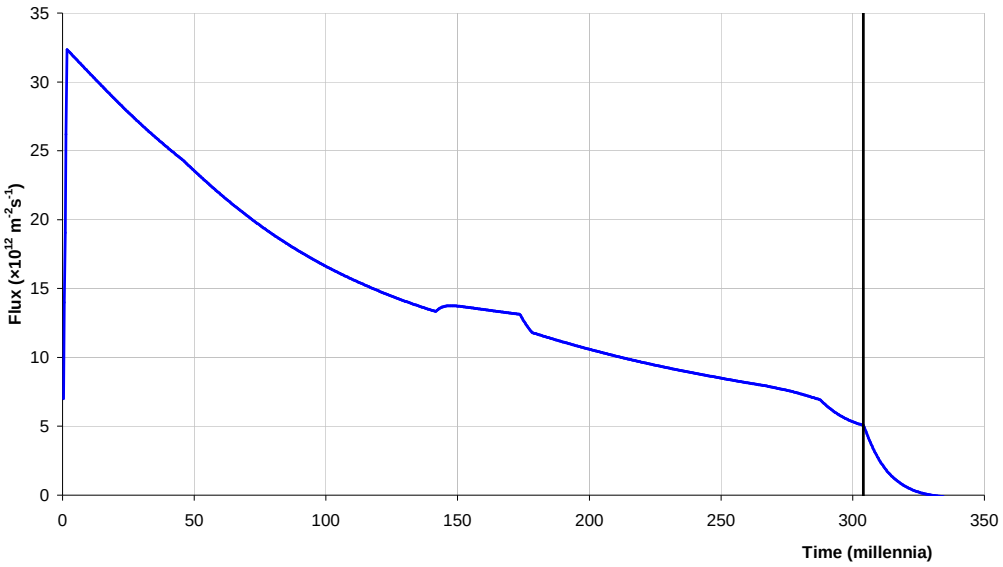

Figure 18: Density of H_2O as a Function of Temperature used for QSS Calculations in Mudstone

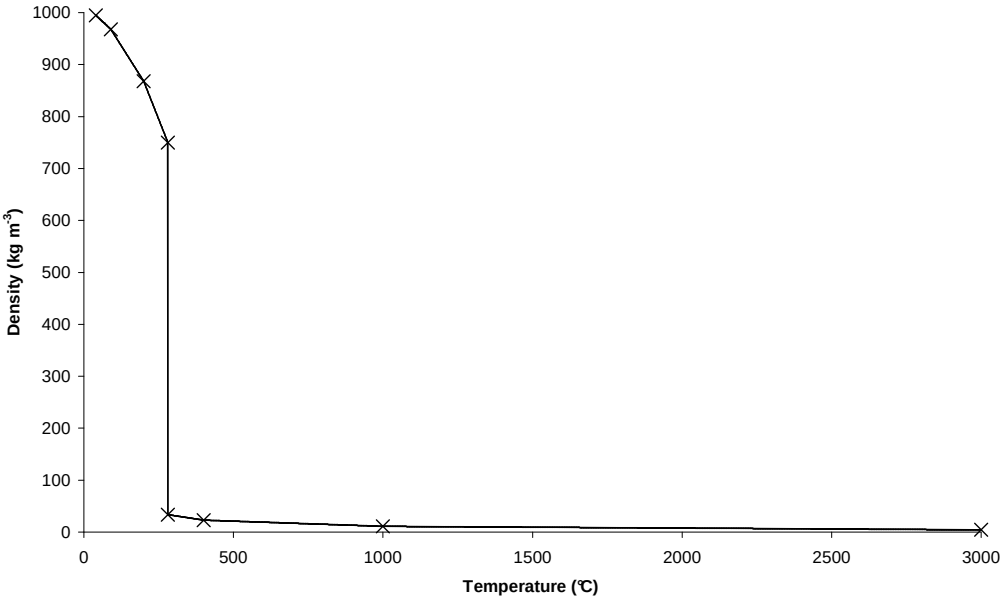

Figure 19: Reactivity as a Function of Temperature for a $^{235}UO_2$ Critical System with Radius 1.1025 m in Mudstone

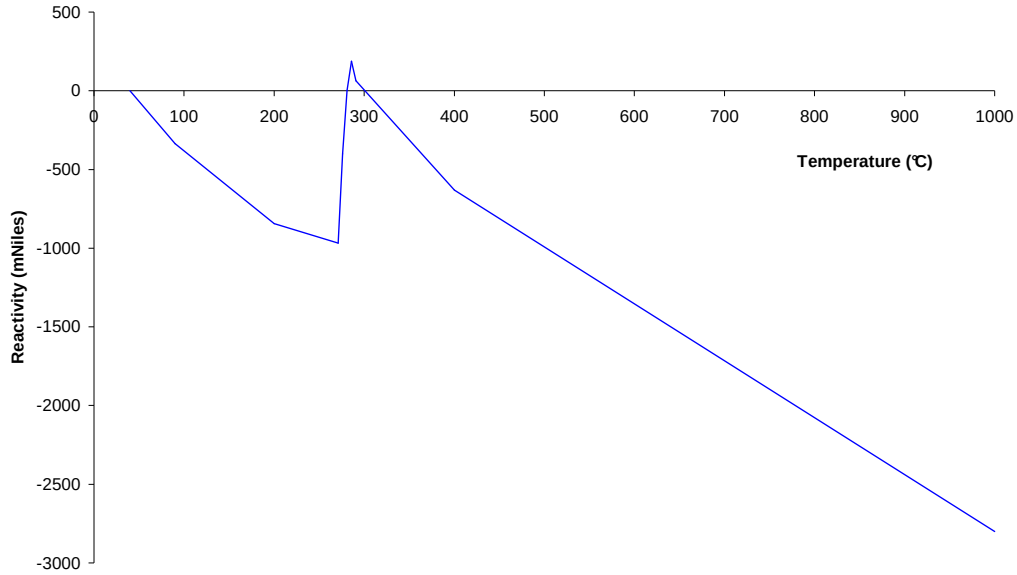

Figure 20: Reactivity as a Function of Temperature at the Composition of 5 kg m^{-3} $^{235}UO_2$ and Selected Concentrations of $^{236}UO_2$ and PbO_2 kg m^{-3} in Mudstone

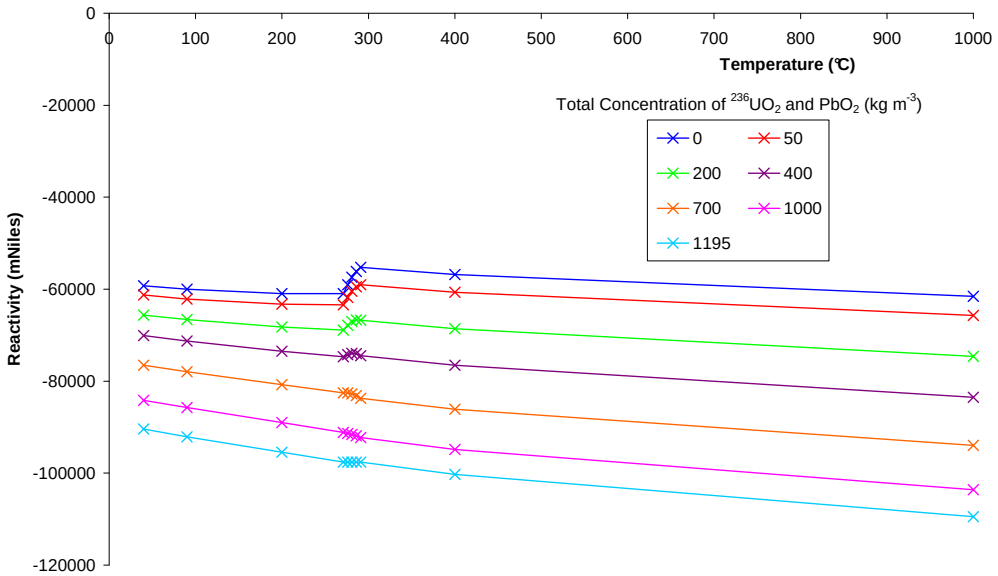

Figure 21: Reactivity as a Function of Temperature at the Composition of 11.27 kg m^{-3} $^{235}UO_2$ and Selected Concentrations of $^{236}UO_2$ and PbO_2 kg m^{-3} in Mudstone

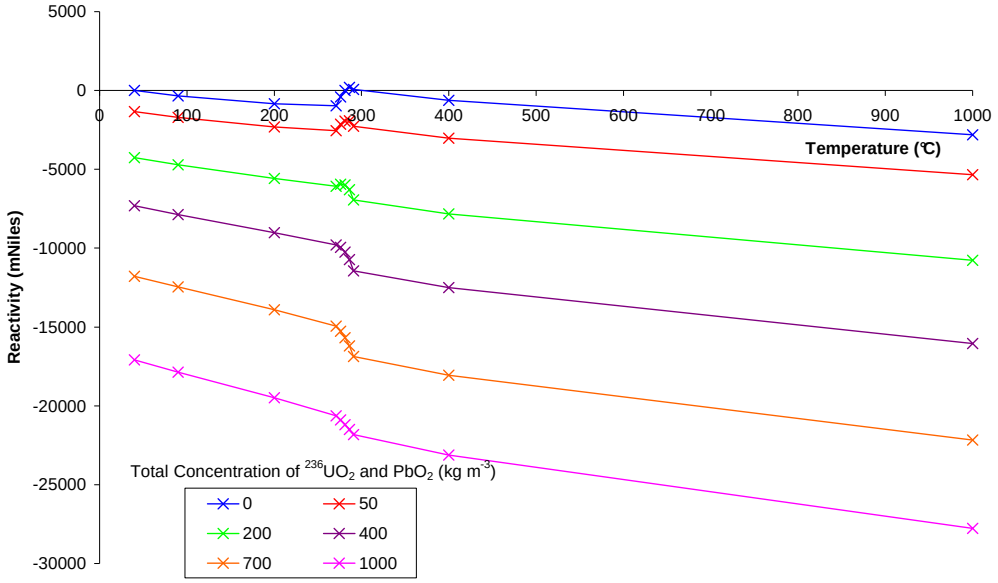

Figure 22: Reactivity as a Function of Temperature at the Composition of 20 kg m^{-3} $^{235}UO_2$ and Selected Concentrations of $^{236}UO_2$ and PbO_2 kg m^{-3} in Mudstone

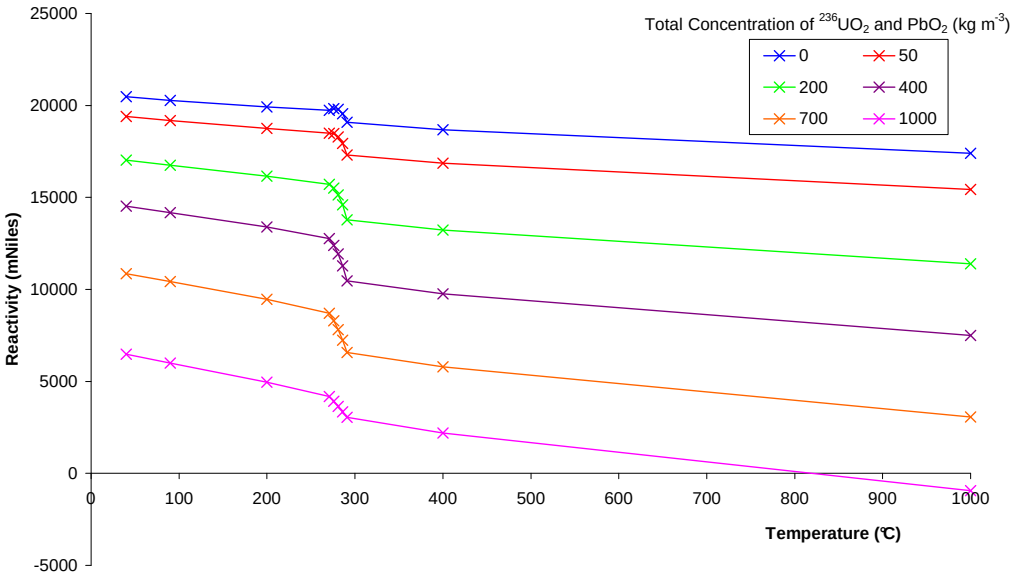

Figure 23: Reactivity as a Function of Temperature at the Composition of 50 kg m^{-3} $^{235}UO_2$ and Selected Concentrations of $^{236}UO_2$ and PbO_2 kg m^{-3} in Mudstone

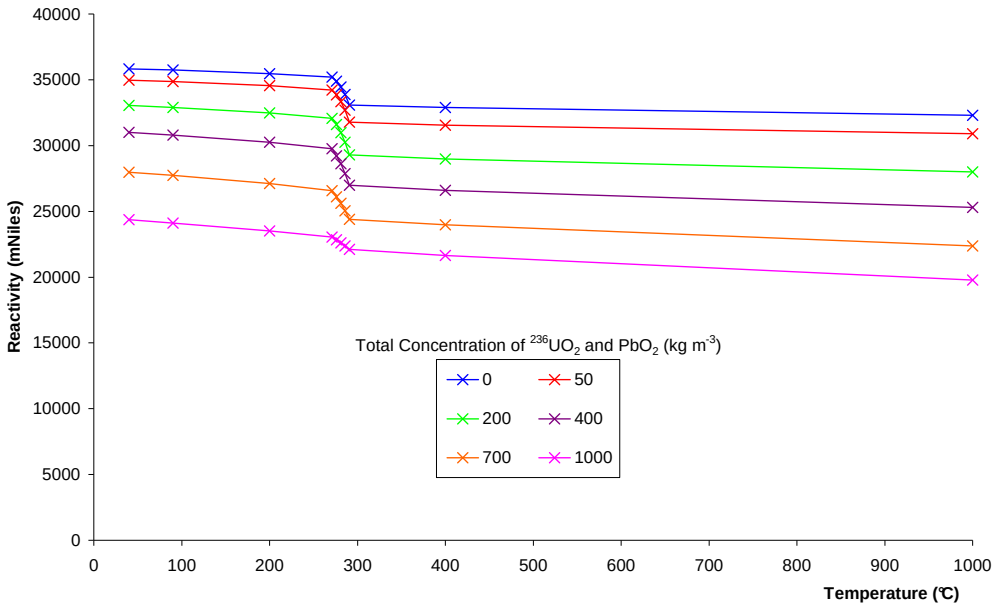

Figure 24: Temperature Increase as a Function of Time for Mudstone QSS Calculations at Various Arrival Rates

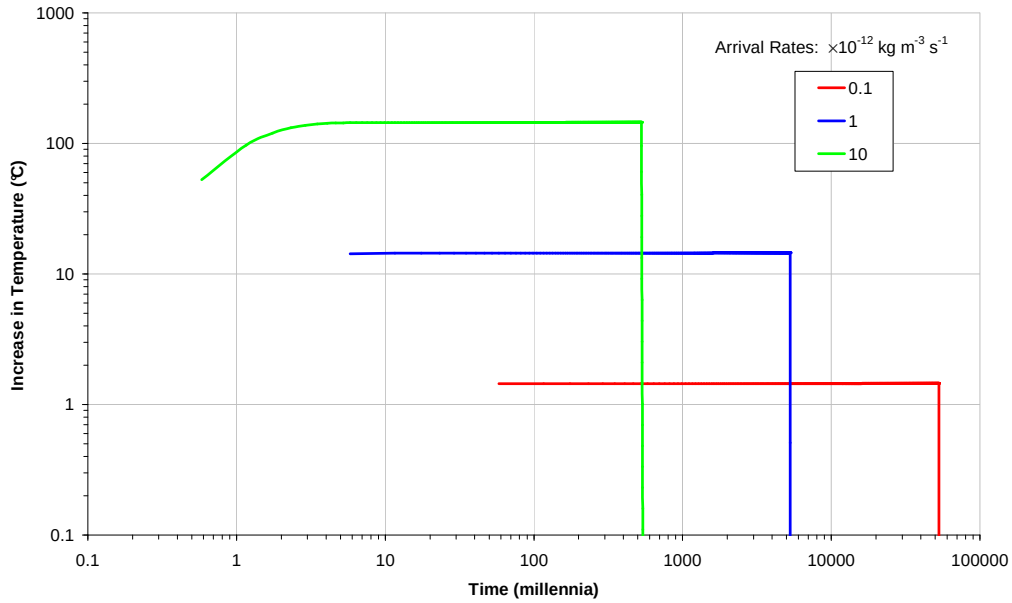

Figure 25: $^{235}UO_2$ Concentration as a Function of Time for Mudstone QSS Calculations at Various Arrival Rates

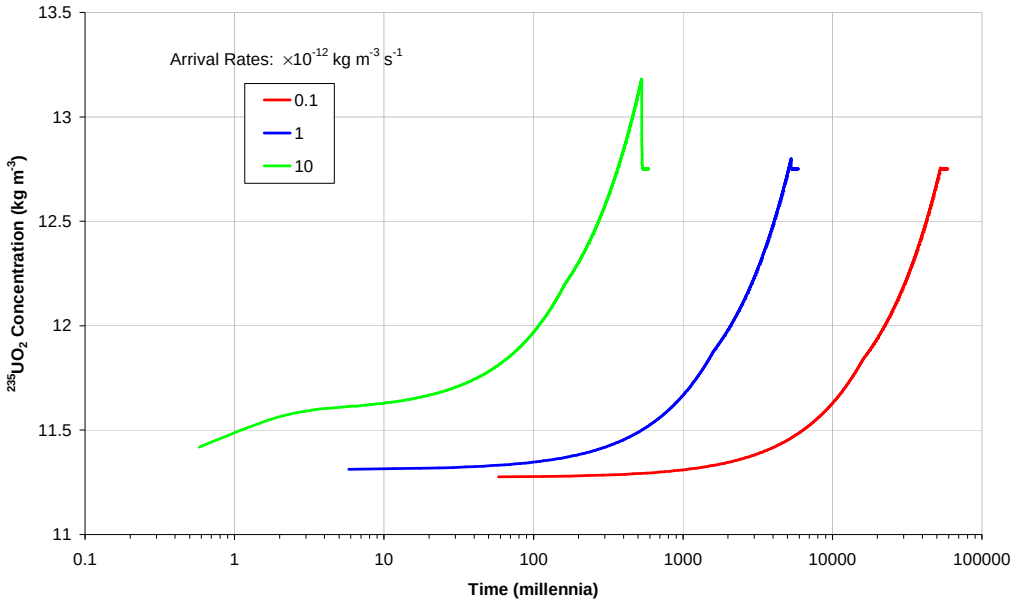

Figure 26: $^{236}UO_2$ Concentration as a Function of Time for Mudstone QSS Calculations at Various Arrival Rates

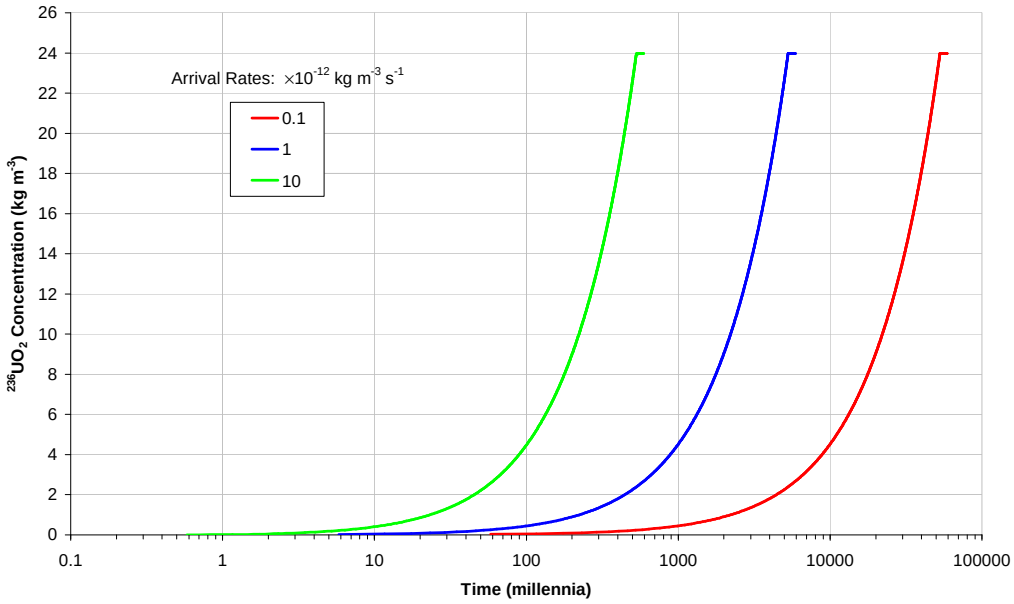

Figure 27: PbO_2 Concentration as a Function of Time for Mudstone QSS Calculations at Various Arrival Rates

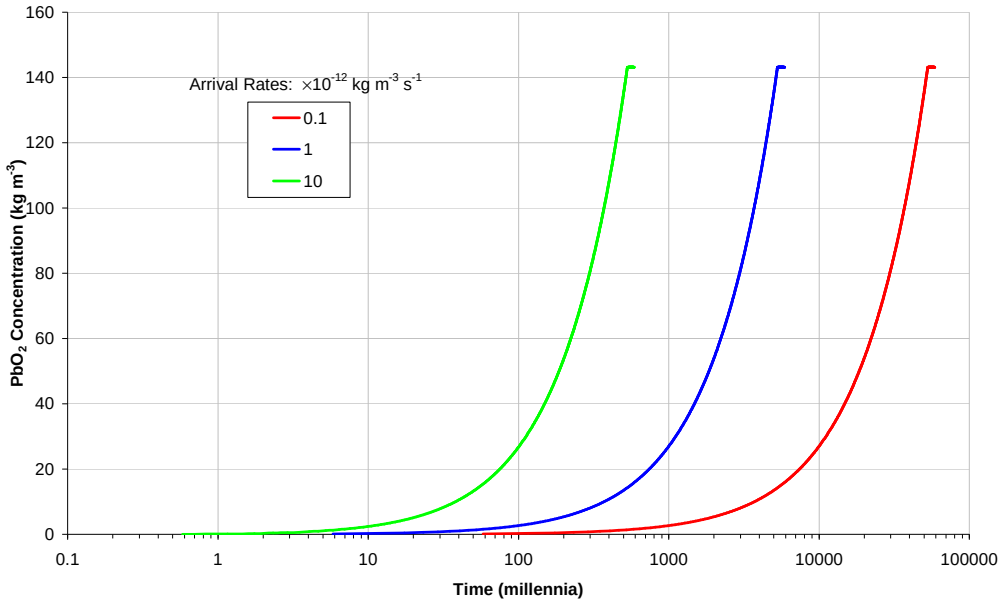

Figure 28: Power as a Function of Time for Mudstone QSS Calculations at Various Arrival Rates

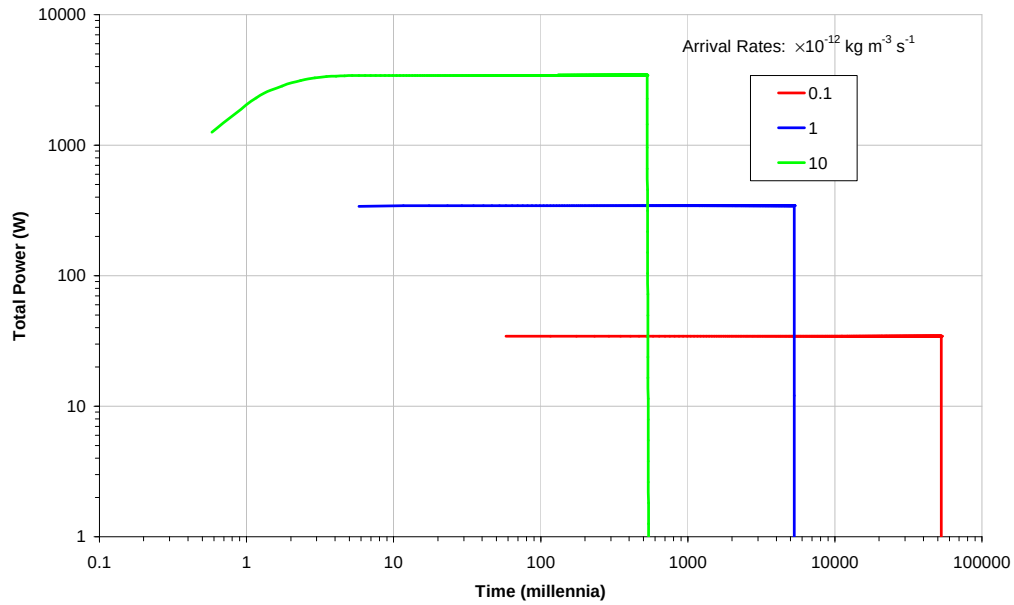

Figure 29: Neutron Flux as a Function of Time for Mudstone QSS Calculations at Various Arrival Rates

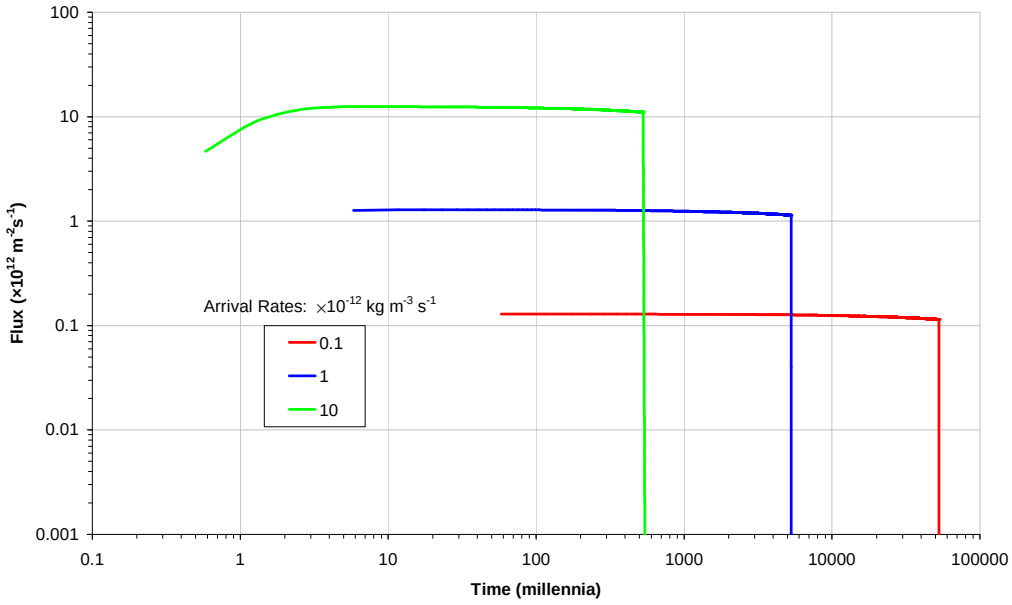

Figure 30: Development of a New Enthalpy Function for NRVB. The function is compared to the older version, and a function derived as an independent check during verification testing

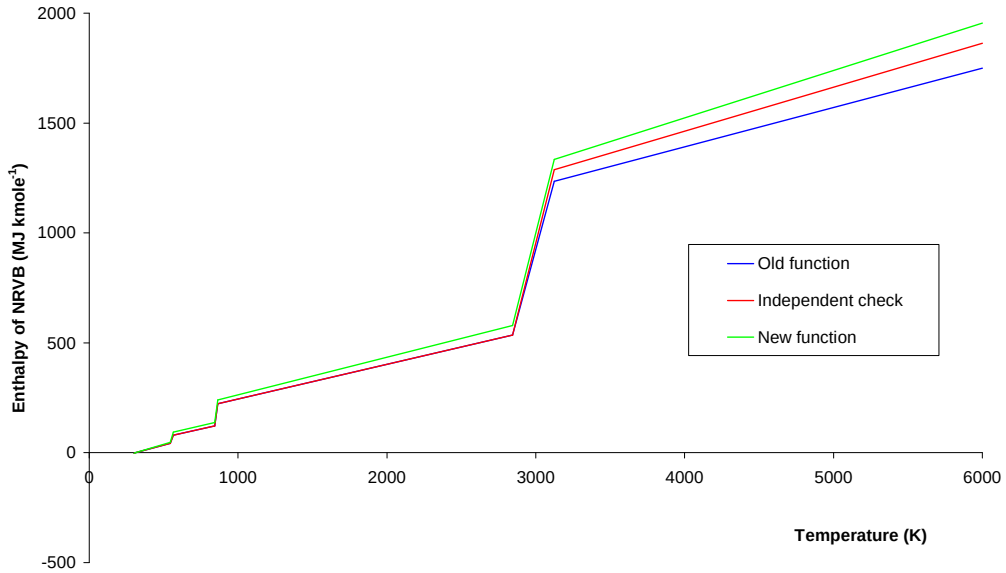

Figure 31: Modifications to the Function f_s for NRVB Calculations. This function is used in the Equation of State for NRVB

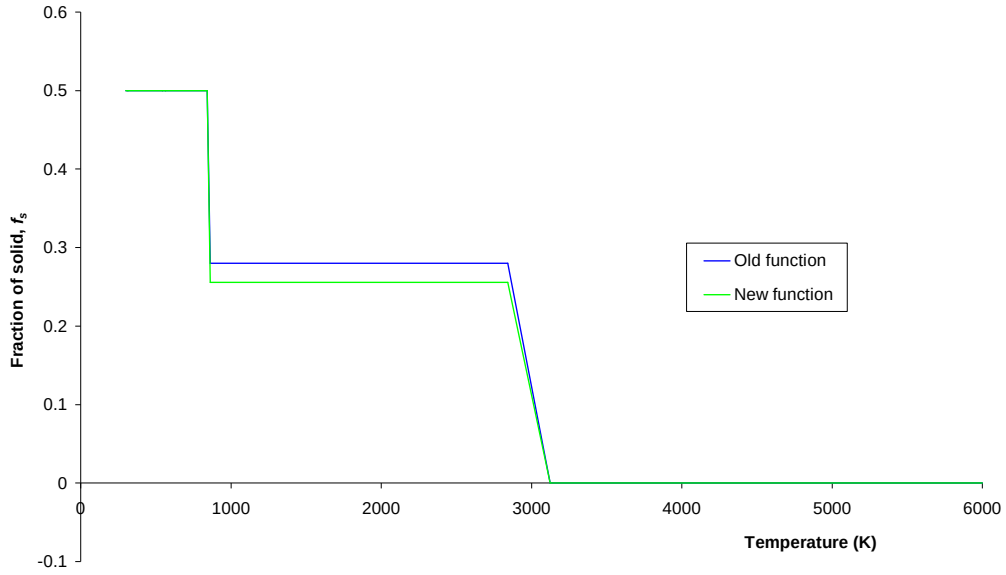

Figure 32: Modifications to the Function θ for NRVB Calculations. This function is used in the Equation of State for NRVB

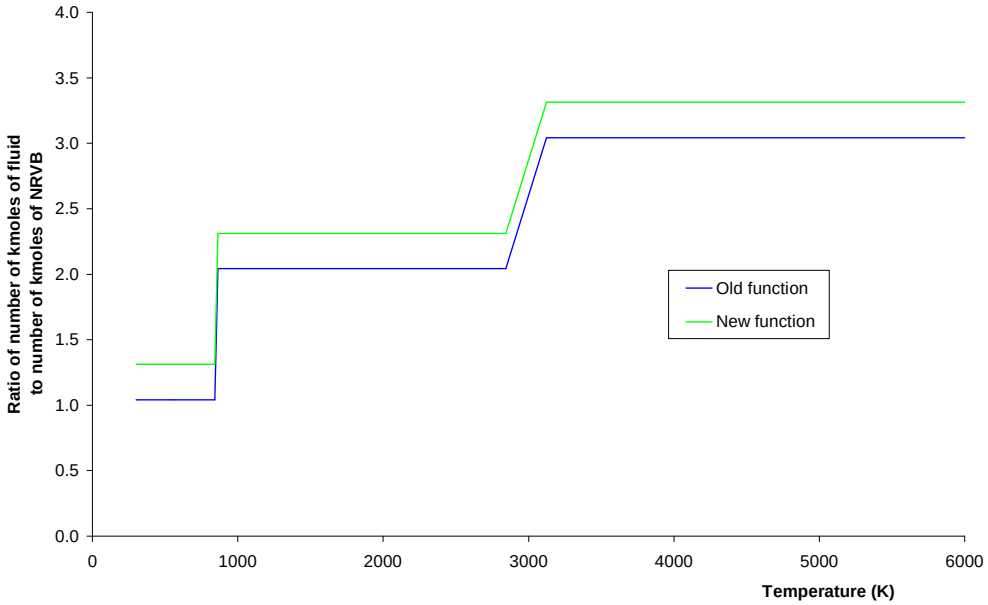

Figure 33: Reactivity as a Function of Radius at Each Temperature for which WIMS9 Calculations are Undertaken for the RTM Model with 3.684 kg of $^{239}PuO_2$ in NRVB. The system is initially just critical

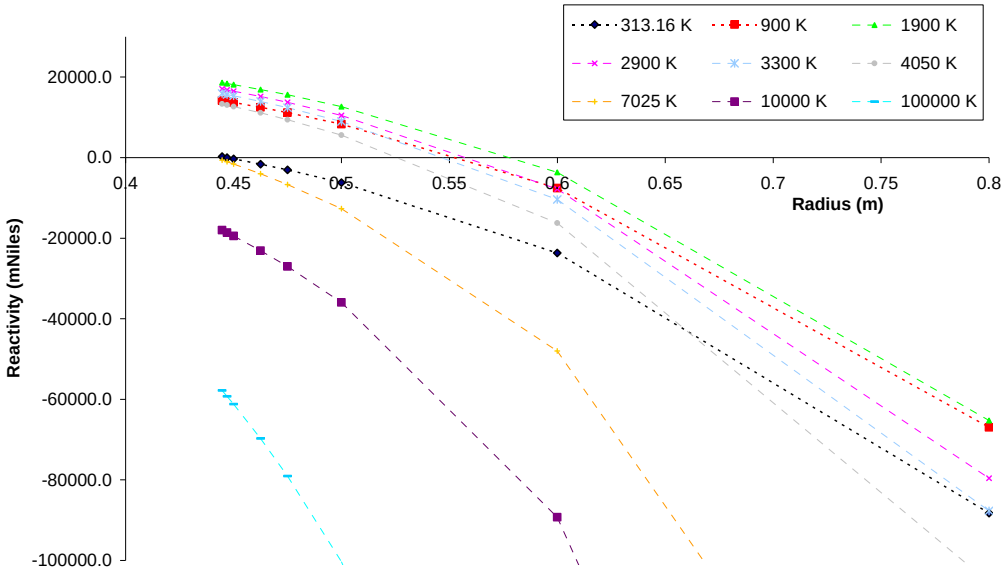

Figure 34: Reactivity as a Function of Radius at Each Temperature for which WIMS9 Calculations are Undertaken for the RTM Model with 10 kg of $^{239}PuO_2$ in NRVB. The system is initially just critical

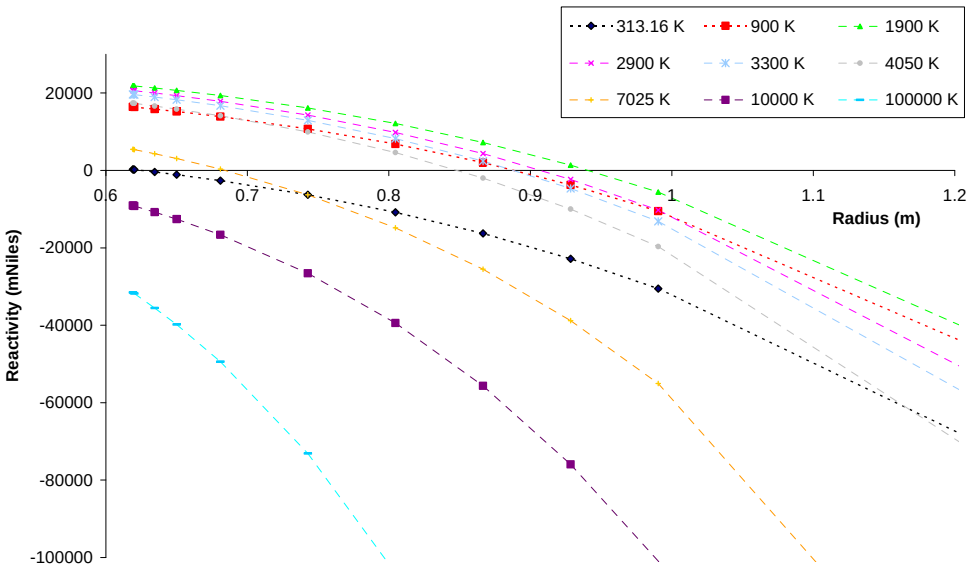

Figure 35: Reactivity as a Function of Radius at Each Temperature for which WIMS9 Calculations are Undertaken for the RTM Model with 100 kg of $^{239}PuO_2$ in NRVB. The system is initially just critical

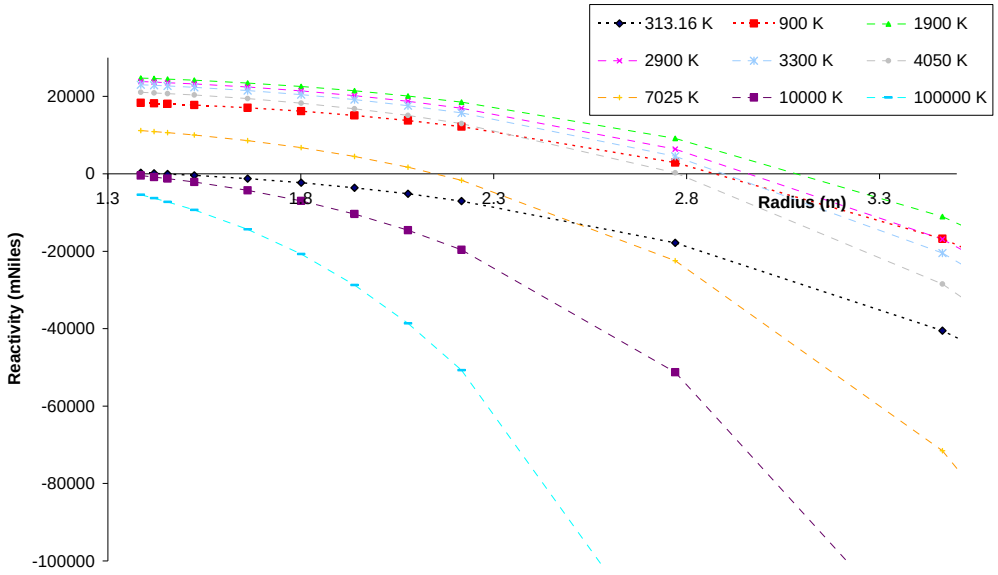

Figure 36: Reactivity as a Function of Radius at Each Temperature for which WIMS9 Calculations are Undertaken for the RTM Model with 200 kg of $^{239}PuO_2$ in NRVB. The system is initially just critical

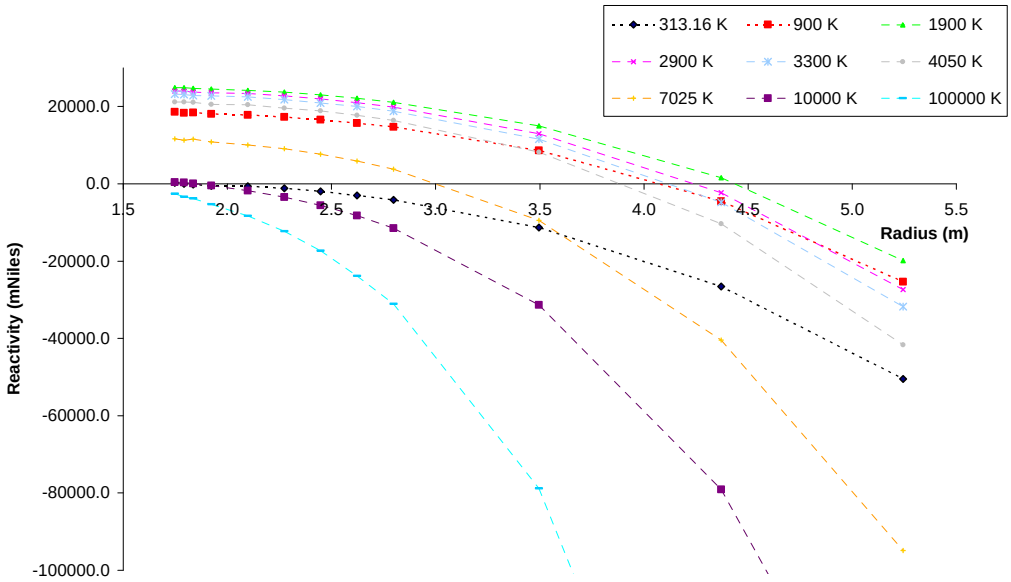

Figure 37: Reactivity as a Function of Radius at Each Temperature for which WIMS9 Calculations are Undertaken for the RTM Model with 1000 kg of $^{239}PuO_2$ in NRVB. The system is initially just critical

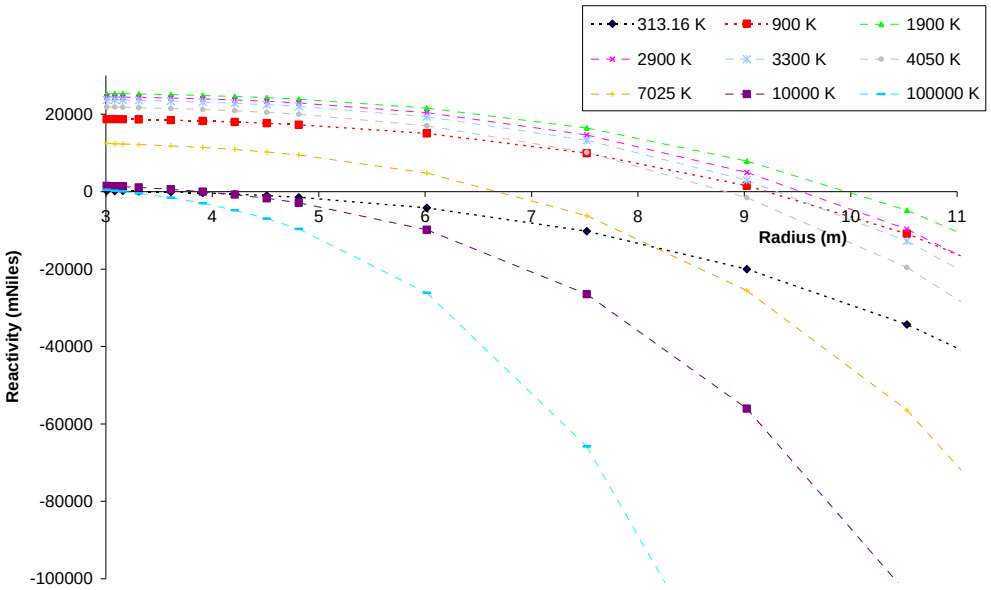

Figure 38: The Relationship between System Mass and Radius for Just Critical $^{239}PuO_2$ systems in NRVB

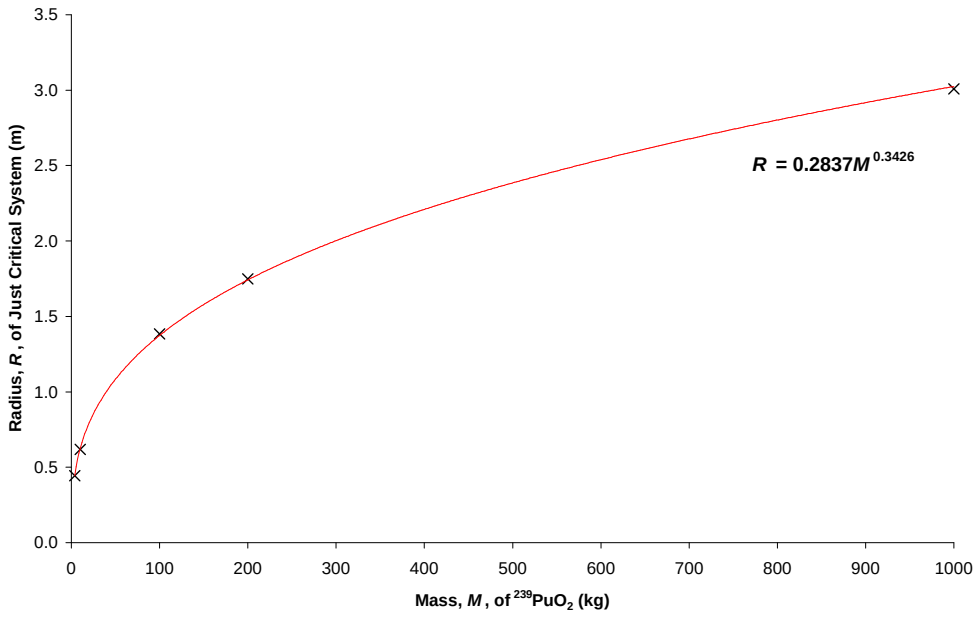

Figure 39: Reactivity as a Function of Radius at Each Temperature for which WIMS9 Calculations are Undertaken for the RTM Model with 15.7 kg of $^{235}UO_2$ in NRVB. The system is initially just critical

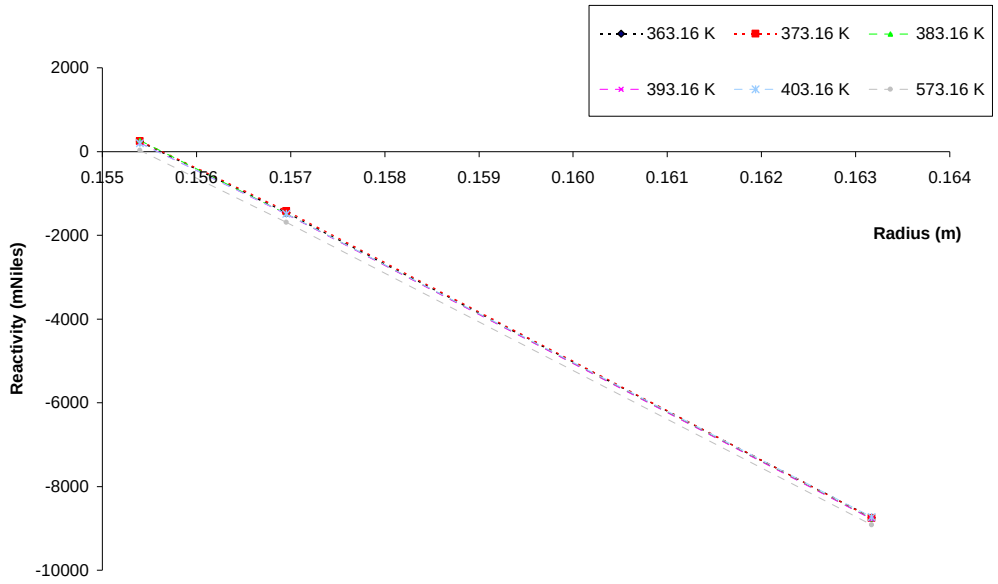

Figure 40: A Zoom of Figure 39 at Radii Close to the Initial Value

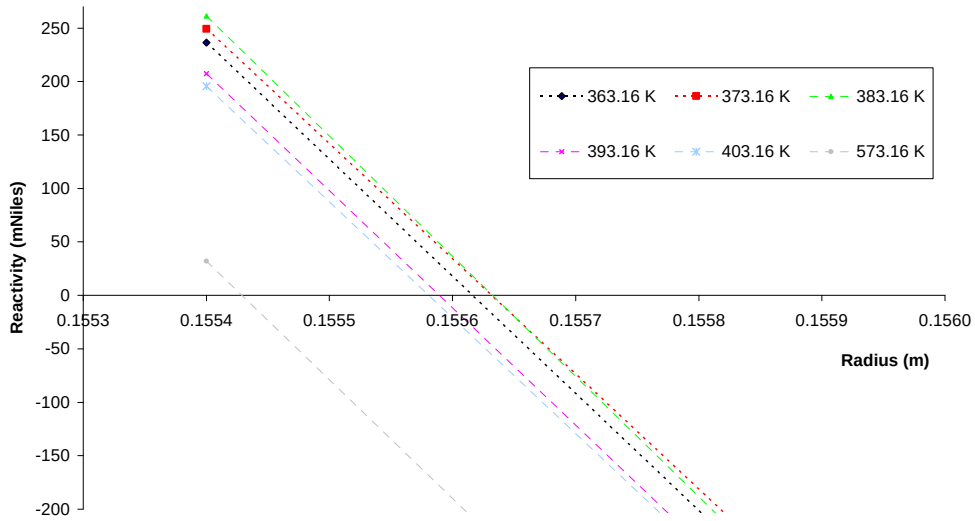

Figure 41: Reactivity as a Function of Radius at Each Temperature for which WIMS9 Calculations are Undertaken for the RTM Model with 13.4 kg of $^{239}PuO_2$ in NRVB. The system is initially supercritical

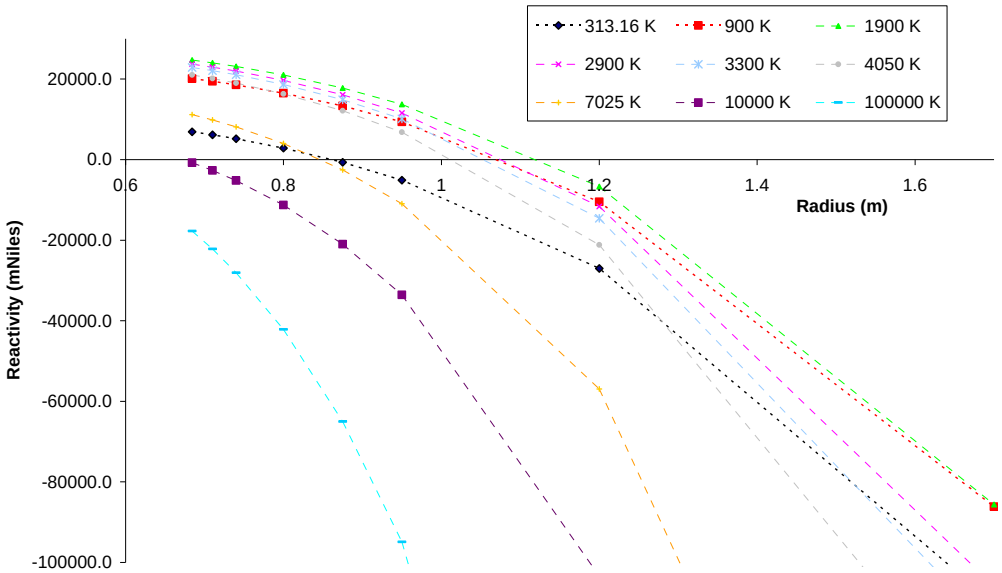

Figure 42: Reactivity as a Function of Radius at Each Temperature for which WIMS9 Calculations are Undertaken for the RTM Model with 200 kg of $^{239}PuO_2$ in NRVB. The system is initially supercritical

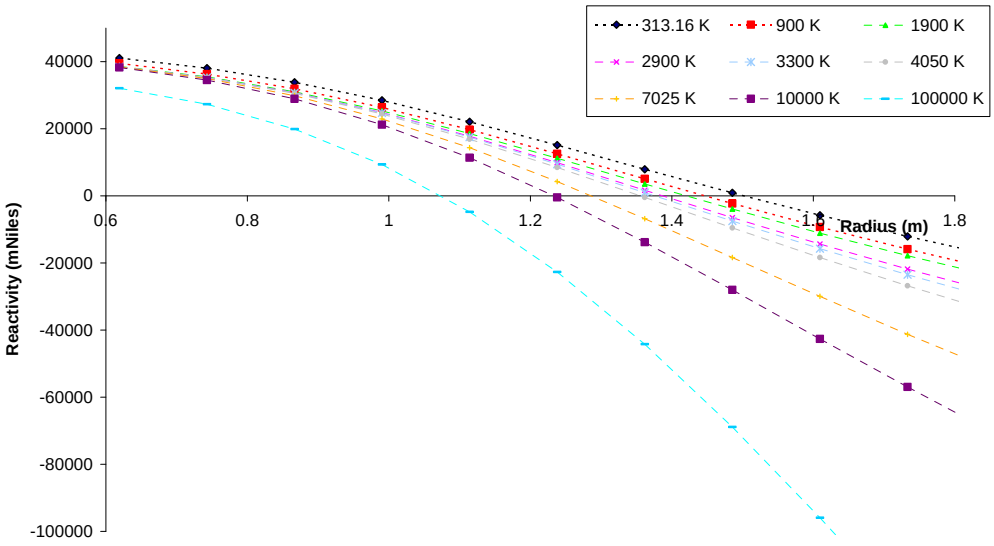

Figure 43: Reactivity as a Function of Radius at Each Temperature for which WIMS9 Calculations are Undertaken for the RTM Model with 500 kg of $^{239}PuO_2$ in Granite. The system is initially just critical

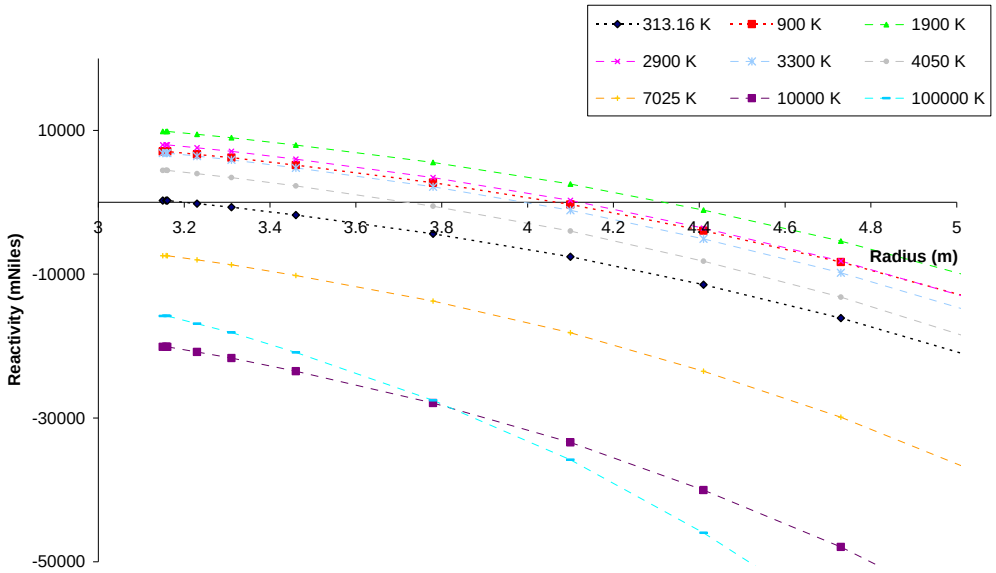

Figure 44: Reactivity as a Function of Radius at Each Temperature for which WIMS9 Calculations are Undertaken for the RTM Model with 988 kg of $^{239}PuO_2$ in Granite. The system is initially just critical

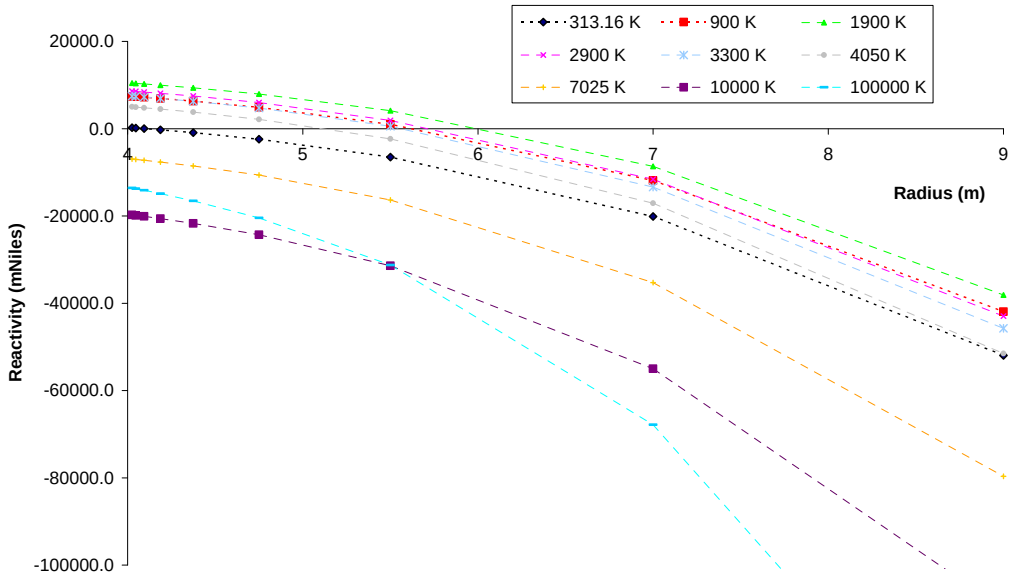

Figure 45: Reactivity vs. Time for Case 4

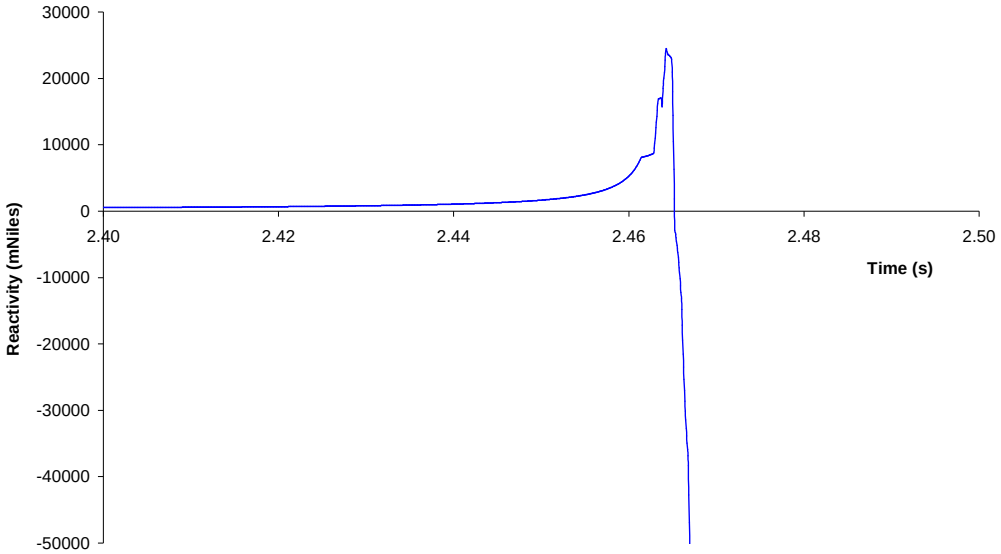

Figure 46: Power History for Case 4

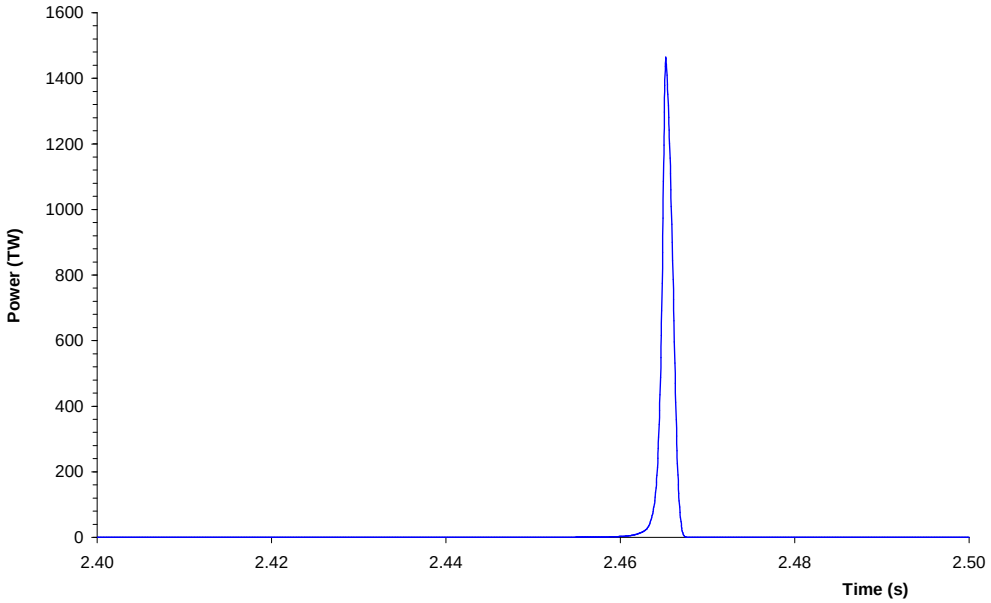

Figure 47: Temperature History for Case 4

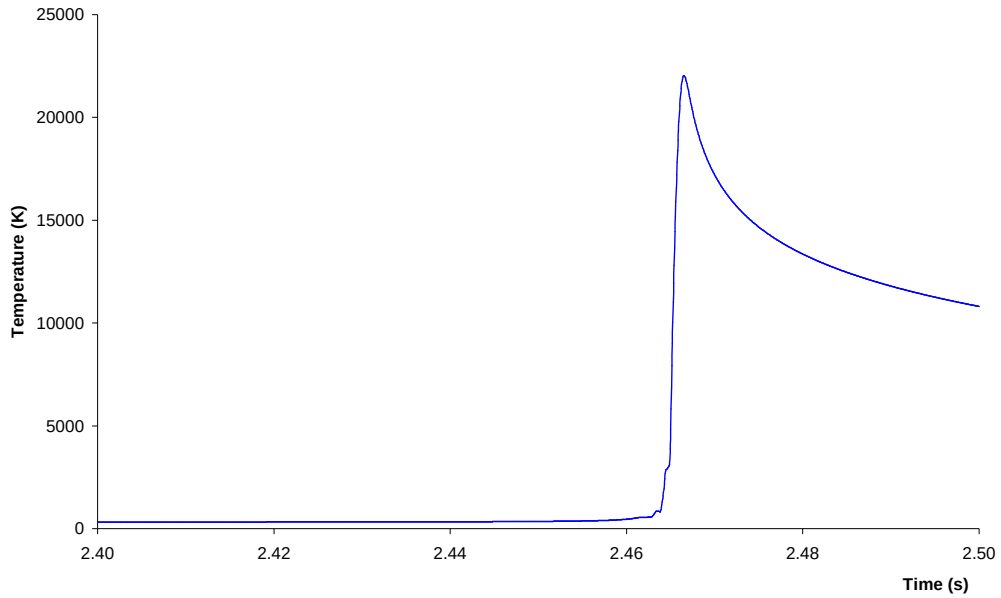

Figure 48: Pressure History for Case 4

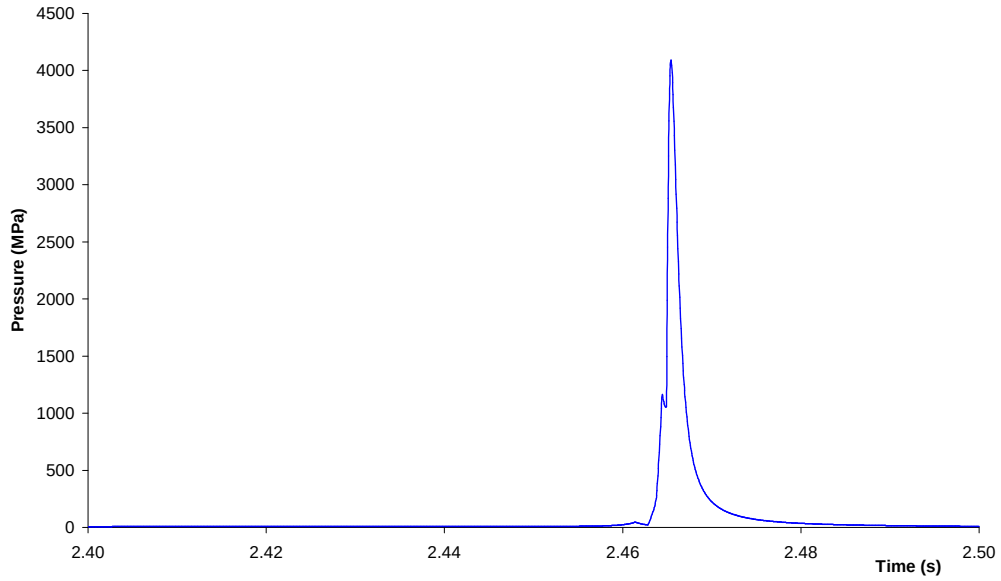

Figure 49: Radius vs. Time for Case 4

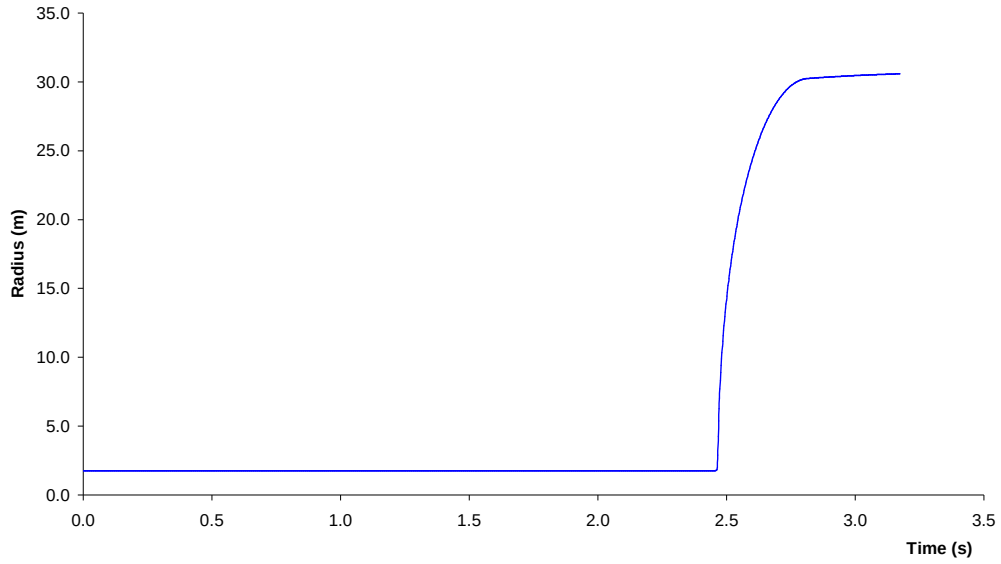

Figure 50: The Relationship between System Mass and Yield for Just Critical $^{239}PuO_2$ systems in NRVB

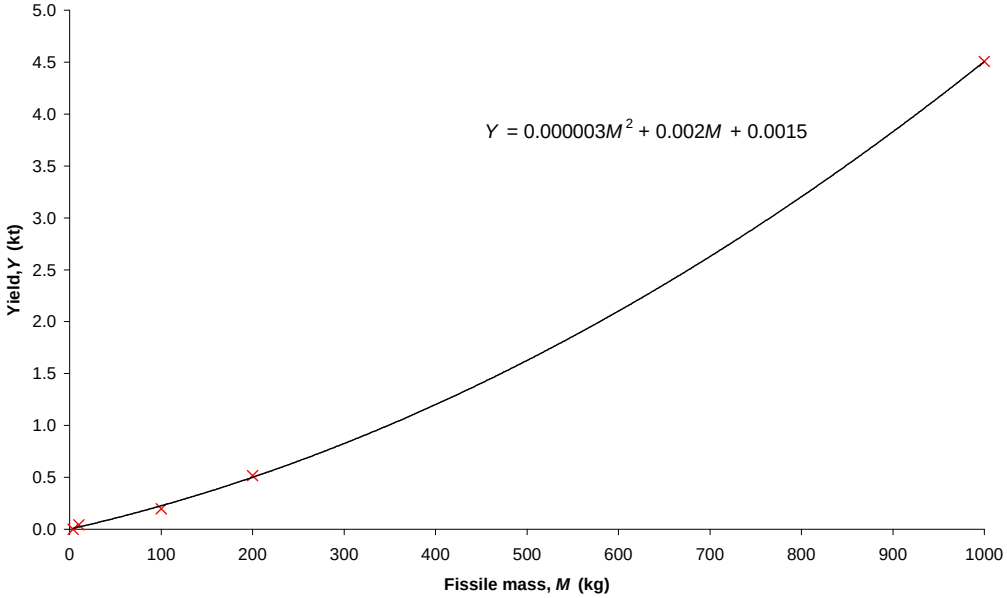

Figure 51: Reactivity vs Time for Case 6

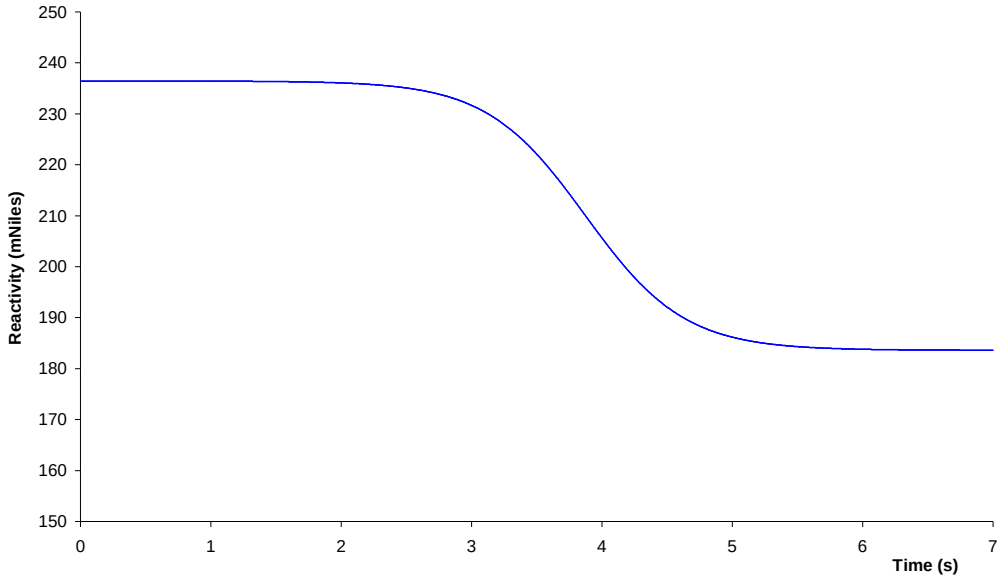

Figure 52: Power History for Case 6

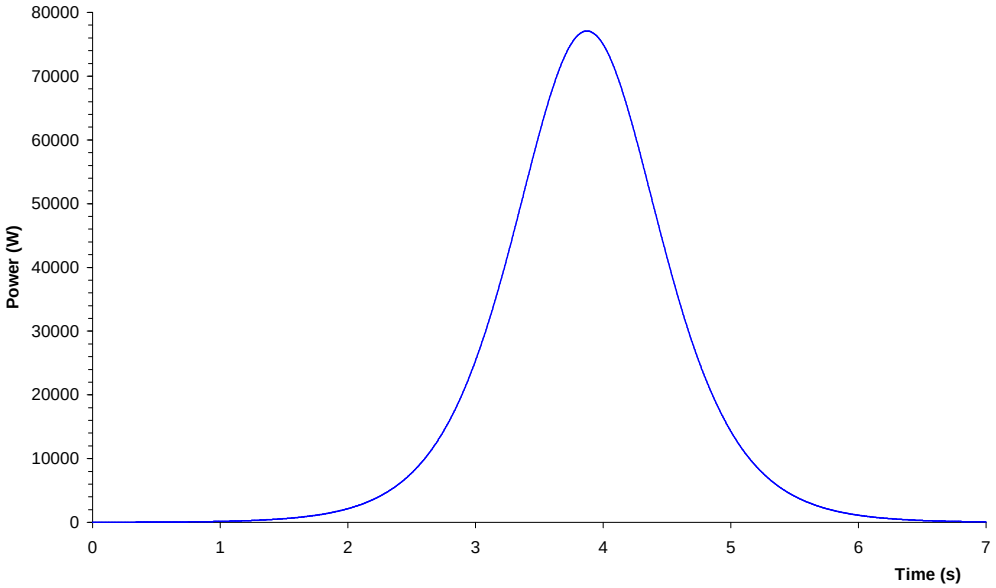

Figure 53: Variation of Flux with Time for the NRVB QSS Transient

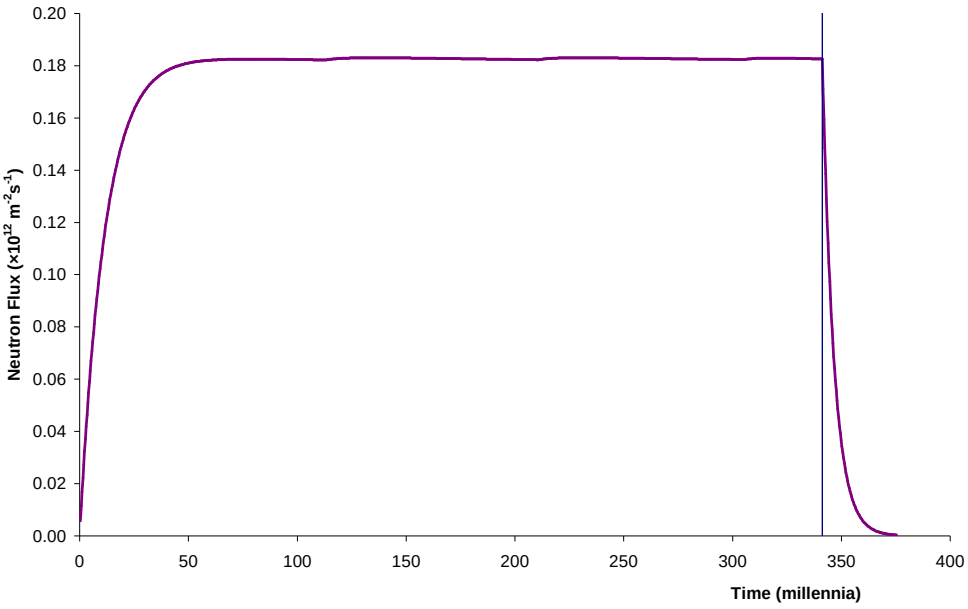

Figure 54: Variation of Power with Time for the NRVB QSS Transient

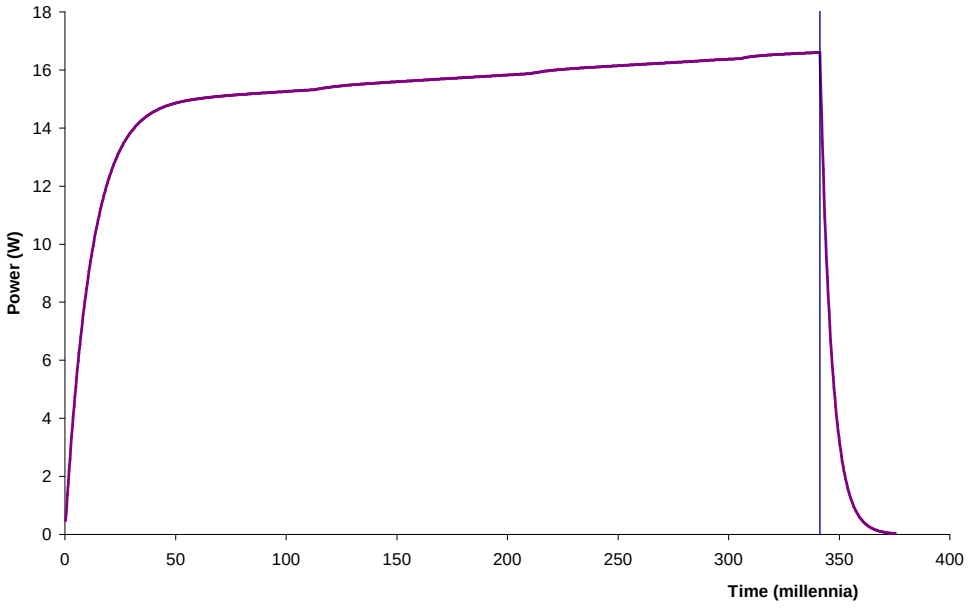

Figure 55: Variation of Temperature with Time for the NRVB QSS Transient

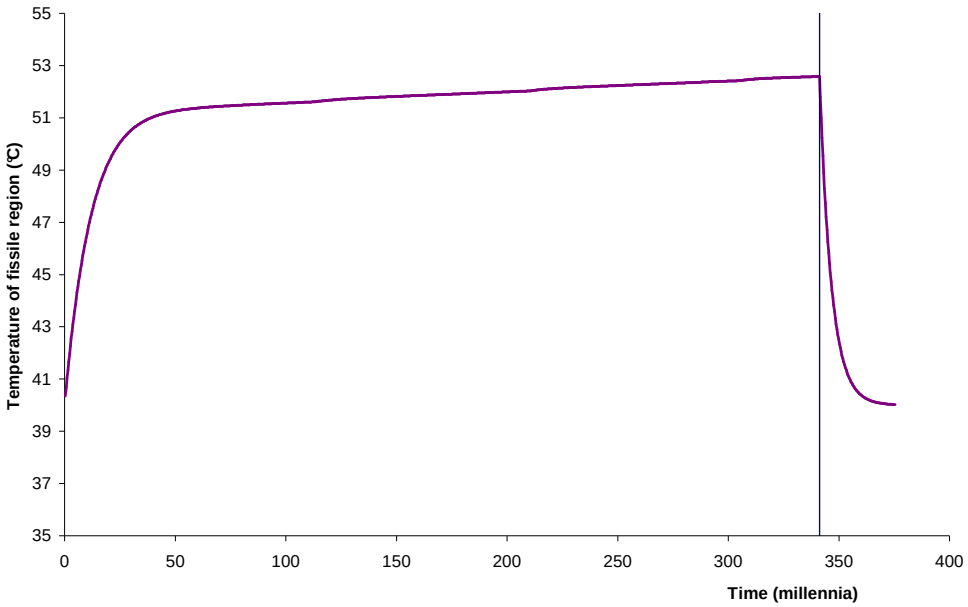

Figure 56: WIMS9 Neutron Energy Spectra

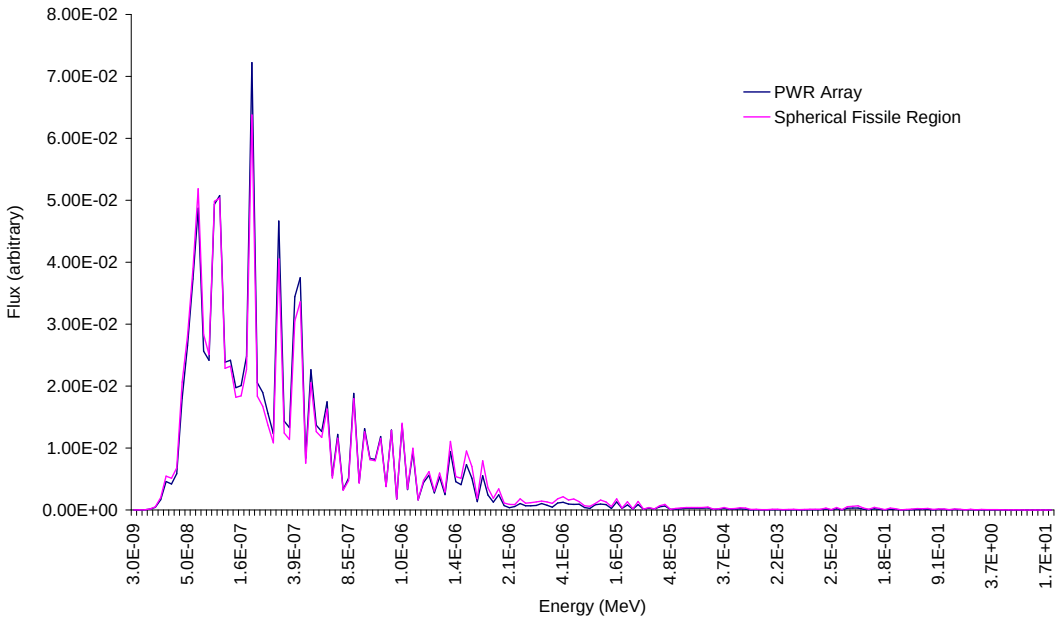

Figure 57: Variation of Power with Time for the NRVB QSS Transient

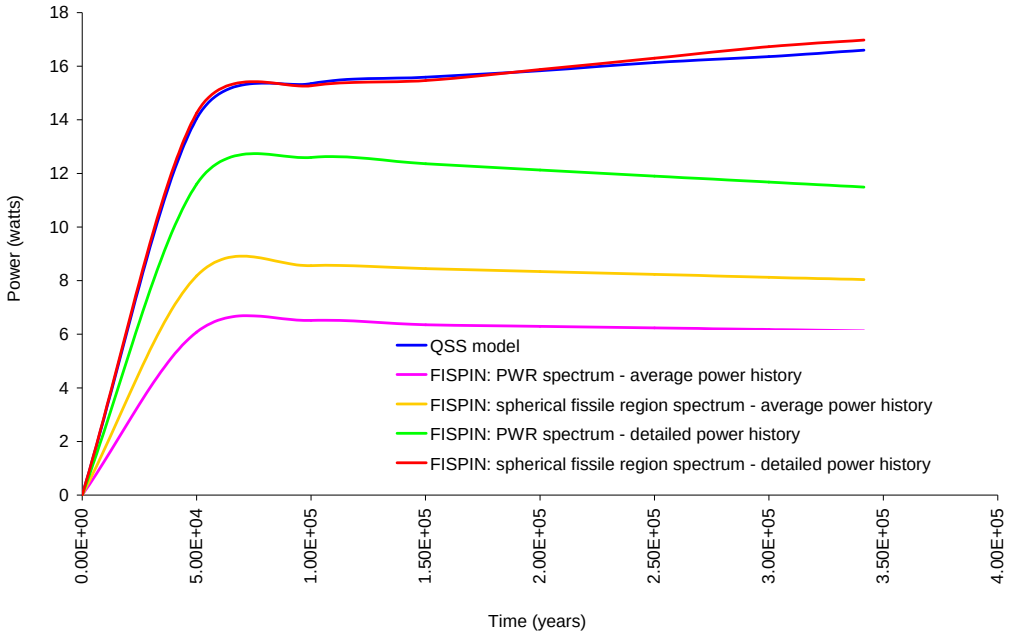

Figure 58: Variation of ^{235}U Mass with Time for the NRVB QSS Transient

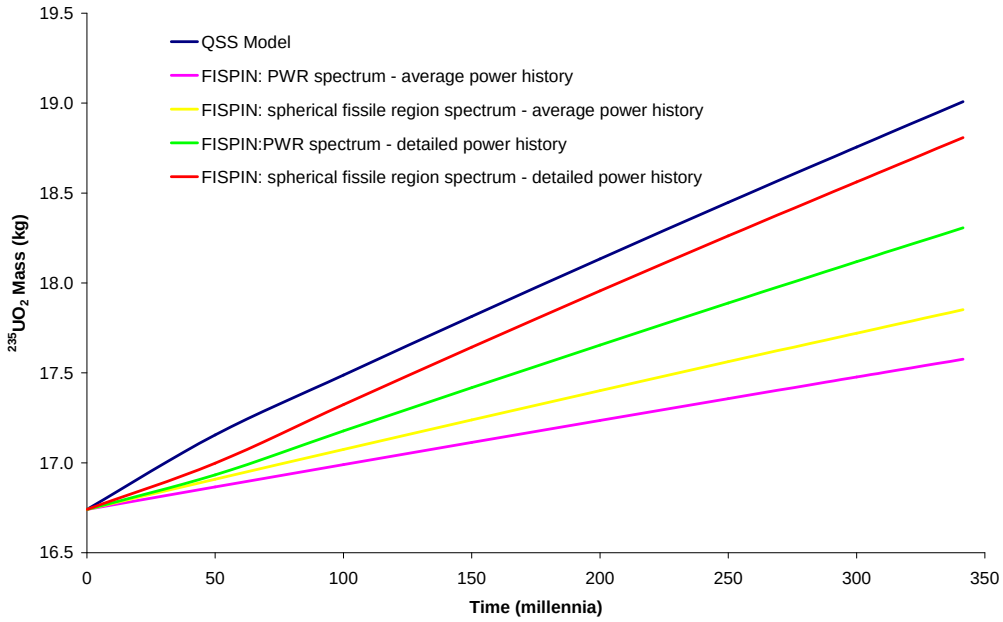

Figure 59: Variation of Fission Product Mass with Time for the NRVB QSS Transient.
FISPIN – PWR Array Spectrum and Average Power History

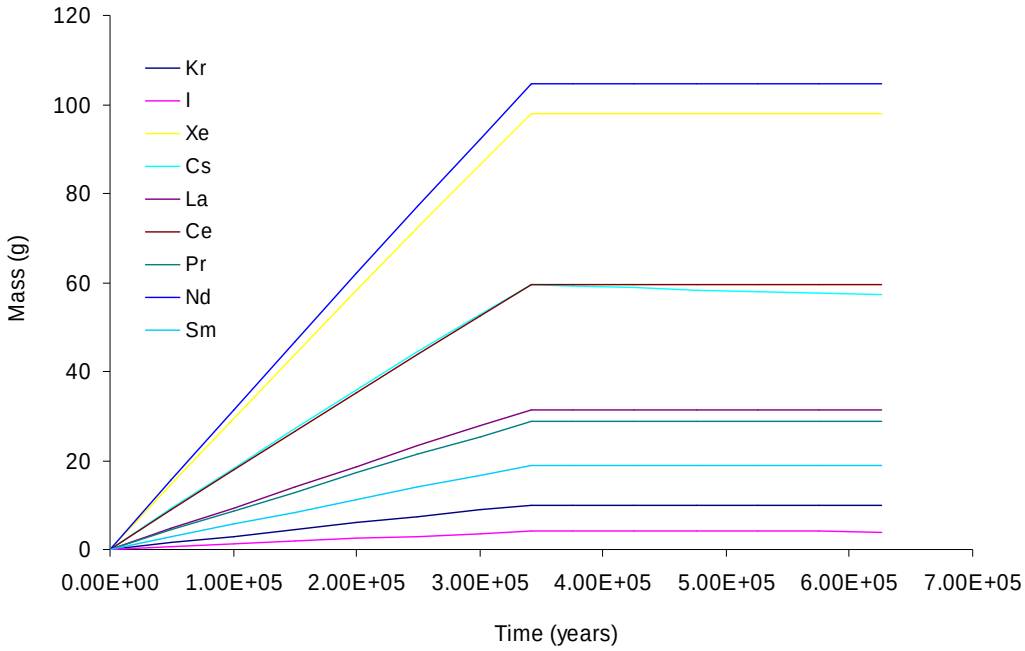

Figure 60: Variation of Fission Product Mass with Time for the NRVB QSS Transient.
FISPIN – Spectrum from a Spherical Fissile Material Region and Average Power History

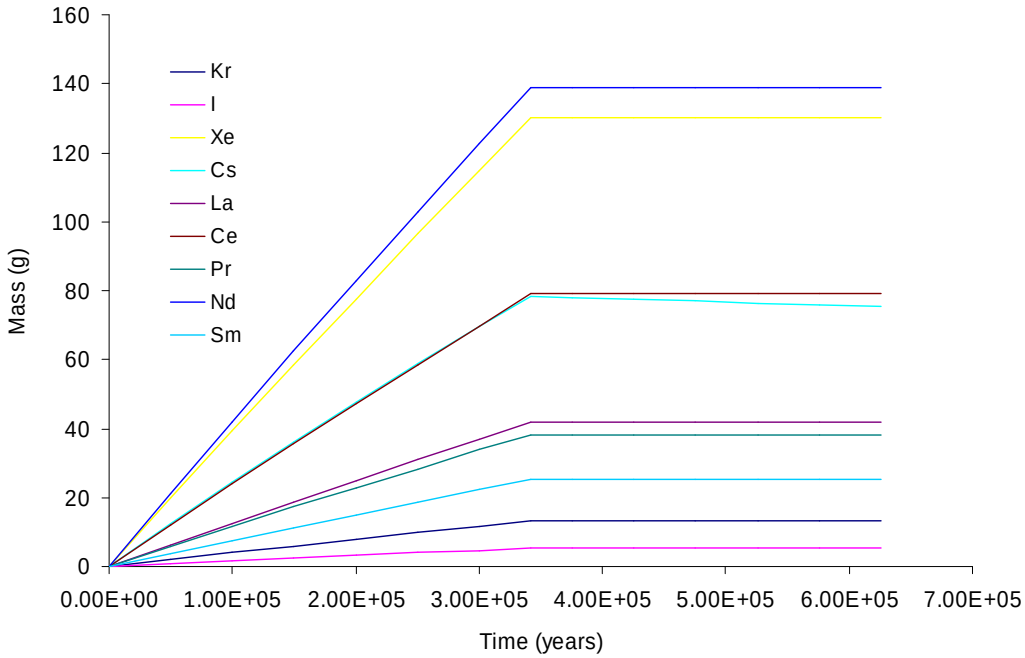

Figure 61: Variation of Fission Product Mass with Time for the NRVB QSS Transient.
FISPIN – PWR Array Spectrum and Detailed Power History

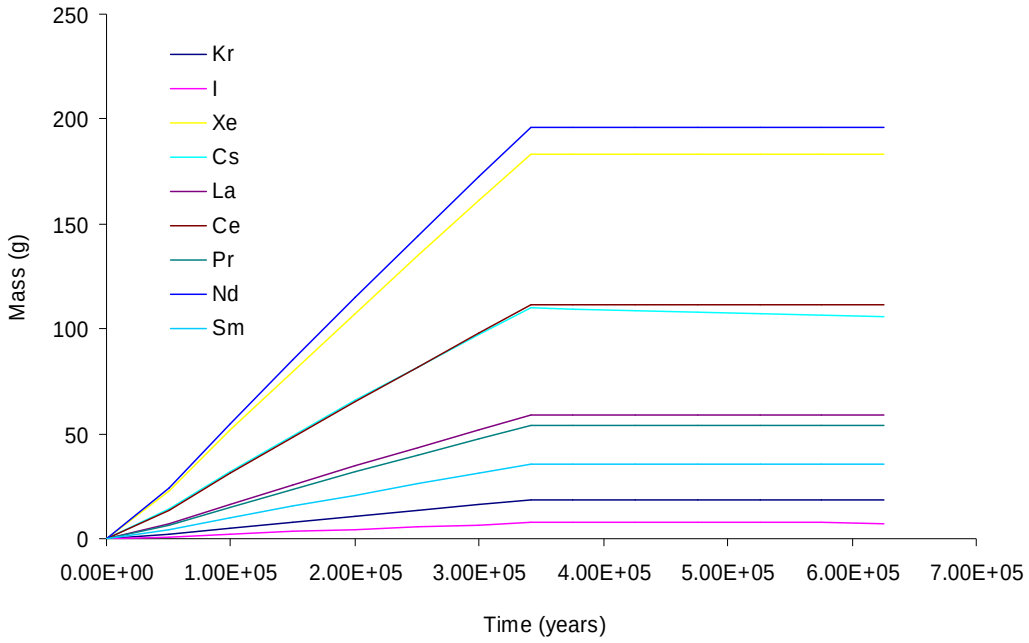

Figure 62: Variation of Fission Product Mass with Time for the NRVB QSS Transient.
FISPIN – Spectrum from a Spherical Fissile Material Region and Detailed Power History

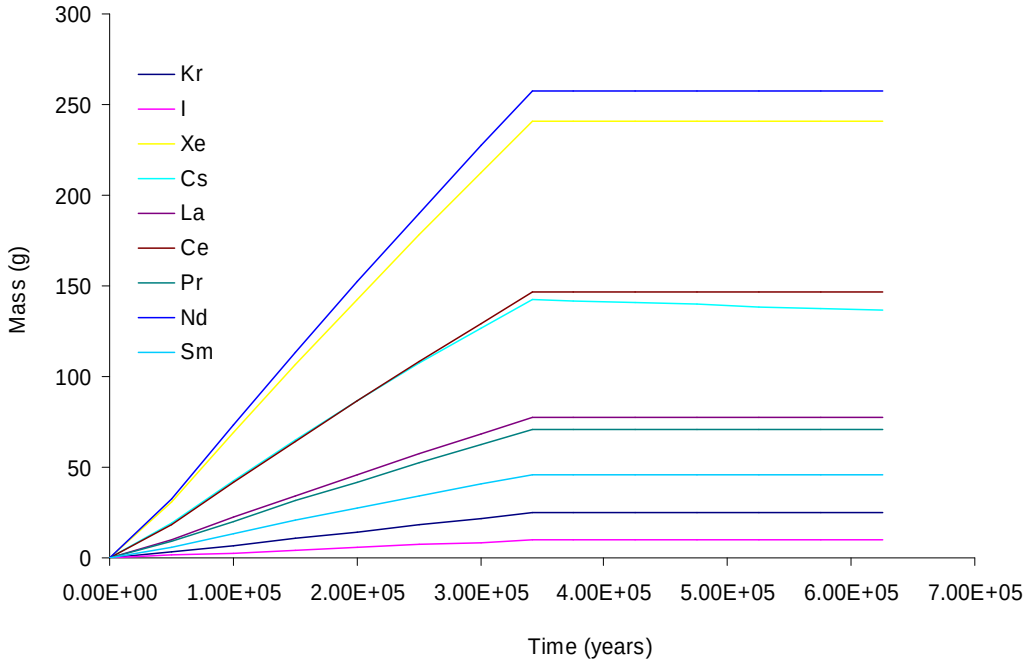

Figure 63: Variation of Fission Product Activity with Time for the NRVB QSS Transient.
FISPIN – PWR Array Spectrum and Average Power History

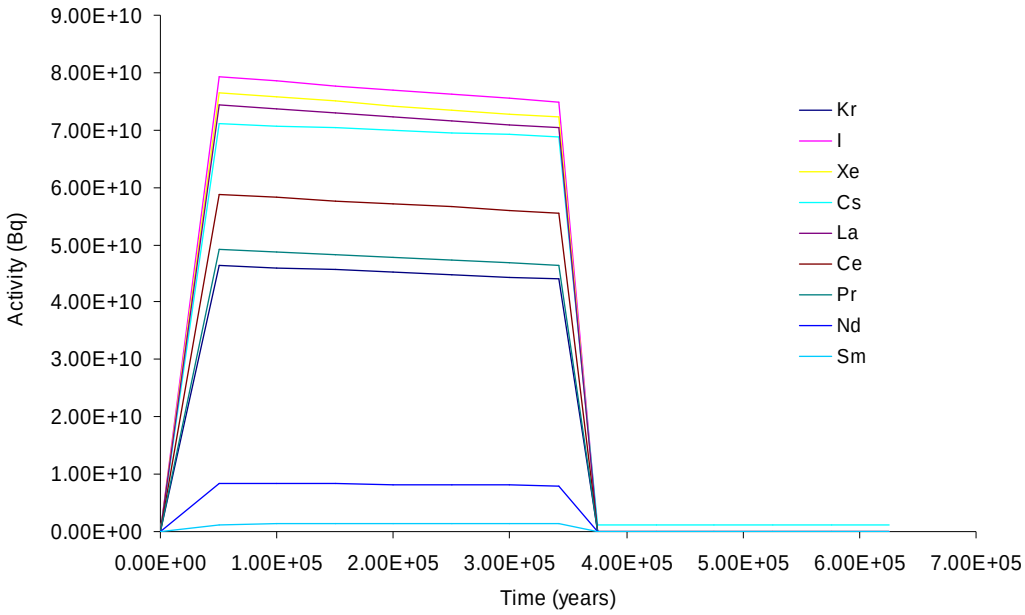

Figure 64: Variation of Fission Product Activity with Time for the NRVB QSS Transient.
FISPIN – Spectrum from a Spherical Fissile Material Region and Average Power History

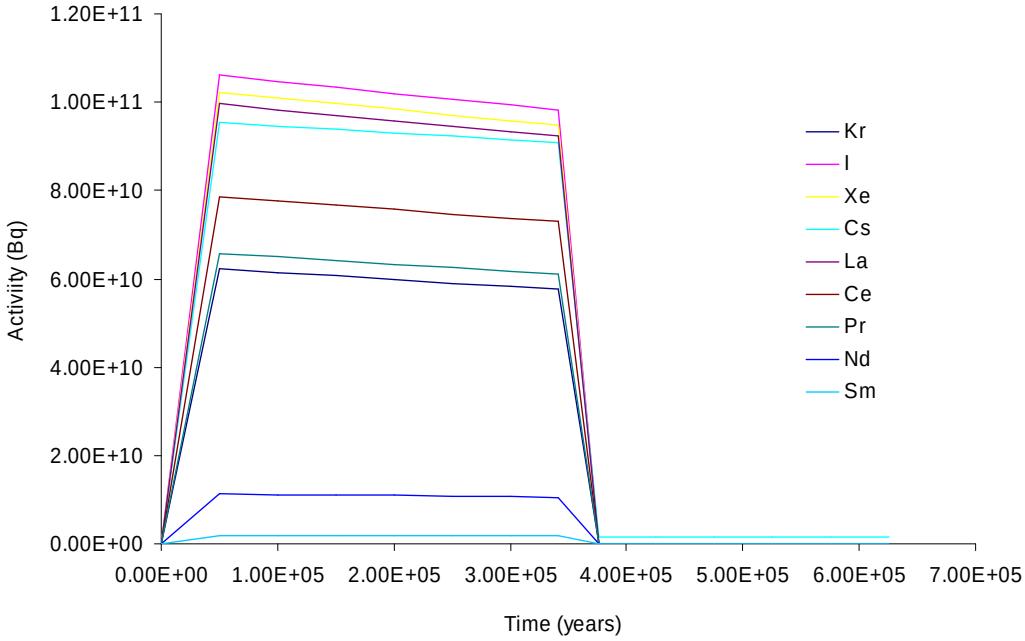

Figure 65: Variation of Fission Product Activity with Time for the NRVB QSS Transient.
FISPIN – PWR Array Spectrum and Detailed Power History

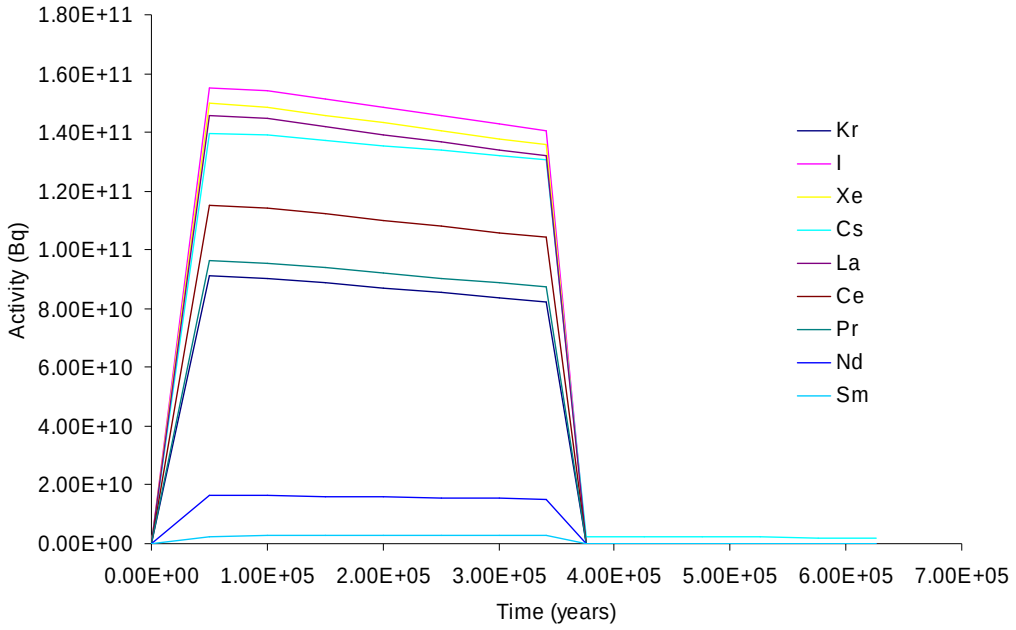

Figure 66: Variation of Fission Product Activity with Time for the NRVB QSS Transient
FISPIN – Spectrum from a Spherical Fissile Material Region and Detailed Power History

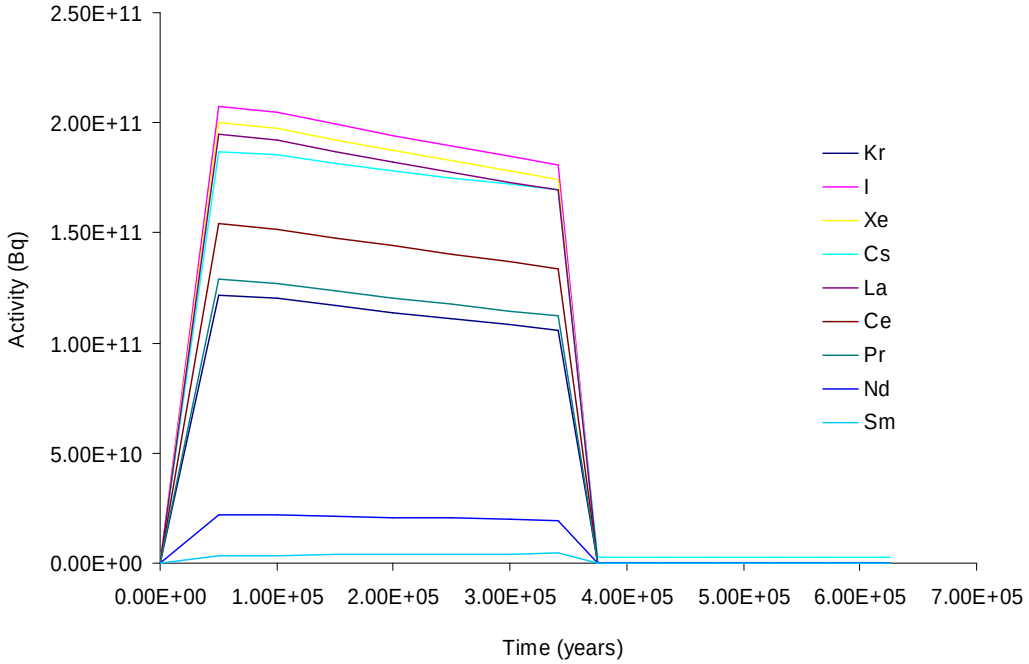

Figure 67: Variation of Power with Time for the RTM Transient – 10 kg of $^{239}PuO_2$ in NRVB

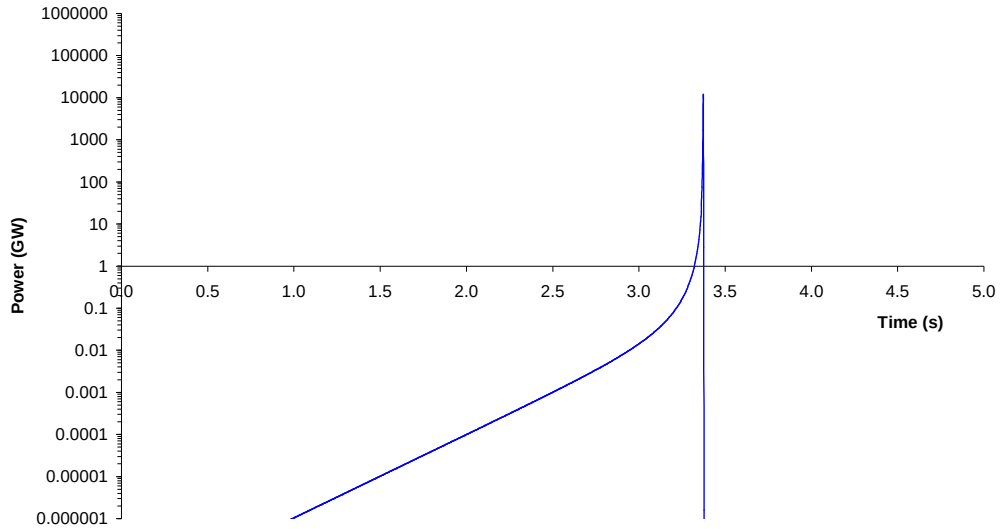

Figure 68: Variation of Power with Time for the RTM Transient - 100 kg of $^{239}PuO_2$ in NRVB

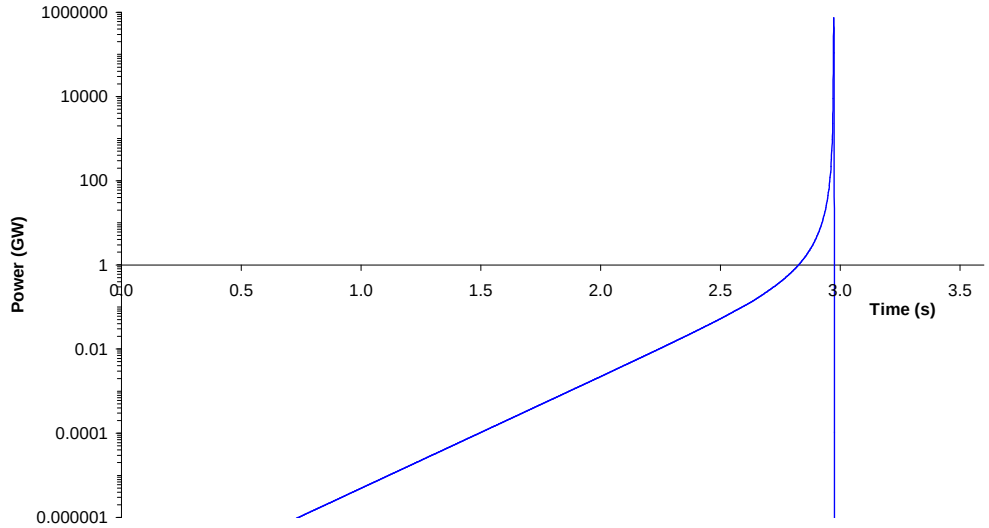

Figure 69: Variation of Power with Time for the RTM Transient - 1000 kg of $^{239}PuO_2$ in NRVB

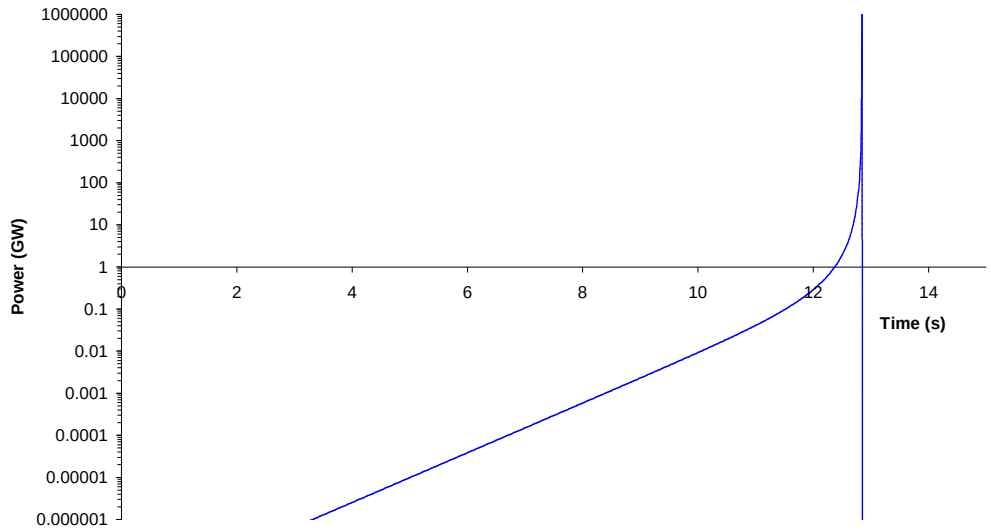

Figure 70: Inventory at One Hour After the RTM NRVB Transient